

Abstract

Disruption of Trio GEF Function and Regulation in Neurodevelopmental Disorders

Ellen Elizabeth Corcoran

2023

There is a critical need to elucidate the biochemical events that control dendrite and synapse function to develop better targeted therapeutic strategies for neurodevelopmental disorders. Functionally damaging mutations in *TRIO* are enriched in individuals with neurodevelopmental disorders. *TRIO* encodes a synaptic regulatory protein with three catalytic domains (Hence the name, *TRIO*) - two guanine nucleotide exchange factor domains, GEF1 (Rac1 and RhoG) and GEF2 (RhoA), and a putative kinase domain. Broadly speaking, Trio serves as a signaling hub to integrate signals from cell surface receptors and coordinate cytoskeletal rearrangements by activating small GTPases. However, the mechanistic details of how Trio GEF1 and GEF2 are regulated in cells and how these processes become disrupted in neurodevelopmental disorders remains largely unclear. Therefore, the goal of my thesis was to answer one fundamental signaling question, which is how Trio GEF activity is regulated in vitro and in cells.

In Chapter One of my thesis, I begin by providing a general overview of the genetic, biochemical, and model organism studies that indicate that disrupted

function of the *TRIO* gene is a risk factor for neurodevelopmental disorders. Next, I detail the extensive toolkit I generated to probe the regulatory mechanisms and binding partners of Trio in vitro. I conclude Chapter One by briefly describing applications of this toolkit.

Chapter Two covers my co-first author work with former graduate student Josie Bircher, where we discovered a novel mechanism wherein Trio spectrin repeats autoinhibit GEF1 activity. In this work, I leveraged the recombinant Trio constructs and in vitro GEF assay from Chapter One to show that when spectrin repeats 6-9 are appended to GEF1 (SR6-GEF1), GEF activity is significantly inhibited in vitro, that disease variants relieve this autoinhibition, and that this phenotype is also observed in cells.

Based on my finding that the spectrin repeats autoinhibit GEF1 activity in vitro and in cells, the next question I sought to answer was how Trio GEF1 activity is regulated spatiotemporally in cells. More specifically, I hypothesized that tails of cellular receptors engage and activate Trio SR6-GEF1 or post-translational modifications (PTMs) activate Trio SR6-GEF1 in a tightly coordinated manner. In Chapter Three, I detail my unpublished work in this project.

In Chapter Four, I conclude my thesis with a brief overview of future directions of this project and the current scope of the field.

Disruption of Trio GEF Function and Regulation in Neurodevelopmental Disorders

A Dissertation

Presented to the Faculty of the Graduate School

Of

Yale University

In Candidacy for the Degree of

Doctor of Philosophy

By

Ellen Elizabeth Corcoran

Dissertation Director: Anthony J. Koleske

December 2023

© 2023 by Ellen Elizabeth Corcoran

All rights reserved.

Table of Contents

List of Figures	xiii
List of Tables	xvi
List of Abbreviations	xvii
Acknowledgements	xx
Dissertation Overview	xxiii
Chapter 1	1
Tools to Probe Disease Impact on Trio GEF Signaling	1
1.1 Summary	2
1.2 Background and Significance	3
1.2.1 Neurological disorders lack effective targeted therapies and are characterized by altered dendritic spine morphologies	3
1.2.2 Trio is a major new risk gene for neurodevelopmental disorders	4
1.2.3 Trio is a large multidomain protein with various isoforms	6
1.2.4 Trio controls dendrite and synapse development and function	7
1.2.5 Disease-associated mutations in the GEF1 domain impair Trio function	11
1.2.6 TRIO variants exhibit distinct patterns in different disorders	12
1.2.7 Spectrin repeats serve as protein scaffolds and cytoskeletal interactors	12

1.3 Generating a Library of Recombinant Trio Fragments	14
1.4 Optimizing an in vitro fluorescence GEF assay	16
1.4.1 Summary	16
1.4.2 Purification of GST-RhoA and GST-Rac1	18
1.4.3 Purification of TRIO His-GEF domains	21
1.4.4 BODIPY-FL-GDP nucleotide exchange assays	22
1.4.5 Data Processing and Analysis	23
1.5 Applying and Expanding the Toolkit	26
1.5.1 Summary	26
1.5.2 Trio Ig Kinase does not have kinase activity toward promiscuous substrates in vitro	26
1.5.3 Trio SR6-GEF1 does not co-sediment with F-actin	30
1.5.3 Trio may functionally interact with PDE4A5	32
1.5.3.1 Summary	32
1.5.3.2 Background	32
1.5.3.3 Methods	33
1.5.3.4 Trio GEF1 directly interacts with PDE4A5	36
1.6 Discussion	41
Chapter 2	42

Autoinhibition of Trio GEF1 is disrupted by neurodevelopmental disorder-related genetic variants	42
2.1 Summary	43
2.2 Overview	43
2.3 Results	45
2.3.1 Inclusion of SRs 6-9 reduces Trio GEF1 activity	45
2.3.2 NDD-associated variants in SR8 increase Trio GEF1 activity in the context of SR6-GEF1	48
2.3.3 NDD-associated variants in SR6 decrease GEF1 activity in the context of SR6-GEF1	48
2.3.4 GEF1 variant D1368V increases GEF activity only in the context of SR6-GEF1	51
2.3.5 The SRs and GEF1 form distinct stable interacting domains	54
2.3.6 The SRs reduce GEF1 binding to Rac1	60
2.3.7 SRs 6-9 inhibit GEF1-induced cell spreading	62
2.4 Discussion	66
2.4.1 Inclusion of Trio SRs autoinhibits GEF1 activity in vitro	66
2.4.2 SRs make direct contact with GEF1 and impair interactions with Rac1	67

2.4.3 NDD associated mutations in SR8 and GEF1 disrupt SR-mediated GEF1 inhibition	68
2.4.4 NDD-associated variants in SR6 may reinforce SR-mediated GEF1 inhibition	69
2.4.5 The SRs may serve as a target for activators of Trio GEF1 activity	70
2.5 Conclusions	71
2.6 Methods	71
2.6.1 Expression Cloning and Protein Purification	71
2.6.2 BODIPY-FL-GDP nucleotide exchange assays	72
2.6.3 Protein Structure Predictions	74
2.6.4 Limited proteolysis	74
2.6.5 Crosslinking mass spectrometry	76
2.6.6 BioLayer interferometry	77
2.6.7 Measurement of GEF and SR6-GEF1 impact on cell morphology	78
Chapter 3	80
Studies Toward the Elucidation of Mechanisms of Trio GEF Activation and Regulation	80
3.1 Summary	81
3.2 Determining whether and how receptors engage and activate Trio GEF1	81

3.2.1 Overview	81
3.2.2 Generating Cytoplasmic Tails of Receptors that Functionally interact with Trio	86
3.2.3 Measuring receptor binding and activation of Trio SR6-GEF1	89
3.2.3.1 Methods	89
3.2.3.2 Trio directly interacts with each candidate activator intracellular region	90
3.2.3.3 No receptor tail candidate activates Trio SR6-GEF1 in vitro	96
3.3 Determining whether and how phosphorylation impacts Trio GEF activity	99
3.3.1 Overview	99
3.3.2 Generating and testing Trio Sr6-GEF1 isosteric phosphomimic constructs	102
3.4 Discussion	105
Chapter 4	107
Ongoing Work and Future Directions	107
4.1 Summary	108
4.2 Do candidate activators increase Trio SR6-GEF1 activity in cells?	108
4.3 What are other Trio signaling pathways?	110
4.4 Is there crosstalk between Trio GEF1 and GEF2?	112
4.5 Concluding Remarks	114

List of Figures

Fig 1.1 Domain structure of Trio with disease-associated variants.....	5
Fig 1.2 Trio Family Proteins are large multi-domain proteins.....	8
Fig 1.3 Major Trio Isoforms.	9
Fig 1.4 Trio regulates neuronal development and function.....	10
Fig 1.5 Library of Recombinant Trio fragments.	15
Fig 1.6 In vitro fluorescence assay for Trio GEF1 activity. <i>Figure adapted from Blaise, Corcoran et al., 2022</i>.....	17
Fig 1.7 Mapping Catalytic Residues of Trio Kinase.....	29
Fig 1.8 Trio SR6-GEF1 does not co-sediment with F-actin.....	31
Fig 1.9 Recombinant Purified PDE4A5.....	35
Fig 1.10 Recombinant Trio Fragments used in pulldown assays.....	37
Figure 1.11 PDE4A5 interacts with Trio GEF1.....	38
Figure 1.12 PDE4A5 interacts with Trio SR6-GEF1.	39
Fig 1.13 PDE4A5 interacts with Trio SR6-SH3-1.	40
Fig. 2.1 Inclusion of SRs 6-9 reduces Trio GEF1 activity on Rac1. <i>Figure adapted from Bircher, Corcoran et al., 2022</i>	46

Fig. 2.2 Mutations in SR6 and SR8 differentially impact GEF1 activity. <i>Figure adapted from Bircher, Corcoran et al., 2022</i>	49
Fig. 2.3 GEF1 variant D1368V increases GEF1 activity in the context of SR6-GEF1. <i>Figure adapted from Bircher, Corcoran et al., 2022</i>	52
Fig. 2.4 AlphaFold predicts an interaction between the SRs and GEF1, which form independent folding units. <i>Figure adapted from Bircher, Corcoran et al., 2022</i>	55
Fig. 2.5 The SRs interact with GEF1. <i>Figure adapted from Bircher, Corcoran et al., 2022</i>	58
Fig. 2.6 Inclusion of SRs 6-9 reduce binding to Rac1. <i>Figure adapted from Bircher, Corcoran et al., 2022</i>	61
Fig. 2.7 SRs 6-9 reduce the impact of GEF1 on cell spreading. <i>Figure adapted from Bircher, Corcoran et al., 2022</i>	64
Fig 3.1 Candidate Trio GEF1 Activating Receptors.....	85
Fig 3.2 Schematic of Purifying Intracellular Tails of Candidate Trio Activators.....	87
Fig 3.3 Purified Candidate Trio Activator Tail Constructs.....	88
Fig 3.4 DCC, Kidins220, ICAM1 and NLGN1 interact with Trio.....	92
Fig 3.5 ADAM22, ADAM23, and VE-Cadherin directly interact with Trio.	93

Fig 3.6 L1CAM directly interacts with Trio.....	95
Fig 3.7 Candidate activator tails do not activate Trio SR6-GEF1 in vitro. ...	98
Fig 3.8 Conserved phosphorylation sites mapped on Trio SR6-GEF1.	101
Fig 3.9 Isosteric Phosphomimic Trio SR6-GEF1 constructs.....	103
Fig 3.10 Phosphomimic Trio SR6-GEF1 constructs do not have altered catalytic activity.	104
Fig 4.1 Cell-based assay for Trio SR6-GEF1 activity. Figure adapted from <i>Katrancha et al. 2017</i>.....	109
Fig 4.2 Preliminary identification of Trio interactors from mouse brain extract.....	111
Fig 4.3 Structural Prediction and Purification of Trio SR6-GEF2.....	113

List of Tables

Table 1: Recombinant Trio Fragments	117
Table 2: Recombinant Trio Primer sequences	120
Table 3: Primer sequences and vectors used for Trio constructs. Table adapted from Bircher, Corcoran et al., 2022	124
Table 4: Candidate Protein Activators of Trio	125
Table 5: Primer sequences used for candidate activators of Trio.....	127
Table 6: Trio and Kalirin phosphorylation peptide sequences	128
Table 7: Evolutionarily conserved Trio and Kalirin phosphorylation residues	129
Table 8: Primer sequences and vectors used for isosteric phosphomimic Trio SR6-GEF1 constructs	130

List of Abbreviations

ADAM23	ADAM metallopeptidase domain 23
ASD	Autism Spectrum Disorder
AU	Arbitrary Units
BME	β -mercaptoethanol
BPD	Bipolar Disorder
BS3	Bis(sulfosuccinimidyl)suberate
CV	Compensation voltage
DCC	Deleted in colorectal cancer
DD	Developmental Delay
DH	Dbl Homology
DNA	Deoxyribonucleic acid
dTrio	<i>Drosophila</i> Trio protein
Dtrio	<i>Drosophila</i> Trio gene
DTT	1,4-dithiothreitol
EDTA	Ethylenediaminetetraacetic acid
EGTA	Ethylene glycol-bis(2-aminoethylether)-N N N'N'-tetraacetic acid
FAIMS	Field asymmetric ion mobility spectrometry
FL	Full-length
fl	<i>Flox</i>
Fn	<i>Fibronectin</i>
GDP	Guanosine diphosphate
GDP-FL-BODIPY	GDP-fluorescein-BODIPY
GEF	Guanine nucleotide exchange factor
GFP	Green fluorescent protein
GST	Glutathione-s-transferase
GTP	Guanosine triphosphate
GTPase	Guanosine triphosphate hydrolase
HTA	
Hr	Hours
HRP	Horseradish peroxidase
ICAM1	Intercellular Adhesion Molecule 1
ID	Intellectual disability
Ig	Immunoglobulin

IP	Immunoprecipitate
Kalirin	Human Kalirin protein
Kalirin	Human Kalirin gene
kcat	Rate constant for conversion of substrate into product
Kd	Dissociation constant
KDa	Kilodalton
Kidins220	Kinase D substract interacting substrate of 220 kDa
Km	Michaelis constant
KO	Knockout
Kobs	Observed rate coefficient
L1CAM	L1 cell adhesion molecule protein
LC-Ms/MS	Liquid chromatography-mass spectrometry
Lgi1	Leucine-rich glioma inactivated 1
MBP	Maltose Binding Protein
MES	2-ethanesulfonic acid
Min	Minutes
NDDs	Neurodevelopmental disorders
NLGN1	Neuroigin1 gene
NTA	Nitrilotriacetic acid
PCR	Peptidylglycine a-amidating monooxygenase
PH	Pleckstrin homology
PIs	Phosphatidyl inositols
PDE4A5	Phosphodiesterase 4A Isoform 5
PMSF	Phenylmethylsulfonyl fluoride
Rac1	Ras-related C3 botulinum toxin substrate 1
RFP	Red fluorescent protein
Rho	Ras homology family member
S200	Superdex 200
SAXs	Small angle x-ray scattering
SCZ	Schizophrenia
SDS-PAGE	Sodium dodecyl sulfate – polyacrylamide gel electrophoresis
Sec	Seconds

SEC	Size exclusion chromatography
SH3	Src homology 3
SR	Spectrin repeat
TBS	Tris buffered saline
Trio	Human Trio protein
TRIO	Human Trio gene
Unc-73	UNCoordinated 73
Unc-73	<i>C. elegans</i> trio protein
Unc-73	<i>C. elegans</i> trio gene
UPLC	Ultra performance liquid chromatography
VE-Cadherin	Vascular endothelial cadherin

Acknowledgements

First and foremost, I would like to thank my thesis advisor, Tony Koleske. Over the span of four and a half years, Tony pushed and encouraged me to become a better scientist every single day. Leading by example, Tony taught me to plan experiments efficiently and effectively, to think for myself, to read voraciously, and to maintain a growth mindset. Personal growth and being challenged is never comfortable, but in retrospect, I am undoubtedly grateful that I had Tony as a steadfast mentor to guide me toward my full potential. Tony's enthusiasm for research is contagious, and I am appreciative I got to learn from his daily demonstrations of how to be a productive, careful, ethical, and collegial scientist. I would also like to thank the other three members of my committee: Titus Boggon, Charlie Greer, and Mark Hochstrasser. My project and I always benefitted from the fruitful discussion and constructive criticism my committee had to offer.

Steadfast mentors have been a recurring theme in my academic journey, even before I arrived at Yale, and are the reason why I have gotten to where I am today. I would like to thank Sheryl Hemkin, who ignited my passion for scientific research at Kenyon College. Sheryl continues to provide me with endless support (and endless recommendation letters), for both of which I owe her many thanks. Sheryl is a wonderful role model and great inspiration for the type of mentor I aspire to be in the future. I would also like to thank the Kenyon College Chemistry Department for their efforts to create such an enthusiastic, supportive, and inclusive scientific community.

Next, I would like to thank several of my fellow lab members in the Koleske lab, all of whom served as wonderful mentors to me. First, I must thank Josie Bircher, who was my co-author and mentor in the lab. I owe an endless amount of thanks for Josie's patience when we worked together on the Trio project. Josie taught me how to work smarter, be a rigorous scientist, and she helped me navigate every step of the graduate school process. I have Josie, Juliana Shaw, Wanqing Lyu, Kuanlin Wu, Amanda Jeng, and Tony Koleske to thank for teaching me everything I know about protein biochemistry. I always turned to Juliana, Josie, Wanqing, Kuanlin, and Amanda when I was getting started in the lab. Starting graduate school and working in a lab, my anxiety was at an all-time high. I truly don't think I could've made it through graduate school if I didn't have this patient, kind, and supportive group of older students in lab and I thank them from the bottom of my heart. I would like to thank Xianyun Ye, Liz Vellali, and Amber Thammavongsa for all the administrative and technical assistance that make the daily operation of our lab possible. I would like to thank my fellow peers in the lab whom I had the privilege to mentor and helped me with the project outlined in this thesis. I would like to thank Eve Wattenberg, Matt Vitarelli, Maria Mendoza, Jasmine Simmons, Pauline Lining Pan, and Camila Garcia for their patience as I learned how to grow as a mentor and for all their help in pushing this project forward. Finally, I value all the advice and support from all other members of the Koleske lab, past and present, not explicitly mentioned, who helped me during my time at Yale.

Next, I owe an endless amount of thanks to my dear friends who were all incredibly supportive throughout my time in graduate school. Anna Nelson (Stanton) is my oldest friend and has been my steadfast friend throughout my highest of highs and my lowest of lows. I cannot thank her enough for always being there for me to help me navigate life. I also want to thank Julia Josowitz, who, despite living across the country, still came to visit me multiple times at Yale. Finally, I want to thank all my Yale friends. I could write multiple pages of thanks for every one of my friends at Yale, but to say briefly, I want to thank Michelle Worthington, Rafi Castellanos, Elizabeth Gordon, Acadia Kocher, Jake Thrasher, Rebecca Starble, and Matt Jones for being such wonderful, supportive friends and making Yale/New Haven feel like home.

Saving the best for last, I would like to thank my parents, Everard and Julie Corcoran, and my sister, Claire Corcoran. I have so much gratitude that I was raised by two loving, encouraging parents that showed me the great value of hard work from an early age and that I have such a kind, caring older sister as a best friend. My parents and sister are always my biggest cheerleaders, and their endless support has allowed me to build a life that I love. I love our family, and I love you all everything.

My work in this thesis was funded in part by 1F31MH127891-01 and CMBTP T32GM007223.

Dissertation Overview

This dissertation is composed of four chapters. Chapter One provides a framework for the thesis by introducing the set of tools I generated to answer critical Trio signaling questions in my thesis. Chapter Two includes my co-first author publication, where I discovered a novel mechanism of Trio GEF1 regulation by the spectrin repeats and showed that disease variants relieve this autoinhibitory constraint. Chapter Three details my unpublished preliminary work to answer how Trio GEF activity is regulated in a spatiotemporal manner in cells. In Chapter Four, I provide an overview of future directions of this project to fully understand how Trio GEF activity is regulated in cells and how dysregulation of these processes contributes to disease pathology.

For Aunt Kathleen and Grandma Paula.

Chapter 1

Tools to Probe Disease Impact on Trio GEF Signaling

1.1 Summary

Schizophrenia (SCZ) and autism spectrum disorder (ASD) are complex, debilitating neurodevelopmental disorders that affect up to 3% of the worldwide population. Current therapies remain insufficient, as they do not ameliorate all symptoms and have significant side effects. Better targeted therapeutics are imperative but cannot advance without identifying biochemical events and pathological processes that cause disease.

These disorders are characterized by aberrant dendritic and synaptic pathology. Intriguingly, allelic loss-of-function (LOF) or rare variants spread throughout the entire *TRIO* gene are significantly enriched in individuals with SCZ and ASD and related disorders. Studies in model organisms have demonstrated that *TRIO* is required to control synaptic development and function. However, the fundamental questions of how mutations in *TRIO* disrupt biochemical signaling pathways and impacts neuron development is completely unknown.

In this Chapter, I begin by providing a brief overview of Trio protein function from a mechanistic level to implications in neurodevelopmental disorders, with written sections modified from my qualifying proposal. I next detail the extensive list of tools I generated to probe the biochemical functions of Trio and easily test the impact of disease variants on these processes, including a library of recombinant Trio fragments, and my contributions to optimizing an in vitro fluorescence guanine nucleotide exchange factor assay (modified from my second author paper, Blaise, Corcoran 2022). The written sections included from this manuscript were sections that I contributed intellectually to and co-wrote with

Alyssa Blaise were taken directly from the manuscript. I conclude this chapter with a brief overview of applying and expanding this toolkit to probe the biochemical function of Trio.

1.2 Background and Significance

1.2.1 Neurological disorders lack effective targeted therapies and are characterized by altered dendritic spine morphologies

Neuropsychiatric disorders are the leading cause of medical disability in the United States¹. Bipolar disorder, schizophrenia, autism, intellectual disability, are complex neurodevelopmental disorders that affect millions of people and bring tremendous emotional and financial burdens to families^{2,3}. Current therapies for these disorders are insufficient, as they do not fully ameliorate neurological disease symptoms and have significant side effects⁴⁻⁷. Better targeted therapeutics are imperative, but therapeutic progress for these diseases is hindered by poor understanding of the biochemical events underlying these disorders.

Dendritic spines are the major receptive sites for synaptic input, and their dynamic morphology is linked to learning and memory. For each of these disorders, both dendritic spines and their associated synapses do not develop normally or become destabilized⁸⁻¹². Dendritic spines are drastically reduced in the prefrontal cortices of individuals with bipolar disorder and schizophrenia and increased in individuals with autism spectrum disorder¹²⁻¹⁴. The prevalence of altered spine pathology and high level of genetic overlap in these disorders,

notably in genes related to synapse function, suggest the disruption of common biochemical pathways involved in dendritic stability ^{7, 15-21}. Intriguingly, there is an enrichment of disease associated loss-of-function and rare variant damaging mutations in the *TRIO* gene that encodes a synaptic regulatory protein ^{7, 16, 22-25}.

1.2.2 Trio is a major new risk gene for neurodevelopmental disorders

The *TRIO* gene has been implicated as a significant risk gene in multiple neurodevelopmental disorders ^{7, 15, 19, 22-24, 26-32}. Our lab and others have identified an enrichment of predicted damaging variants (from sequencing pedigrees) and ultrarare variants in *TRIO*. Exome sequencing analyses in control individuals classify Trio as highly intolerant to mutation, therefore likely to contribute to disease ^{7, 33, 34}. Distinct patterns of these deleterious mutations are linked with different disorders, such as schizophrenia (SCZ), autism spectrum disorder (ASD), intellectual disability (ID), developmental delay, (DD) and bipolar disorder (BPD) (Fig 1.1).

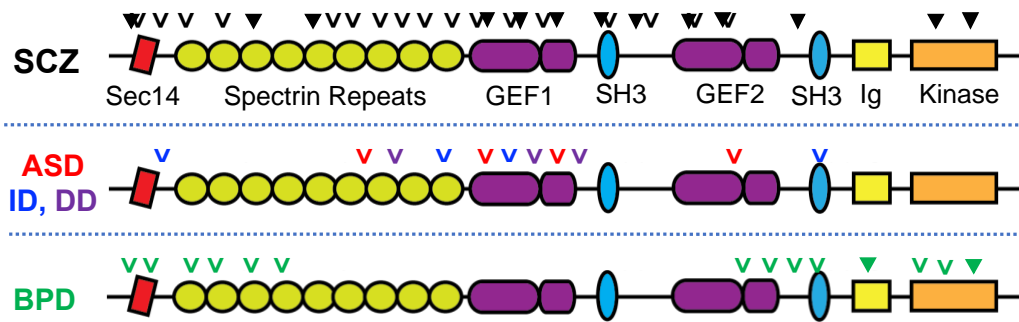


Fig 1.1 Domain structure of Trio with disease-associated variants.

Schematic representation of the domain structure of TRIO with positions of genetic mutations associated with schizophrenia (SCZ), autism (ASD), intellectual disability (ID), developmental delay (DD), and bipolar disorder (BPD). ▼ indicate nonsense mutations, ∨ indicate predicted-to-be-damaging missense mutations. All mutations are heterozygous.

De novo missense mutations and rare variants in the GEF1 domain and the adjacent regulatory spectrin repeats are enriched in autism, intellectual disability, and developmental delay, suggesting that dysregulated GEF1 activity is linked to these disorders ^{7, 24, 25}. However, the mechanism by which the spectrin repeats regulate GEF1 and the impact of disease mutation remained completely unknown.

1.2.3 Trio is a large multidomain protein with various isoforms

Human Trio is the founding member of the Trio family proteins that contain two Rho-GEF domains ^{35, 36}. The Trio family of proteins is made up of highly conserved large, multi-domain proteins, including vertebrate Trio and Kalirin, as well as *Drosophila* dTrio, and *C. elegans* unc-73 (Fig 1.2) ^{37, 38}. *TRIO* encodes a large (>300 kDa) multi-domain protein with three catalytic domains (Hence the name, *TRIO*) – two guanine nucleotide exchange factor (GEF) domains, and a putative serine/threonine kinase domain. Biochemically, the two GEF domains display different specificities to regulate the actin cytoskeleton ^{39, 40}. The N-terminal GEF (GEF1) is responsible for the activation of the Rho GTPases Rac1 and RhoG, which further activates CDC42, while the C-terminal GEF domain (GEF2) activates RhoA ^{35, 41-43}. The function of the kinase domain remains unknown. Trio also contains an N-terminal lipid-binding Sec-14 domain and nine spectrin repeat domains, ⁴⁴ and SH3 and Ig-like domains^{45, 46}. Alternative splicing of *TRIO* yields four major isoforms expressed in the nervous system (Fig 1.3). Beyond the

potential for protein-protein and protein-lipid interactions, the functions of these accessory domains remain poorly understood.^{7, 47, 48}

1.2.4 Trio controls dendrite and synapse development and function

These isoforms of Trio all localize to axons and dendrites, where they function to integrate diverse guidance signals presented by cell surface receptors and cell-cell interactions^{29, 35, 49-51}. Trio interfaces with cell-receptors to orchestrate cytoskeletal rearrangements by interacting with small guanine triphosphatases to carry out essential morphological changes during neuronal development (Fig 1.4).

TRIO is an essential gene in mice, as *TRIO* knockout in mice is embryonic lethal⁵². Our lab also generated a *TRIO* haploinsufficient mouse model and demonstrated that ablation of a single *TRIO* allele in excitatory neurons in the cortex and hippocampus cause severe behavioral deficits in mice, including increased anxiety, and impaired social preference and motor coordination⁵³. Trio loss also reduced forebrain size and dendritic arborization. Overall, because of the implication of *TRIO* as a significant risk gene and its known involvement in synapse and dendrite development, elucidating the function and regulation of Trio GEF activity will improve our understanding of complex neurodevelopmental disorders characterized by aberrant dendritic spine pathologies.

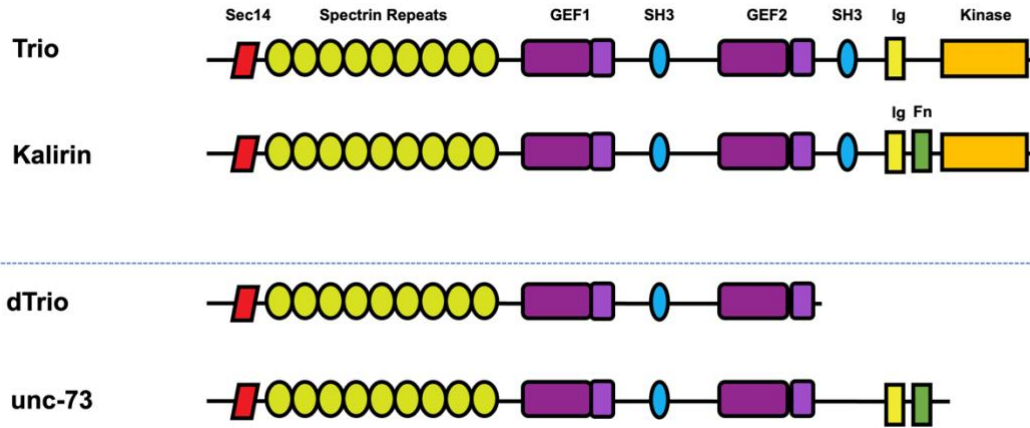


Fig 1.2 Trio Family Proteins are large multi-domain proteins.

Trio family proteins are large multi-domain proteins that contain several accessory domains and up to three catalytic domains. The Trio family proteins has four well studied members – two vertebrate paralogs (Trio and Kalirin) and two invertebrate orthologs (unc-73 in *C. elegans* and dTrio in *Drosophila*). The invertebrate orthologs do not contain a putative kinase domain, suggesting this was an evolutionary addition.

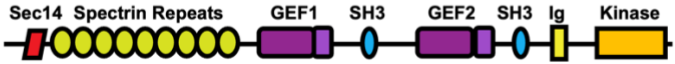


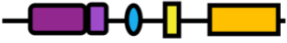
Name	MW (kDa)	Location of Expression	Protein Product
Full length Trio	347	Ubiquitous (low)	
Trio 9S (Trio A)	264	Cortex	
Trio 8 (Trio C)	217	Cerebellum	
Duet (Trio E)	145	Cortex	

Fig 1.3 Major Trio Isoforms.

The *TRIO* gene is alternately spliced. Full length Trio is ubiquitously expressed in all cells, where four main Trio isoforms are specific to the nervous system. Trio9s and Trio 8 are enriched in the cortex and cerebellum, respectively, and Trio Duet is enriched in the cortex.

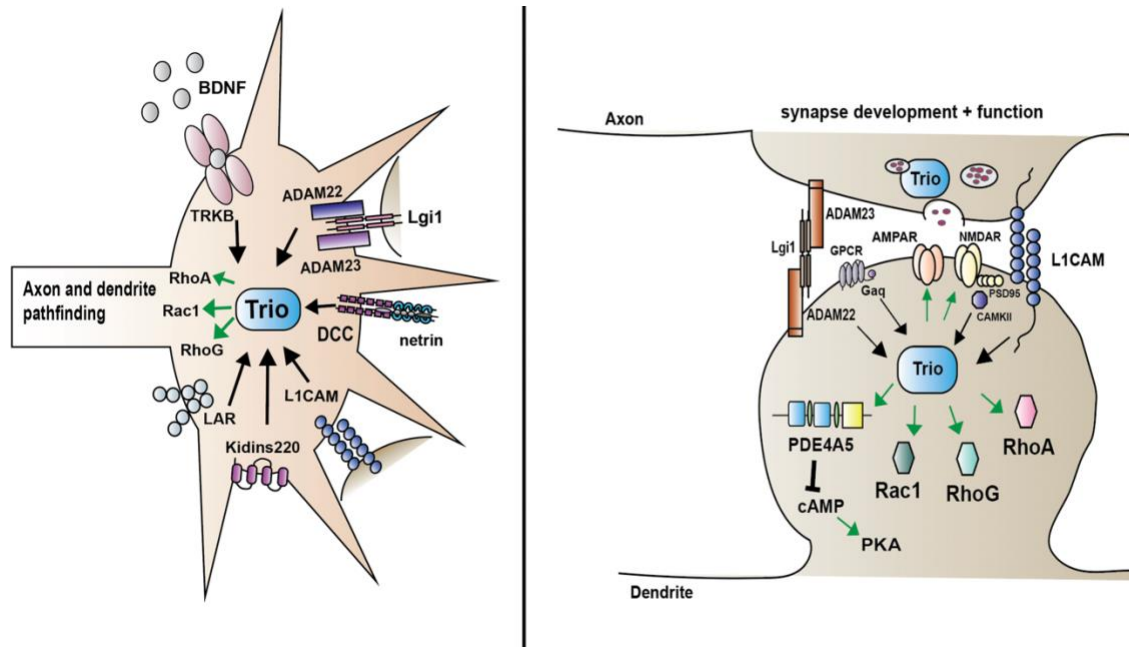


Fig 1.4 Trio regulates neuronal development and function.

(Left) Trio mediates signaling from guidance receptors in axonal and dendritic growth cones to regulate cytoskeletal rearrangements that power proper outgrowth and guidance. (Right) In synapses, Trio regulates release probability, spine structure, and glutamate receptor function. This illustration is adapted from a figure made by Tony Koleske (*unpublished*).

1.2.5 Disease-associated mutations in the GEF1 domain impair Trio function

Genetic analyses in *C. elegans* and *Drosophila* indicate that Trio controls axon guidance and dendrite development and function via its GEF activity^{49, 50, 54-56}. The distinct roles for the two GEF domains in Kalirin and Trio have been characterized by both *in vitro* and *in vivo* studies. The two GEF domains have opposing functions: The GEF1 domain signals through Rac1 to promote dendritic spine stability, whereas GEF2 signals through RhoA to promote dendritic spine *instability*^{49, 57, 58}. *De novo* mutations that disrupt the Trio GEF1 domain are enriched in individuals with ASD and SCZ. Our lab and others have shown that these mutations disrupt the ability of GEF1 to catalyze Rac1 activation^{7, 25}. These studies highlight the essential role of the Trio GEF1 domain and the clear deleterious impact of disease mutation. The central goals of my thesis were to begin to answer two fundamental signaling questions: 1) How is Trio GEF1 activity regulated in cells? 2) How does disruption of these processes contribute to disease pathology?

Several members of the RhoGEF family contain regulatory autoinhibitory N-terminally adjacent domains, where removal of the N-terminal sequence led to constitutive GEF activation when expressed *in vivo*⁵⁹⁻⁶³. Almost all GEFs are multi-domain proteins regulated by protein-protein interactions^{64, 65}. It is hypothesized that autoinhibitory constraint is relieved by proteins interacting with the N-terminal domain of these proteins. However, in most cases, the mechanism of how autoinhibition is released is unknown. The possibility of a flanking domain

regulating GEF1 in Trio, either by autoinhibition or mediated protein interaction had previously not been tested. However, previous studies suggest that the spectrin repeats may also function as an autoinhibitory N-terminally adjacent domain, where removal of the spectrin repeats in Trio leads to a large gain of function in GEF1 activity *in vivo*^{56, 66}. In Chapter 2 of my thesis, I detail my efforts to elucidate the mechanism of regulation of Trio GEF1 activity via its own spectrin repeats.

1.2.6 *TRIO* variants exhibit distinct patterns in different disorders

A recent study by Barbosa et al. demonstrated that two variant hotspots in Trio exhibit distinct patterns in different disorders³². More specifically, it was shown that variants in the spectrin repeat domains and GEF1 domains yield distinct phenotypes – whereas most GEF1 variants inhibit the ability of Trio to activate Rac1 and are linked to patients with intellectual disability and microcephaly, variants in the spectrin repeat 8 domain result in hyperactive Rac1 activity and are enriched in patients with developmental delay and macrocephaly. However, the role of the spectrin repeats in Trio function and the mechanism of spectrin repeat 8 variant -mediated increase in Rac1 activity remained unclear.

1.2.7 Spectrin repeats serve as protein scaffolds and cytoskeletal interactors

While the distinct biochemical functions of the two Trio GEF domains are well-characterized, the relevance of the Trio spectrin repeats remains unclear. The spectrin repeat is a core structural element composed of three α -helices that often

occur as tandem arrangements of multiple repeats in many different proteins ^{67, 68}. Spectrin repeats are the fundamental unit of the spectrin superfamily of proteins (spectrin, a-actinin, dystrophin, and utrophin) ⁶⁹. Spectrin family proteins provide structural support to the plasma membrane, linking the actin cytoskeleton to soluble and integral membrane proteins ⁶⁹⁻⁷¹. More specifically, the spectrin repeats in spectrin and dystrophin have been shown to contribute to actin binding ^{72, 73}, and repeats can directly interact with the cytoplasmic domains of transmembrane proteins, including integrins ^{74, 75}, ICAMs ^{76, 77}, and NMDA receptors ^{78, 79}. However, little is known regarding whether and how the Trio spectrin repeats act as protein scaffolds or contribute to cytoskeletal interactions.

The Trio spectrin repeats have been shown to bind multiple soluble and transmembrane proteins, suggesting that Trio does serve as a protein scaffold. For example, Trio's spectrin repeats interact with Piccolo and Bassoon. Piccolo, and Bassoon, proteins embedded within a cytoskeletal matrix assembled at the presynaptic active zone (CAZ), localize Trio to the presynaptic active zone to modulate the dynamic assembly of F-actin during cycles of synaptic vesicle exocytosis ⁸⁰. The spectrin repeats also bind Kidins220, an integral membrane protein, recruiting Trio to specific membrane domains to promote neurite elongation ⁸¹. A recent study also suggests that spectrin repeats class tightly associate with the Golgi ⁸², and localize Trio to the Golgi and complex with the guanine exchange factor RABIN8 to regulate RAB8- and RAB10-mediated membrane trafficking during neurite outgrowth ⁸³. However, it remains poorly understood whether and how the Trio spectrin repeats coordinate cytoskeletal

interactions by binding to actin, or whether and how Trio spectrin repeats serve as a switchboard for interactions that serve a regulatory role for the catalytic activity of Trio. In Chapter 3 of my thesis, I detail my efforts to determine cellular binding partners of the Trio spectrin repeats, Trio GEF1, and Trio SH3-1. In Chapter 4 of my thesis, I provide a roadmap for future studies to test how these binding interactions mediate Trio GEF1 activity.

1.3 Generating a Library of Recombinant Trio Fragments

To perform quantitative binding and catalytic assays to probe the biochemical regulation of Trio and determine how disease variant disrupt Trio signaling, I generated and purified a library of recombinant Trio fragments spanning the entire length of Trio (Fig 1.5). The cloning was done by me or in collaboration with Tony Koleske, unless otherwise noted, and all subsequent purification and solubility tests were performed by me. Two detailed tables of each of the constructs generated with pertinent information are included in the Appendix section of this thesis (Table 1, Table 2).

While numerous constructs of Trio fragments have been generated and preliminary solubility tests have been performed, several constructs remain largely insoluble. Therefore, future studies are needed to optimize conditions to improve solubility of outstanding constructs, such as altering borders of recombinant fragments or performing solubility matrices to optimize buffer conditions and induction conditions.

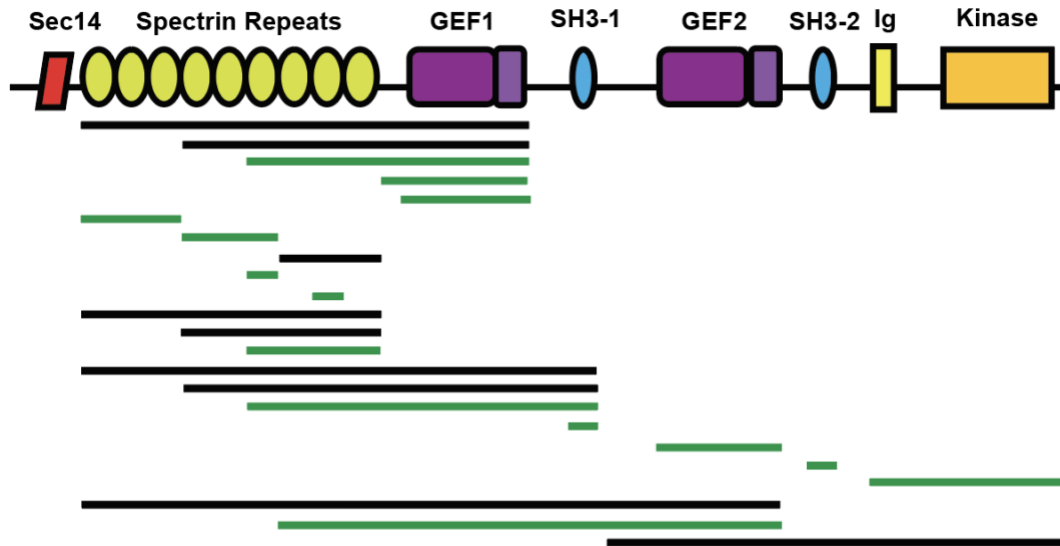


Fig 1.5 Library of Recombinant Trio fragments.

Schematic Diagram of Trio fragments that have been generated. Constructs successfully expressed, purified, and soluble in solution are highlighted in green.

1.4 Optimizing an in vitro fluorescence GEF assay

1.4.1 Summary

As a second author of Blaise et al. 2022, I helped write and optimize a detailed protocol for testing and quantifying the GEF activity of TRIO using an in vitro fluorescence assay. This assay monitors GEF activity by measuring the decrease in fluorescence intensity as fluorescent BODIPY-GDP bound to the Rho-GTPase is exchanged for non-fluorescent GTP (Fig 1.6). First, I optimized purification methods (buffer conditions, utilizing size exclusion chromatography, etc.) for GEF1/GEF2 and Rac1/RhoA and helped write the purification protocol for this methods paper. In addition, I conceptualized a python script to enable facile data processing to calculate catalytic rate and efficiency, wrote a detailed protocol for how to process and analyze the data, and Eve Wattenberg wrote the python script. Our manuscript demonstrates that this assay is scalable for a high-throughput setting for potential use in identifying small-molecule regulators of GEFs and allows for quantitative analysis of GEF activity on many Rho GTPases. This paper was accepted by Biology Methods and Protocols in 2021, and the following sections that I contributed intellectually to and co-wrote with Alyssa Blaise were taken directly from the manuscript.

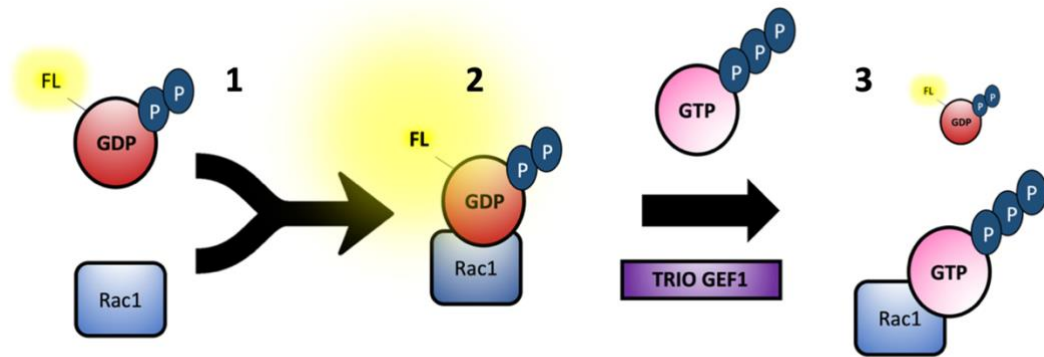


Fig 1.6 In vitro fluorescence assay for Trio GEF1 activity. *Figure adapted from Blaise, Corcoran et al., 2022*

Our in vitro fluorescence assay measures the ability of GEF domains to catalyze the exchange of GDP for GTP on small GTPases. (1) Free BODIPY-FL-GDP has low fluorescence in solution, which (2) greatly increases when bound to Rac1. Trio GEF1 catalyzes exchange of BODIPY-FL-GDP for GTP on Rac1, leading to (3) decreased BODIPY-FL-GDP fluorescence.

1.4.2 Purification of GST-RhoA and GST-Rac1

Day 0: Plasmids were transformed fresh into BL21 cells and plated onto agar plates containing 100 $\mu\text{g}/\text{mL}$ ampicillin. The plates were incubated at 37°C overnight.

Day 1: A single BL21 colony was used to inoculate 50 mL of 2XYT media (16 g/L Tryptone, 10 g/L Yeast, 5.0 g/L NaCl, pH = 7.0) containing 200 $\mu\text{g}/\text{mL}$ ampicillin to maintain high plasmid copy number, and 0.2% glucose to prevent possible slow growth due to expression of the recombinant protein. Starter cultures were grown for ~12-18 hours at 37°C on a shaking platform at 200 rpm. 16 mL (each) of the starter culture was used to inoculate 4 X 800 mL cultures in 2XYT containing 200 $\mu\text{g}/\text{mL}$ ampicillin. The initial culture density was measured (typically $\text{OD}_{600} \approx 0.050$). These cultures were incubated on a shaking platform at 37°C to an $\text{OD}_{600} = 0.6-0.8$, then shifted to 16°C to equilibrate. After approximately 60 minutes, when $\text{OD}_{600} = 0.8-1.0$, expression of the GTPase proteins was induced by adding IPTG to 0.5mM and incubating the culture on a shaking platform at 200 rpm in 16°C overnight. We have found that overnight induction at 16°C of Trio GEF1 domain, Trio GEF2 domain, and Rho-family GTPases reduces protein degradation. Overnight induction 16°C also provides the optimal timing for bacterial cell mass to grow, allowing the investigator to begin protein purification first thing in the morning.

Day 2: Bacteria were pelleted via centrifugation for 20 minutes at 15,00 rpm in an SA-600 centrifuge. Cell pellets were resuspended in a total volume of 48 mL of ice-cold lysis buffer containing 1X PBS (8 mM $\text{Na}_2\text{HPO}_4 \cdot 7\text{H}_2\text{O}$, 2 mM KH_2PO_4 ,

137 mM NaCl, 2.7 mM KCl), 5% glycerol, 1 mM EDTA, 1 mM DTT, 1 mM PMSF, and protease inhibitors (in all cases, we use 1X Sigma Aldrich cOmplete protease inhibitor cocktail). If needed, the resuspended cell pellets can be frozen in 50 mL Falcon tubes using liquid nitrogen and stored at -80°C for later purification. We have stored material in this manner for up to 2 weeks with no loss in the quality of the purified material.

Resuspended cell pellets were thawed in a water bath and quickly put on ice. The pellets were subject to sonication at maximal output on a 50% duty cycle for 4 X 3 minutes, pausing in between cycles to swirl the lysates on ice and cool the sample. Following sonication, Triton X-100 was added to 1% to the lysate and gently mixed. This mixture was allowed to incubate for 20 minutes on ice. The lysate was loaded into Oak Ridge tubes and centrifuged at 4°C in an SA600 Rotor for 30 minutes at 15,000 rpm. The supernatant was loaded into a 50 mL syringe and filtered through a 0.45 µm syringe top filter. 2 mL of glutathione-agarose bead slurry (Pierce) were washed 3X in ice-cold 1X PBS (1.5 mM KH₂PO₄, 155 mM NaCl, 2.7 mM Na₂HPO₄•7H₂O). The beads were packed into a 10 mL disposable chromatography column (Pierce Protein Solutions, ThermoFisher). The lysate supernatant was run through the column 3X and washed 3 times with 10 mL of 1X PBS, 5% glycerol, 1 mM DTT, and 1 mM PMSF, and equilibrated with 10 mL of equilibration buffer (20 mM Hepes pH 7.25, 150 mM KCl, 5 % glycerol, 1 mM DTT, 0.01 % Triton X-100, and 1 mM PMSF). Fractions were eluted in 1 mL aliquots of elution buffer (20 mM Hepes pH 7.25, 150 mM KCl, 5% glycerol, 1 mM DTT, 0.01% Triton X-100, 10 mM glutathione, buffered to pH = 7.25). Protein

elution was monitored using a Bradford assay. Eluted protein fractions were pooled and incubated with PreScission Protease (5 units/mg) overnight to cleave off the GST- tag. The following day, the protein mixture was concentrated by centrifugal filter, and GST was separated from GTPase by size exclusion chromatography into GTPase exchange buffer (20 mM Hepes pH 7.25, 150 mM KCl, 5% glycerol, 1 mM DTT, 0.01% Triton X-100) on a Superdex 75 column (GE). A series of twofold dilutions of a bovine serum albumin (BSA) protein standard in Bradford reagent ranging from 0 mg/mL to 2 mg/mL were prepared to create a standard curve used for calculating protein concentration. 2 μ L of each BSA dilution was added to 200 μ L of diluted Bradford reagent. Often, the eluted protein was too concentrated to be in the linear range of detection when added to Bradford reagent. The purified protein sample was diluted in elution buffer, 1:5, 1:10, and 1:20, depending on the concentration of protein eluted. 2 μ L of each protein dilution was added to 200 μ L of Bradford reagent. Absorbance levels of both the BSA and protein dilutions were measured at 595 nm on a spectrophotometer. The standard curve was created for the BSA dilutions using absorbance (A_{595}) versus concentration. The unknown concentration of the purified protein was determined from an absorbance (A_{595}) versus BSA concentration plot. Protein purity was evaluated after running 10 μ g of protein using SDS-Page and Coomassie blue staining with analysis in Image J. GTPase was aliquoted for assay use and stored at -80°C.

1.4.3 Purification of TRIO His-GEF domains

Days 0-1 were followed as described above using plasmids encoding His-tagged TRIO GEF domains, His-GEF1 and His-GEF2.

Day 2:

Bacteria were pelleted via centrifugation for 20 minutes at 4,000 rpm in an RC3B centrifuge and cell pellets were resuspended in a total volume of 48 mL of ice-cold His lysis buffer (20 mM Hepes pH= 7.25, 500 mM KCl, 5% glycerol, 1% Triton X-100, 20 mM imidazole pH 7.25, 5 mM β -mercaptoethanol, 1 mM DTT, 1 mM PMSF, protease inhibitors). The resuspended cells were sonicated as described above and centrifuged at 4°C in an SA600 Rotor for 30 minutes at 15,000 rpm. The supernatant was loaded into a 50 mL syringe and filtered through a 0.45 μ m syringe top filter. 1 mL of Ni-NTA agarose bead slurry (Thermo Fisher) was washed 3X with ice-cold buffer (20 mM Hepes pH= 7.25, 150 mM KCl, 5% glycerol, 1% Triton X-100, 20 mM Imidazole pH 7.25, 5 mM β -mercaptoethanol, 1 mM DTT, 1 mM PMSF, protease inhibitors) and packed into a 10 mL disposable chromatography column (Pierce Protein Solutions, Thermo Fisher). The clarified lysate was passed through the column 3X and washed with 10 mL of wash buffer A (20 mM Hepes pH 7.25, 150 mM KCl, 5% glycerol, 0.1% Triton X-100, 20 mM Imidazole pH 7.25, 5 mM β -mercaptoethanol, 1 mM DTT, 1 mM PMSF), 10 mL of wash buffer B (20 mM Hepes pH 7.25, 150 mM KCl, 5% glycerol, 0.01% Triton X-100, 5 mM MgCl₂, 10 mM ATP, 1 mM DTT, 1 mM PMSF, adjusting pH to 7.25 with KOH, if needed), and 10 mL of wash buffer C (20 mM Hepes pH 7.25, 150 mM KCl, 5% glycerol, 0.01% Triton X-100, 1 mM DTT, 1 mM PMSF). Bound protein

was eluted in 0.5 mL aliquots of His elution buffer (20 mM Hepes pH 7.25, 150 mM KCl, 5% glycerol, 0.01% TritonX100, 1 mM DTT, 250 mM Imidazole pH 7.25, 1 mM PMSF, protease inhibitors). The protein concentration and purity were determined as stated above. We typically do not cleave the His-tag, as cleaving it from the Trio GEF1 and GEF2 domains does not impact GEF catalytic activity. Purified protein fractions were dialyzed for 4-6 hours using 2 L of dialysis buffer (20 mM Hepes pH 7.25, 150 mM KCl, 5% glycerol, 1 mM DTT, 0.01% Triton X-100, 1 mM PMSF) then overnight in 2 L of fresh dialysis buffer. The Trio GEF domains were aliquoted, flash frozen in liquid nitrogen, and stored at -80°C for later use.

1.4.4 BODIPY-FL-GDP nucleotide exchange assays

Prior to assay use, all protein aliquots were thawed on ice and centrifuged for 10 minutes at 15,000 rpm to remove any debris. Protein concentration was measured again via Bradford to verify protein concentration. 12.8 μ M Rac1, RhoA, or Cdc42 were loaded with 3.2 μ M BODIPY-FL-GDP in 1X exchange buffer (20 mM Hepes pH 7.25, 150 mM KCl, 5% glycerol, 1 mM DTT, 0.01% Triton X-100) plus 2 mM EDTA to a total volume of 25 μ L per reaction, then incubated for 1 hour at room temperature. The reaction was protected from light with aluminum foil. GTPases were loaded at a ratio of 1:4 BODIPY-FL-GDP to GTPase, respectively, to minimize background fluorescence. Loading of BODIPY-FL-GDP was halted by the addition of 5 μ L of MgCl₂ to block further GDP binding to GTPase, for a total

volume of 30 μL with a final MgCl_2 concentration of 30 mM. Prior to initiating the reaction with Trio GEF, 30 μL of GTPase (12.8 μM) plus MgCl_2 (30 mM) or blank (3.2 μM BODIPY-FL-GDP, 2 mM EDTA, 1X exchange buffer) was added to appropriate wells, followed by shaking the plate for 30 s and 10 min of room temperature incubation. During this incubation period, various Trio GEF1/GEF2 concentrations were prepared in 1X Buffer (20 mM HEPES pH 7.25, 150 mM KCl, 5% glycerol, 1 mM DTT, 0.01% Triton X-100), 4 mM GTP, and 2 mM MgCl_2 . GEF mixes were mixed well and placed on ice until use. Exchange reactions were started by adding 10 μL of respective Trio GEF concentration mixture to each well, for a total reaction volume of 40 μL . Reactions were mixed carefully to avoid bubbles. After shaking the plate again for 30 s, real-time fluorescence data was measured every 10 seconds for 30 minutes monitoring BODIPY-FL fluorescence by excitation at 488 nm and emission at 535 nm. For these measurements, we set the PMT gain to 325 V, but this variable may change depending on the sensitivity of the instrument.

1.4.5 Data Processing and Analysis

Data from the assay were processed using a custom script in Anaconda distribution of Python (see Supplemental Materials). The script is a text-based program that runs from a command line. The code takes in raw time-series plate reader data as a .xls spreadsheet. The user must convert the .xls to .xlsx prior to processing the data via the script. The user specifies which wells were used for background and which wells contained each experimental condition. Data from

wells that were not part of the experiment are discarded. Wells for which some or all observations fell below the background value are automatically flagged as possibly containing a bubble. The program then calculates the average time series for each experimental condition and subtracts the background value. The user can opt to normalize the data so that the first observation for each averaged time series has a value of 1. Raw or normalized fluorescence averages are then visualized in a time-series line plot that may be saved in a .png format. The relabeled data may be saved for further analysis as either a .csv or .xlsx file, with or without the averages and normalizations. We have run the program successfully on macOS High Sierra using the built-in Terminal and Windows 10 using Anaconda Prompt, processing data from a Molecular Devices SpectraMax M5 plate reader. Data saved as .csv can be imported to GraphPad Prism 8. Because the fluorescence of GDP-FL-BODIPY decreases exponentially over time, the fluorescence curves can be fit to a one-phase exponential decay function to determine the catalytic rate (λ) of Trio GEF activity using equations 1-3:

$$(1) \quad Y_t = Y_0 e^{-t/\tau}$$

$$(2) \quad \lambda = \frac{1}{\tau}$$

$$(3) \quad t_{1/2} = \frac{\ln(2)}{\lambda} = \tau * \ln(2)$$

where Y_t is the fluorescence intensity at time t and Y_0 is the initial intensity at time $t=0$. τ is the time constant, expressed in the same units as the X-axis. It is computed as the reciprocal of the catalytic rate, λ . The half-life, $t_{1/2}$, is the time

required for the amplitude to be one half of its initial value. A pseudo first order rate constant (observed rate constant or K_{obs}) can be calculated from the data because the reaction contains a large excess of GTP over GTPase.

GraphPad Prism 8 can be used to execute this fit. After opening GraphPad Prism 8 and creating a new XY table, the time can be entered into X and fluorescence readings into Y. The X units can be marked "Seconds" for analysis by selecting "Format Data Table" from the Change Menu. After entering data (X units) the "Analyze" button can be selected, followed by "Nonlinear Regression" from the list of XY analyses. "One phase exponential decay" can be selected to obtain the first order K_{obs} value, or λ (sec^{-1}). Because the derivative of an exponential decay equals $-\lambda \cdot Y$, the initial rate can be calculated as $-\lambda \cdot Y_0$. When testing multiple GEF concentrations, the catalytic efficiency (K_{cat}/K_M) can be extracted from a plot of catalytic rate (sec^{-1}) vs. GEF concentration that is fit with a linear function using Microsoft Excel.

1.5 Applying and Expanding the Toolkit

1.5.1 Summary

By generating a library of recombinant Trio fragments, I created a set of proteins to probe the biochemical function and regulation of Trio. While Trio has been studied extensively in the context of GEF activity and small GTPase regulation, fundamental biochemical Trio signaling questions remained unanswered: What is the role of the Trio Kinase domain? Does Trio interact with F-actin? What Trio signaling pathways are vulnerable to disease-associated dysregulation? In this section, I give a brief overview of applications of the recombinant protein Trio library I generated, questions that remain unanswered, and detail current and future applications of this toolkit.

1.5.2 Trio Ig Kinase does not have kinase activity toward promiscuous substrates *in vitro*

A fundamental question that remains unanswered is what the cellular function of the Trio kinase domain is. While only a portion of Trio splice isoforms contain this putative serine/threonine kinase domain, previous studies suggest that this domain may have functional significance. More specifically, expression of the Trio paralog Kalirin kinase (Kal Kinase) in cultured rat hippocampal neurons enhances neurite outgrowth, while a catalytic-dead Kal Kinase blocks neurite outgrowth^{84, 85}. While these findings strongly suggest that the Trio kinase domain

has a physiological purpose, the fundamental questions of what substrates are targeted and how this kinase activity would be regulated remains unanswered.

While previous members of our lab had attempted to isolate and purify the Trio kinase domain alone, solubility remained a limiting factor. In addition, mapping of catalytic kinase residues on Trio suggests that the catalytic residues are present in the Ig and Kinase domains (Fig 1.7). To generate soluble, pure protein, I purified a construct that contained both the Ig and Kinase domain with an N-terminal 6xHis Tag and C-terminal MBP (maltose binding protein) tag that could be expressed and purified from bacteria. One advantage of a dual tag kinase construct was the ability to use two steps of affinity chromatography to obtain pure protein, avoiding having to run the protein over a Sephadex size exclusion column that may contain trace kinase contamination from other purifications.

To purify Ig Kinase, I first purified Ig Kinase via amylose chromatography, cleaved the MBP tag with Tev protease, buffer exchanged Ig Kinase into His lysis buffer using a G-25 buffer exchange column, and further purified cleaved Ig Kinase via Ni-NTA chromatography.

To determine whether Trio Ig Kinase had catalytic activity, I performed an in vitro kinase assay by incubating an excess amount of Trio Ig Kinase (50 nM) with radioactive ATP and one of four promiscuous substrates (10 μ M): calmodulin, Myelin Basic Protein, Histone H1, and α -casein in a standard serine threonine kinase buffer (20 mM Hepes, 5 mM MgCl₂, 3% glycerol, 40 mM NaCl). My results suggested that Ig Kinase has no catalytic activity (data not shown). However, there are several caveats to consider moving forward: the main Trio isoform that

contains the kinase isoform is Trio Duet, which contains the GEF2 domain, SH3-2 domain, Ig domain, and kinase domain. It is possible that GEF2 is essential to promote kinase activity. Another caveat to consider is that Trio Ig Kinase was purified from bacteria cells, and that post-translational modifications may be needed to confer kinase activity. Moving forward, strides should be taken to design a construct of Trio Duet that expresses well in insect cells for in vitro use.



Fig 1.7 Mapping Catalytic Residues of Trio Kinase.

Canonical features of a kinase domain shown in left panel. The right panel shows the amino acid sequence of Trio SH3 (2) – kinase. The SH3(2) domain is highlighted in cyan blue, the Ig Domain is highlighted in yellow, and the kinase domain is highlighted in gray. Domain map of Trio SH3 (2) – kinase, with corresponding colors, is shown below for reference. Each canonical catalytic feature from the left panel is highlighted in red in the Trio amino acid sequence in the right panel.

1.5.3 Trio SR6-GEF1 does not co-sediment with F-actin

While spectrin repeat domains of other proteins have been shown to directly bind to actin, this had not yet been tested with Trio. One application of the library of recombinant purified Trio fragments I generated is to perform in vitro co-sedimentation assays to test whether any soluble Trio fragment binds directly to F-actin.

To perform the co-sedimentation assay, I incubated Trio SR6-GEF1 (2 μM) with F-actin (26 μM) for 45 min at 25 °C to allow the reaction to equilibrate, followed by spinning the reaction at 100,000g for 45 min at 4 °C, and determining whether Trio SR6-GEF1 co-sediments with F-actin by boiling supernatant and pellet samples in LSB, running the samples on an SDS-Page gel, and staining with Coomassie Blue.

My results suggest that Trio SR6-GEF1 does not bind to F-actin and remains soluble in solution post spin (Fig 1.8). Therefore, it is likely that actin alone does not interact with spectrin repeats 6-9 or GEF1 to regulate GEF1 activity and other binding partners are needed for Trio to interact with actin. Indeed, previous research from other labs suggests that other binding proteins, such as filamin, are needed for Trio GEF1 to interact with F-actin ⁵¹. However, it remains unclear whether spectrin repeats 1-5 interact directly with F-actin. Intriguingly, recombinant purified Trio fragments that include spectrin repeats 1 -5 do not remain soluble in solution.

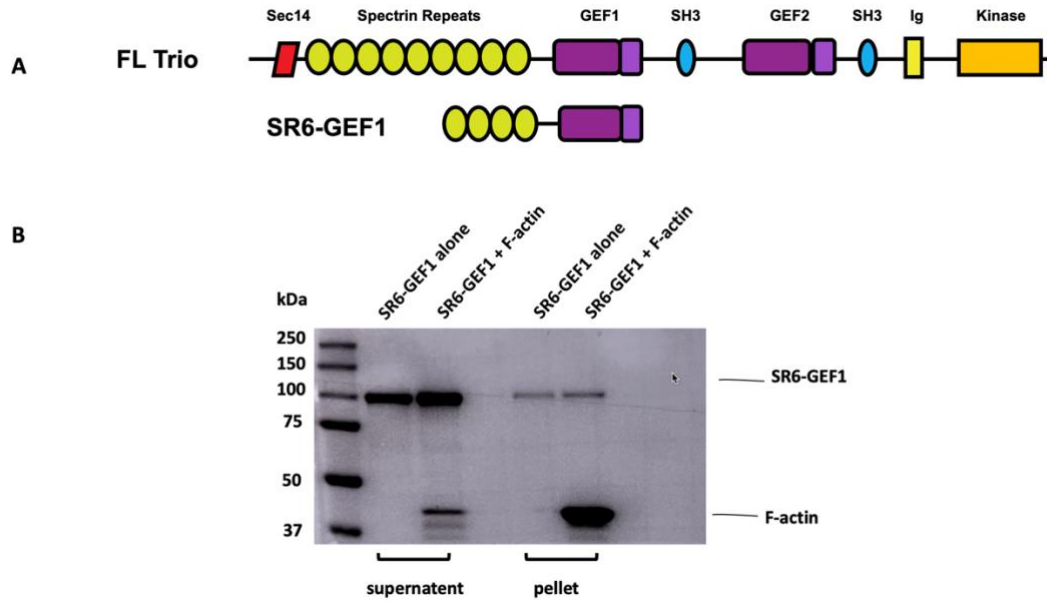


Fig 1.8 Trio SR6-GEF1 does not co-sediment with F-actin.

(A) Schema of Trio SR6-GEF1, with FL Trio shown for context. (B) Excess Trio SR6-GEF1 (2 μ M) was equilibrated with F-actin, and spun at max speed to determine whether Trio SR6-GEF1 co-sediments with F-actin. Samples were analyzed by SDS-Page gel and stained with Coomassie Blue; molecular weight marker also shown.

1.5.3 Trio may functionally interact with PDE4A5

1.5.3.1 Summary

This section contains written excerpts from my 1F31MH127891-01 grant, titled “Disruption of Trio signaling through PDE4A5 in neurodevelopmental disorders”. Our lab identified cAMP phosphodiesterase 4A isoform 5 (PDE4A5) as a new candidate Trio signaling partner due to its reduced levels in Trio-deficient mouse cortex and its ability to co-immunoprecipitate with Trio. My proposal was to test the hypothesis that Trio interacts functionally with PDE4A5 to regulate neuron development and function.

1.5.3.2 Background

Our lab used unbiased mass spectrometry-based proteomic and phosphoproteomic analyses of *NEX-TRIO*^{+/-} and *NEX-TRIO*^{-/-} mouse brains to identify proteins and signaling events altered by reducing Trio levels⁸⁶. Of 8,379 proteins quantified, levels of 193 proteins were increased, and levels of 101 proteins were decreased in the motor cortex of *NEX-TRIO*^{-/-} mice compared to WT age and sex-matched littermate mice⁸⁶. For example, cAMP phosphodiesterase 4A isoform 5 (PDE4A5) was reduced in a *TRIO* gene dose-dependent manner, exhibiting 21% and 44% reductions in *NEX-TRIO*^{+/-} and *NEX-TRIO*^{-/-} cortex, respectively. PDE4A5 coordinates compartmentalized degradation of cAMP, leading to local attenuation of cAMP-dependent signaling pathways, including protein kinase A (PKA) signaling pathways. Comparative

phosphoproteomic analysis found that phosphorylation of the activating sites in PKA, as well as multiple PKA substrates, were consistently increased in *NEX-TRIO*^{+/-} and *NEX-TRIO*^{-/-} mice. Overexpression of PDE4A5, or inhibition of PKA, normalizes dendritic spine density in *TRIO*^{+/-} cortical neurons to WT levels, demonstrating that altered PDE4A5-PKA signaling contributes to dendritic spine phenotype. However, the molecular mechanism by which Trio and the phosphodiesterase PDE4A45 interact to support normal synapse development and function remains poorly understood.

Preliminary data from Amanda Jeng in our lab indicates that PDE4A5 co-immunoprecipitates with TRIO9, the predominant Trio isoform, following co-expression in HEK293 cells (data not shown). While evidence of interaction, co-immunoprecipitation does not show that the interaction is direct or allow measurement of binding affinities.

1.5.3.3 Methods

To determine whether PDE4A5 and Trio directly interact, I purified GST-tagged PDE4A5 from bacteria cells via affinity chromatography, and further purified GST-PDE4A5 via size exclusion chromatography (Sephadex 200 (S200) Increase 10/300 GL column) into standard assay buffer (20 mM Hepes pH 7.25, 150 mM KCl, 5% glycerol, 1 mM DTT, 0.01% Triton X-100) (Fig 1.9). I linked GST-PDE4A5 to amino link beads (5 μ M) with NaCNBH₃ (20 μ L/mL) and blocked unoccupied binding sites with ethanolamine (50 mM). With GST-PDE4A5 serving as my “bait” protein, I purified three different Trio constructs to serve as my “prey”

protein, each of which I have previously shown to be completely soluble and behave properly in solution: Trio His-GEF1, Trio His-SR6-GEF1, and Trio His-SR6-SH3-1 (Fig 1.10). Trio His-GEF1 was purified from bacterial cells as described in section 4.3 of this Chapter, and Trio His-SR6-GEF1 and Trio SR6-SH3-1 were purified from insect cells as described in Chapter 2. Prior to incubation with GST-PDE4A5, Trio constructs were diluted to 5 - 10 μ M in standard assay buffer and pre-cleared with GST-bound aminolink beads (5 μ M) for 1 hr at 4 °C (7.5 μ L beads per 500 μ L reaction) to minimize non-specific interactions. Pre-cleared Trio constructs (500 μ L) were incubated with 7.5 μ L GST-PDE4A5 beads (15 μ L slurry) for 1 hr at 4°C. Beads were washed quickly 5 times with RIPA buffer (10 mM Tris-HCl pH 8.0, 1 mM EDTA, 0.5 mM EGTA, 1 % Triton X-100, 0.1% Sodium Deoxycholate, 0.1% SDS, 140 mM NaCl), resuspended in 25 μ L 1x LSB, and analyzed by SDS-PAGE and stained with Coomassie Blue.

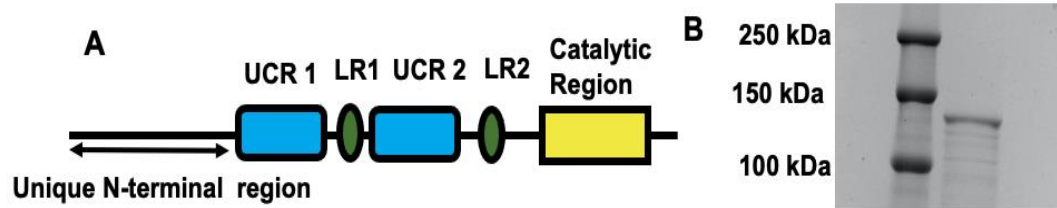


Fig 1.9 Recombinant Purified PDE4A5.

(A) Domain map of PDE4A5. The Unique N-terminal region of PDE4A5 contains three PXXPXXR motifs, which have been shown to provide interaction sites for SH3 domain binding and contribute to intracellular targeting. (B) Purified GST-PDE4A5 (~5 μ g) was analyzed by SDS-PAGE and stained with Coomassie Blue to confirm purity and concentration; molecular weight marker also shown.

1.5.3.4 Trio GEF1 directly interacts with PDE4A5

My preliminary results suggest that GST-PDE4A5 directly interacts with Trio His-GEF1 (Fig 1.11), Trio His-SR6-GEF1 (Fig 1.12), and Trio His-SR6-SH3-1 (Fig 1.13), whereas GST alone showed no interaction.

Future studies will be needed to measure the binding affinity of Trio for PDE4A5, determine the minimal binding interface sufficient to mediate interaction, and also to determine whether Trio:PDE4A5 interaction impacts the catalytic activity of either enzyme.

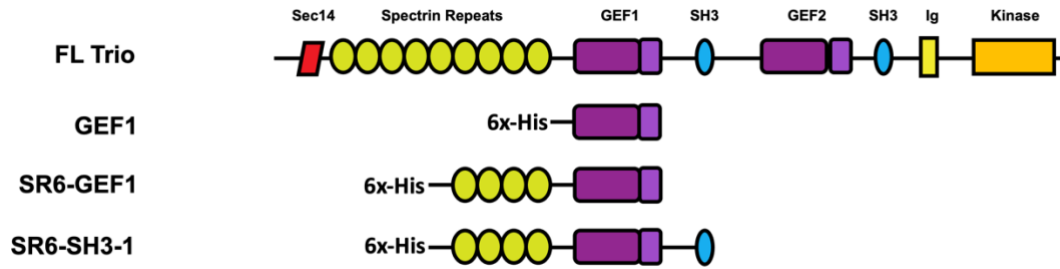


Fig 1.10 Recombinant Trio Fragments used in pulldown assays.

Schema of Recombinant Trio fragments His-GEF1, His-SR6-GEF1, and His-SR6-SH3-1. Trio His-GEF1 was purified from bacterial cells, and Trio His-SR6-GEF1 and Trio SR6-SH3-1 were purified from insect cells.

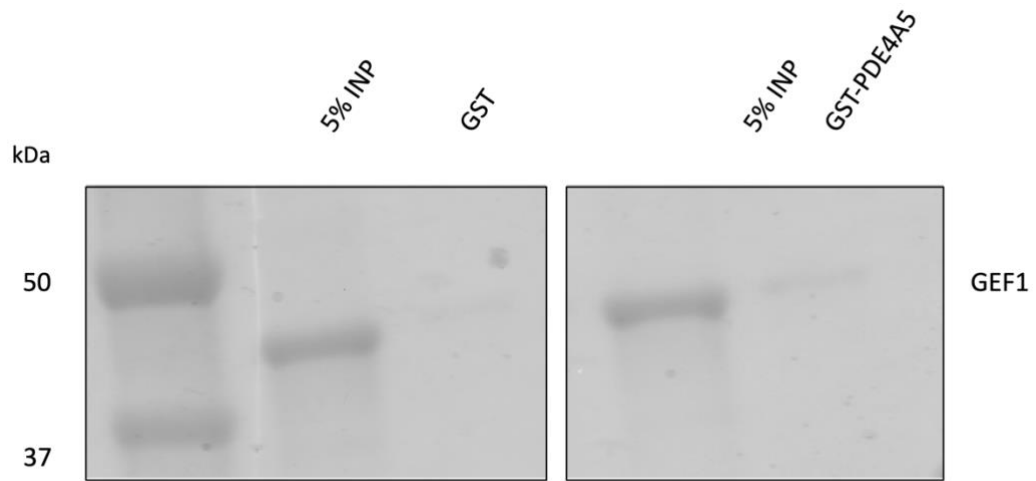


Figure 1.11 PDE4A5 interacts with Trio GEF1.

Trio GEF1 (5 μ M) was incubated with GST-PDE4A5 linked to aminolink beads (5 μ M). Bound Trio GEF1 was analyzed by SDS-Page and stained with Coomassie Blue.

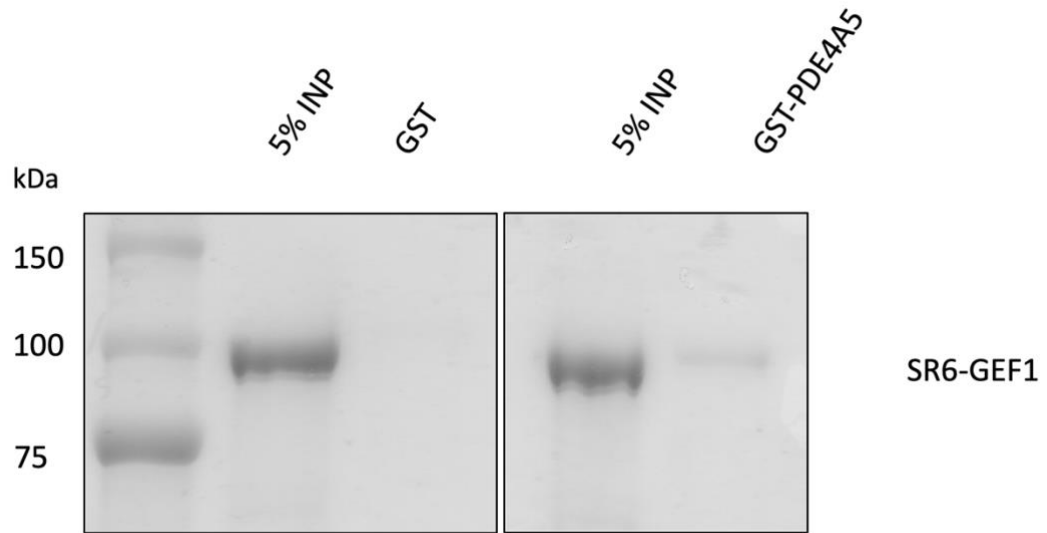


Figure 1.12 PDE4A5 interacts with Trio SR6-GEF1.

Trio SR6-GEF1 (10 μ M) was incubated with GST-PDE4A5 linked to aminolink beads (5 μ M). Bound Trio GEF1 was analyzed by SDS-Page and Stained with Coomassie Blue.

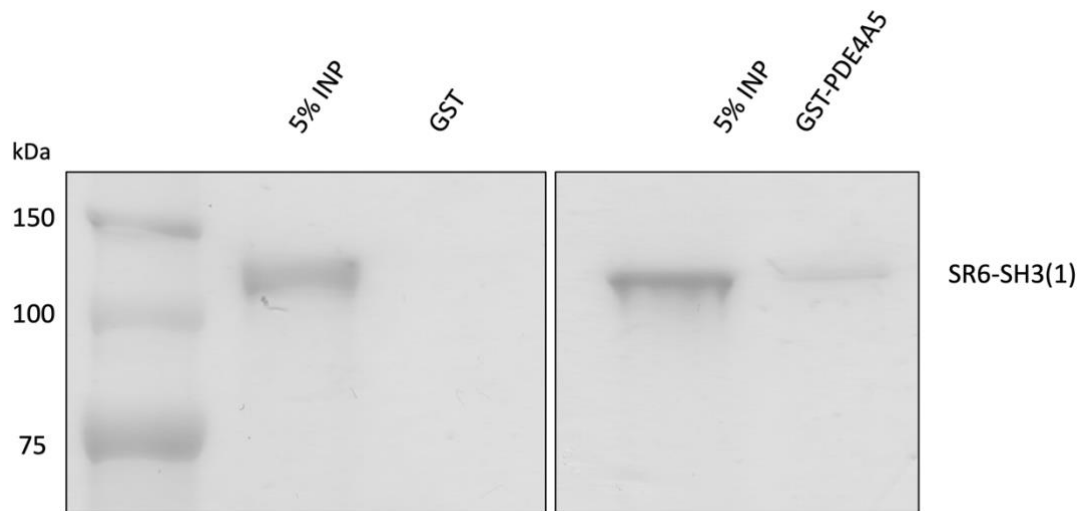


Fig 1.13 PDE4A5 interacts with Trio SR6-SH3-1.

Trio SR6-SH3-1 (5 μ M) was incubated with GST-PDE4A5 linked to aminolink beads (5 μ M). Bound Trio GEF1 was analyzed by SDS-Page and Stained with Coomassie Blue.

1.6 Discussion

From recent genomic studies, *TRIO* continues to emerge as a significant risk gene for multiple neurodevelopmental disorders including schizophrenia and autism spectrum disorders. While Trio has been primarily studied for its ability to coordinate cytoskeletal rearrangements by activating small GTPases, the regulation of GEF activity in cells and the impact of disease variants on these signaling pathways remains poorly understood. Therefore, the development of biochemical tools to probe disease impact on Trio GEF signaling is imperative for improved targeted therapeutic intervention of these disorders.

Chapter 2

Autoinhibition of Trio GEF1 is disrupted by
neurodevelopmental disorder-related genetic variants

2.1 Summary

Chapter Two presents my first author work in collaboration with my co-author, Josie Bircher. This paper was accepted by the Journal of Biological Chemistry in August 2022, and the following sections are taken directly from the manuscript.

2.2 Overview

De novo mutations and ultra-rare variants in *TRIO* are enriched in neurodevelopmental disorders (NDDs)^{7, 24, 25, 87, 88} and the pattern of these variants differs in different disorders. For example, de novo missense and rare damaging variants in the GEF1 domain and adjacent regulatory SRs are enriched in autism, intellectual disability, and developmental delay, suggesting that dysregulated GEF1 activity contributes to the pathophysiology of these disorders. Indeed, our lab and others have shown that some of these variants disrupt the ability of GEF1 to catalyze Rac1 activation^{7, 24, 25, 32}. Clusters of variants in the SR8 and GEF1 domains impacted cellular Rac1 activity in different ways and were associated with distinct endophenotypes in heterozygous carriers: SR8 domain variants were linked to developmental delay, macrocephaly, and hyperactive Rac1 activity in cells, whereas GEF1 domain variants were linked to mild intellectual disability, microcephaly, and reduced Rac1 activity in cells³². However, the role of the SRs in Trio function and the mechanism of SR8 variant-mediated increase in Rac1 activity are unclear.

Previous studies demonstrated that expression of Trio GEF1 increased Rac1 activity in cells and resulted in dominant gain-of-function pathfinding defects in fly retinal axons ^{56, 66}. Appending additional regions of Trio, including the SRs, to GEF1 attenuated both Trio GEF1-dependent processes. These observations strongly suggest that the SRs reduce GEF1 activity in Trio. However, it remains unknown whether the SRs autoinhibit GEF1 activity directly or via the recruitment of cellular cofactor(s). It is also unclear how variants in the SRs would impact this regulatory mechanism in vitro and in cells.

We provide evidence here that SRs 6-9 directly inhibit Trio GEF1 activity in vitro and in cells. Using a GDP-FL-BODIPY nucleotide exchange assay ⁸⁹, we show that inclusion of SRs 6-9 is sufficient to inhibit GEF1 activity in vitro, suggesting an autoinhibitory mechanism. We then find that NDD-associated variants in the SR8 and GEF1 domains increase GEF1 activity by relieving autoinhibition, whereas an NDD-associated variant in SR6 reinforces autoinhibition. Using chemical cross-linking and BioLayer Interferometry, we demonstrate that the SRs make contact with the pleckstrin homology (PH) region of the GEF1 domain and reduce the affinity of GEF1 for Rac1. Together, our findings provide a novel RhoGEF regulatory mechanism by which SRs disrupt Trio GEF1 activation by reducing the interaction of Trio GEF1 with Rac1 and impairing catalytic efficiency. This mechanism appears to be commonly disrupted by NDD-associated variants in *TRIO*, making it a potential target for therapeutic intervention.

2.3 Results

2.3.1 Inclusion of SRs 6-9 reduces Trio GEF1 activity

Genetic variants in SRs 6-9 are associated with NDDs ³², some of which were previously shown to affect Trio-mediated Rac1 activation in cells. To measure the impact of the SRs on GEF1 activity in vitro, we generated and purified Trio GEF1 alone (42 kDa) and a Trio fragment containing SRs 6-9 appended to the GEF1 domain (SR6-GEF1, 99 kDa) (Fig. 2.1A). Both proteins were mono-disperse upon size exclusion chromatography and eluted at a position consistent with being monomers (estimated Stokes radius was 3.8 nm for GEF1, 5.6 nm for SR6-GEF1) (Fig. 2.1B). Using a fluorescence-based guanine nucleotide exchange assay, we measured the catalytic activity of GEF1 and SR6-GEF1. Purified 100 nM GEF1 efficiently catalyzed exchange of BODIPY-FL-GDP for GTP on Rac1, with a first-order dissociation rate constant $k_{\text{obs}} = 2.4 \pm 0.6 \times 10^{-3} \text{ s}^{-1}$ (Fig. 2.1, C and D). Measurement of the rate constant, k_{obs} , as a function of GEF1 concentration yielded a $k_{\text{cat}}/K_{\text{M}} = 1.9 \times 10^4 \text{ M}^{-1} \text{ s}^{-1}$ (Fig. 2.1, E and F). SR6-GEF1 similarly promoted GTP exchange onto Rac1, but with a significantly reduced (~20 fold and 6-fold, respectively) $k_{\text{obs}} = 1.2 \pm 1.8 \times 10^{-4} \text{ s}^{-1}$, and $k_{\text{cat}}/K_{\text{M}} = 3.1 \times 10^3 \text{ M}^{-1} \text{ s}^{-1}$ (Fig. 2.1, C-D and F). These data indicate that inclusion of SRs 6-9 inhibits Trio GEF1 activity for Rac1 in vitro.

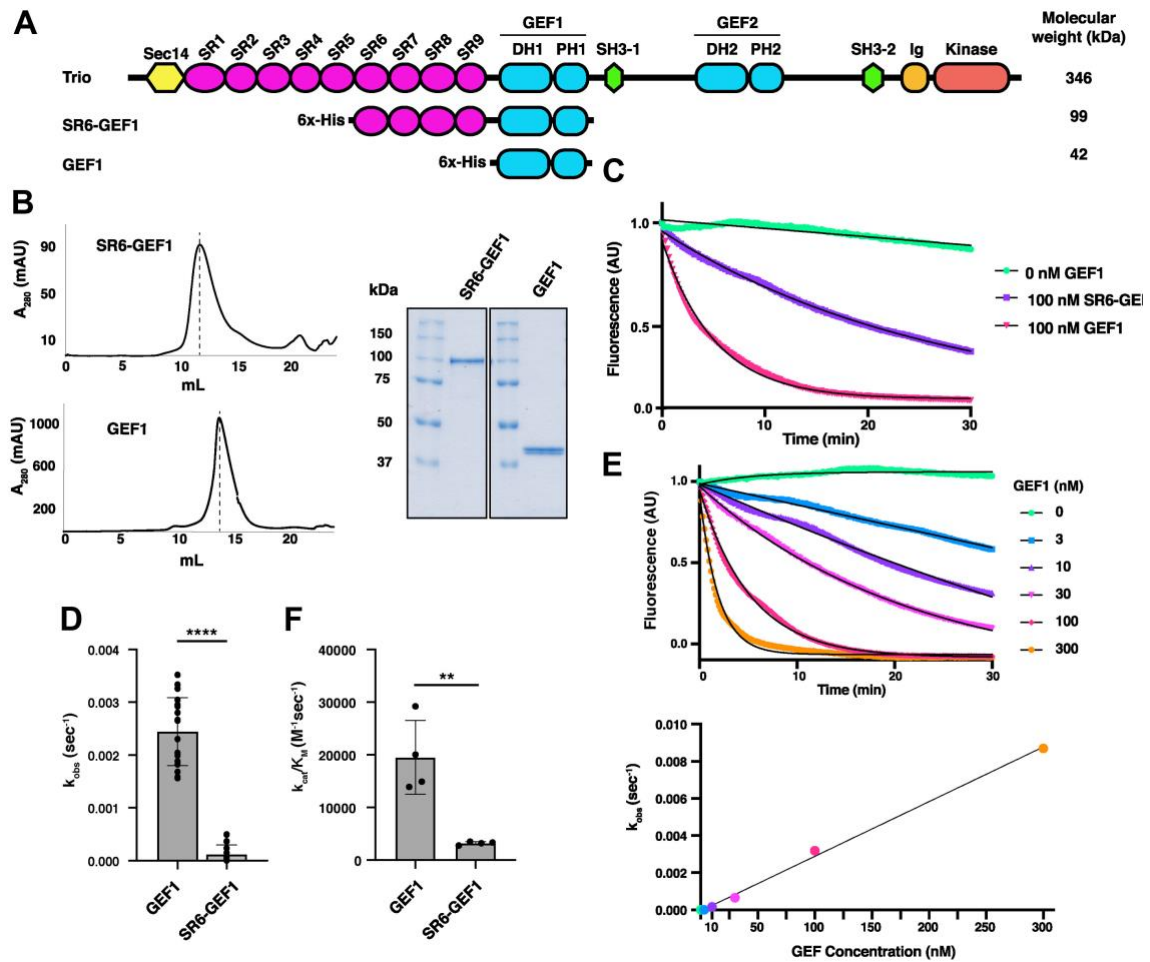


Fig. 2.1 Inclusion of SRs 6-9 reduces Trio GEF1 activity on Rac1. Figure adapted from Bircher, Corcoran et al., 2022

(A) Schematic of Trio proteins: Full-length Trio, SR6-GEF1, and GEF1. SR-spectrin repeat; DH1-Dbl homology domain; PH1-pleckstrin homology domain; SH3-1 – Src homology 3 domain. Ig Ig-like domains. (B) Trio SR6-GEF1 and GEF1 were purified and size exclusion chromatography was performed to verify that proteins were mono-disperse. Dotted lines indicate peak elution volume used to calculate Stokes radii. Samples (approximately 5 μ g) of purified

components were analyzed by SDS-PAGE and stained with Coomassie Blue to assess purity. Gel images were spliced from separate lanes of the same gel, original gel shown in Fig. 2.3B. (C) 100 nM of Trio GEF proteins were incubated with 12.8 μ M Rac1 preloaded with 3.2 μ M BODIPY-FL-GDP, and nucleotide exchange was tracked via the decrease in fluorescence over time. Representative trace shown here; traces in color, exponential fits overlaid in black. (D) Trio SR6-GEF1 had approximately 20-fold lower exchange activity, k_{obs} , compared to GEF1 alone. N=21 independent k_{obs} measurements for overall quantification of rates per group. Bars represent average \pm standard deviation; **** = $p \leq 0.0001$ in a two-tailed t-test. (E) GEF1 catalytic efficiency was determined by measuring the k_{obs} of GEF1 at multiple concentrations (top) and extracting a linear fit from the plot of k_{obs} vs GEF concentration. Sample traces shown with exponential fits overlaid in black. (F) The catalytic efficiency of SR6-GEF1 was 6-fold lower than GEF1 (n=4). Bars represent average \pm standard deviation of four experimental replicates; ** = $p \leq 0.005$ in a two-tailed t-test.

2.3.2 NDD-associated variants in SR8 increase Trio GEF1 activity in the context of SR6-GEF1

We generated and purified SR6-GEF1 expression constructs containing single NDD-associated variants in SR8 and measured their ability to catalyze nucleotide exchange on Rac1 (Fig. 2.2, A and B). When tested at 100 nM, all SR8 variants, except N1080I, increased the k_{obs} by 4-8 fold over that of WT SR6-GEF1 (Fig. 2.2, C and D). In agreement with these findings, one representative SR8 variant, SR6-GEF1_{R1078Q}, which had a significantly increased $k_{\text{obs}} = 1.0 \pm 0.5 \times 10^{-3} \text{ s}^{-1}$, had a $k_{\text{cat}}/K_{\text{M}} = 4.7 \times 10^3 \text{ M}^{-1} \text{ s}^{-1}$, a 1.5-fold increase in catalytic efficiency over WT SR6-GEF1 (Fig. 2.2E). These findings indicate that NDD-associated variants in SR8 are sufficient to relieve SR autoinhibition.

2.3.3 NDD-associated variants in SR6 decrease GEF1 activity in the context of SR6-GEF1

We also generated two SR6-GEF1 constructs harboring individual disease variants in the SR6 domain. While the rate constant (k_{obs}) values obtained for each construct did not significantly decrease compared to WT SR6-GEF1, measurement of catalytic efficiency, $k_{\text{cat}}/K_{\text{M}}$, of both wild-type SR6-GEF1 and SR6-GEF1_{E883D} revealed that SR6-GEF1_{E883D} had a significantly *decreased* catalytic efficiency of a $k_{\text{cat}}/K_{\text{M}} = 1.7 \times 10^3 \text{ M}^{-1} \text{ s}^{-1}$, 1.8-fold lower than WT SR6-GEF1 (Fig. 2.2E). This suggests that NDD-associated variants in SR6 *decrease* GEF1 activity.

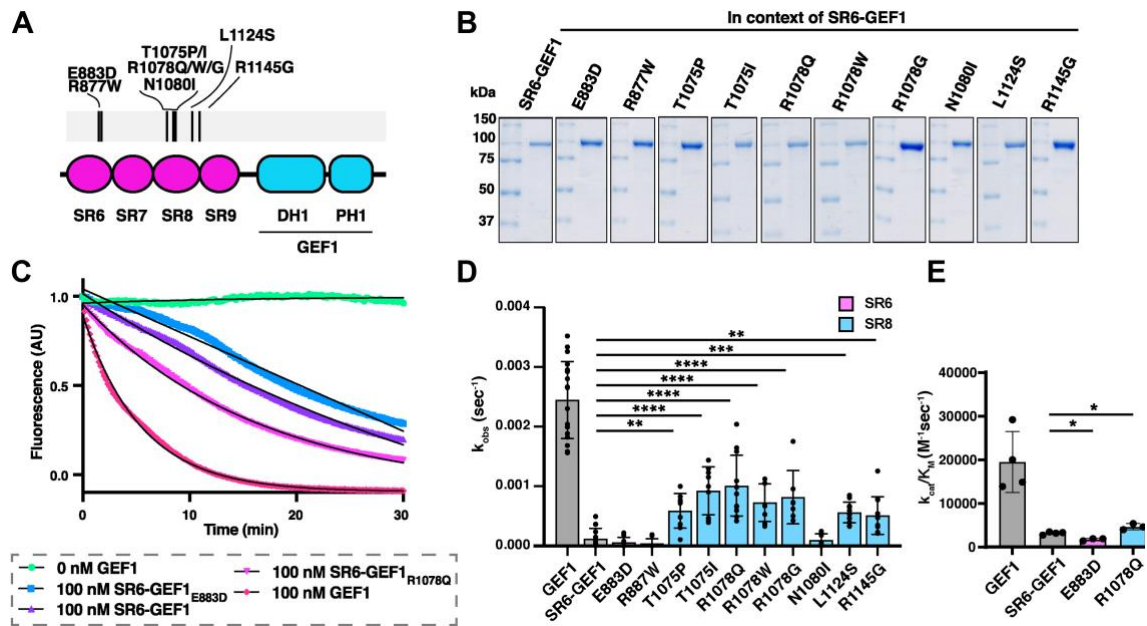


Fig. 2.2 Mutations in SR6 and SR8 differentially impact GEF1 activity.
Figure adapted from Bircher, Corcoran et al., 2022

(A) Schematic of disease associated mutations in the SRs used in this study. (B) Mutants were generated in the context of SR6-GEF1 and purified. (C) Sample GEF assay traces of SR6-GEF1_{E883D} and SR6-GEF1_{R1078Q}. Traces in color, exponential fits overlaid in black. (D) SR8 variants in SR6-GEF1 have significantly enhanced catalytic rates, k_{obs} , at equal molar amounts (100 nM) (except N1080I). ** = $p \leq 0.005$; *** = $p \leq 0.001$; **** = $p \leq 0.001$ for a significant difference compared to SR6-GEF1 in a one-way ANOVA adjusted for multiple comparisons ($n \geq 9$). (E) Catalytic efficiency (k_{cat}/K_M) of representative SR6/8 mutants was determined by measuring the k_{obs} values at different concentrations of GEF, as shown in Fig. 2.1D. The catalytic efficiency of SR6-GEF1_{R1078Q} is ~1.5-fold greater than that of SR6-GEF1, while that in SR6-GEF1_{E883D} is ~1.8-

fold slower (n=3). Data for GEF1 and SR6-GEF1 from Fig. 2.1 are shown again for reference, and all are reported as an average \pm standard deviation of three or more experimental replicates. * = significantly different from SR6-GEF1, $p \leq 0.05$ in a one-way ANOVA adjusted for multiple comparisons.

2.3.4 GEF1 variant D1368V increases GEF activity only in the context of SR6-GEF1

Hypothesizing that the SRs might contact GEF1 to impact catalytic activity, we searched for GEF1 domain variants that might impact potential autoinhibition of GEF1 activity by SRs. Unlike GEF1 disease variants that lie in the GEF1:Rac1 interface and *decrease* GEF1 activity^{7, 24, 25}, D1368V lies in the DH domain but is distal to the GEF1:Rac1 interface, so its impact is less well understood (Fig. 2.3A). However, introduction of the D1368V variant greatly potentiates the ability of the Trio9 splice isoform, which contains all the SRs, to increase activity of a Rac1 reporter in cells²⁵. We introduced D1368V into SR6-GEF1, and found that it significantly increased catalytic activity, with a $k_{\text{obs}} = 1.4 \pm 0.3 \times 10^{-3} \text{ s}^{-1}$ and $k_{\text{cat}}/K_{\text{M}} = 4.8 \times 10^3 \text{ M}^{-1} \text{ s}^{-1}$ (Fig. 2.3, *B-E*), a 1.5-fold increase over the $k_{\text{cat}}/K_{\text{M}}$ for WT SR6-GEF1. In contrast, introducing D1368V into GEF1 alone did not impact its activity compared to GEF1 (Fig. 2.3, *B-E*), indicating that the activating effects of D1368V require SRs 6-9. Together with data reported above, these are consistent with a model in which NDD-associated variants in SR8 and GEF1 relieve inhibition of GEF1 activity by the SRs.

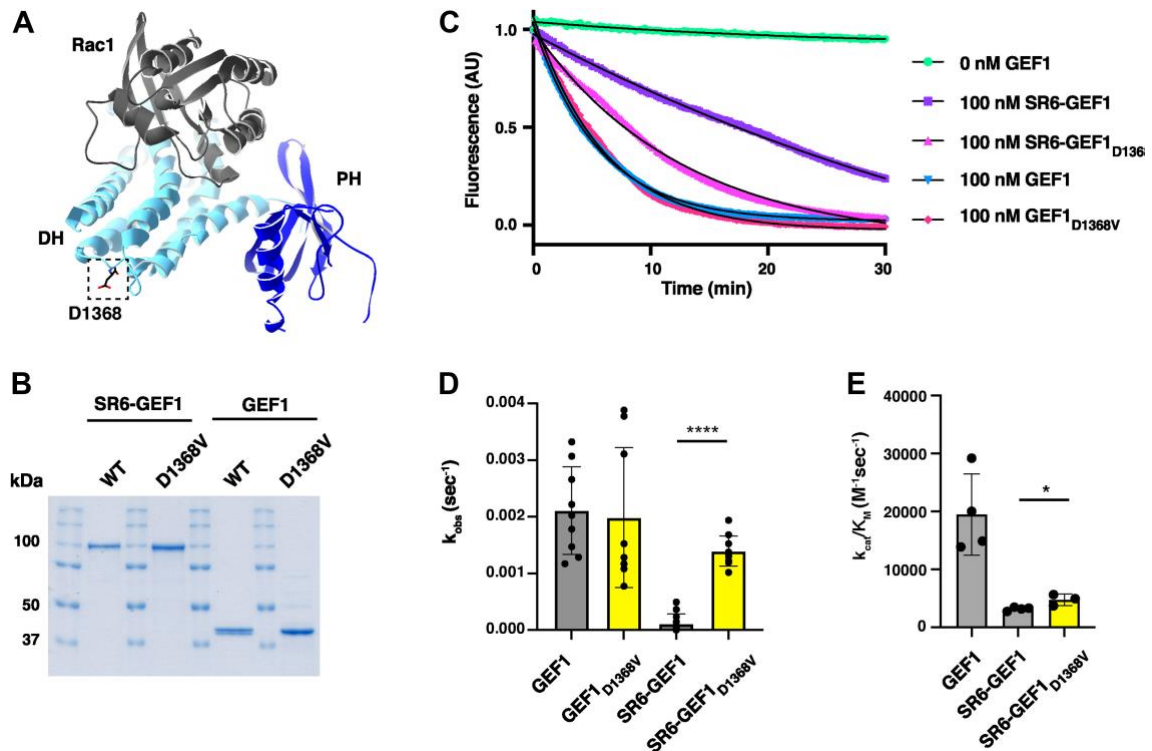


Fig. 2.3 GEF1 variant D1368V increases GEF1 activity in the context of SR6-GEF1. Figure adapted from Bircher, Corcoran et al., 2022

(A) Crystal structure of Trio GEF1 (light and dark blue) and Rac1 (gray), accessed in PDB, ID = 2NZ8⁹⁰. D1368, identified in the box, is distal to the Rac1 binding interface. (B) Samples (approximately 5 μ g) of purified components were analyzed by SDS-PAGE and stained with Coomassie Blue R250 to assess purity. Gel bands for WT SR6-GEF1 and WT GEF1 are the same as shown spliced in Fig. 2.1B. (C) Sample GEF assay traces of D1368V in the context of SR6-GEF1 and GEF1. Traces in color, exponential fits overlaid in black. (D) D1368V in SR6-GEF1 increases catalytic rate, k_{obs} , at equal molar amounts of GEF, but has no impact when inserted into GEF1 alone (**** = $p \leq 0.0001$,

unpaired t-test for mutant vs WT in respective GEF1 or SR6-GEF1, n=3). (E) Catalytic efficiency (k_{cat}/K_M) of SR6-GEF1_{D1368V} was determined by measuring the k_{obs} values at different concentrations of GEF, as in Fig. 2.1D. Data for GEF1 and SR6-GEF1 shown again for reference. The catalytic efficiency, k_{cat}/K_M , of SR6-GEF1_{D1368V} is ~1.5-fold greater than that of SR6-GEF1 (n=3). * = significantly different from SR6-GEF1, $p \leq 0.05$ in a one-way ANOVA adjusted for multiple comparisons.

2.3.5 The SRs and GEF1 form distinct stable interacting domains

We used AlphaFold ^{91, 92} to model human Trio SR6-GEF1 (Fig. 2.4, *A* and *B*). Strikingly, this model suggests that SRs interact with the GEF1 domain, with SR8 closely apposed to GEF1 and the NDD-associated mutations concentrated at this SR8:GEF1 interface. This model of SR6-GEF1 and additional analysis using DISOPRED predicted the existence of an unstructured loop between SR9 and GEF1, suggesting this flexible region may connect the SRs and GEF1 domain (Fig. 2.4C) ⁹³. We used limited proteolysis to probe for the presence of a flexible linker between SR9 and the GEF1 domain that might be susceptible to partial proteolysis. Treatment of SR6-GEF1 at intermediate levels of trypsin yielded two major bands, identified by mass spectrometry as composed of SRs 6-9 and GEF1, respectively. This observation indicates that SRs 6-9 and the GEF1 domain each make up distinct folding units with increased relative resistance to protease (Fig. 2.4D). Together, these findings support a model in which the SRs make contact with GEF1.

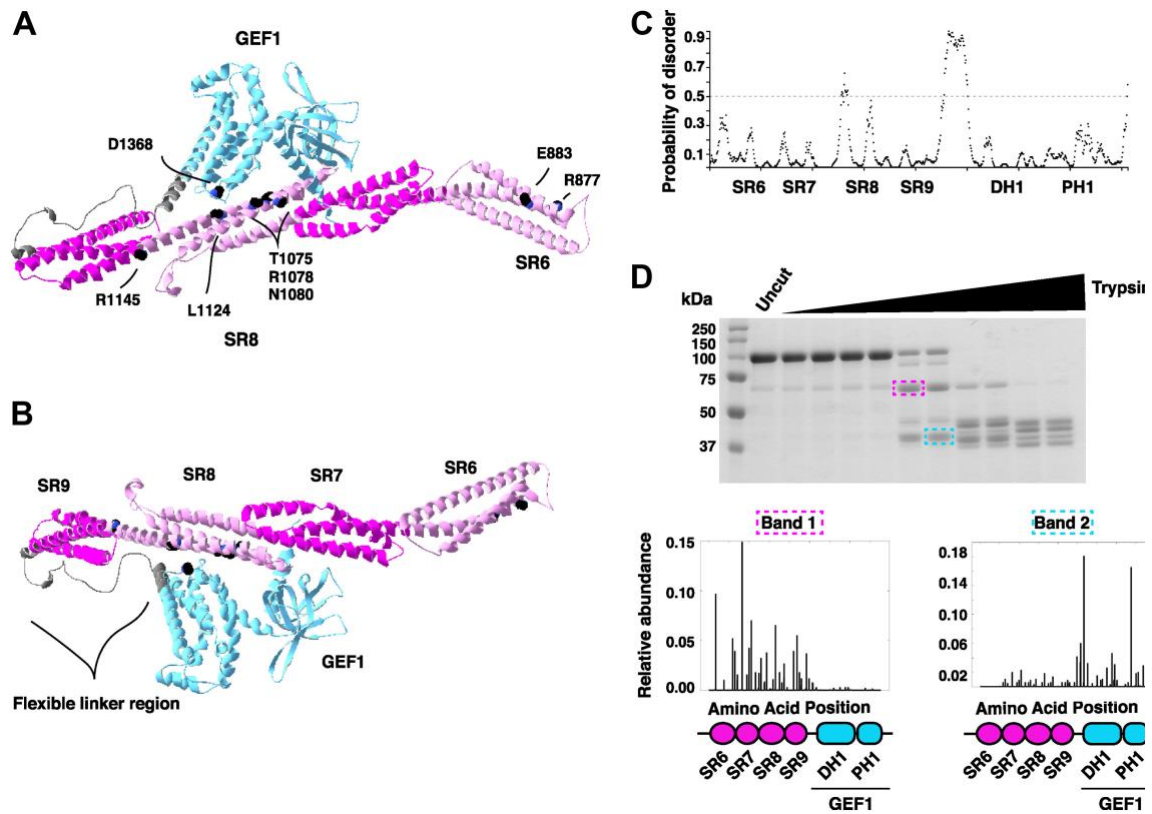


Fig. 2.4 AlphaFold predicts an interaction between the SRs and GEF1, which form independent folding units. Figure adapted from Bircher, Corcoran et al., 2022

(A) AlphaFold model of human Trio SR6-GEF1. SR6, 8 in light pink, SR 7,9 in dark pink, linker region in gray, GEF1 in blue. Sites of mutations used in this study are modeled as black spheres, with amino acids labeled. This model predicts an interaction between SR8 and GEF1. (B) SR6-GEF1 from AlphaFold model, rotated to view flexible linker region between GEF1 and SR9. (C) Probability of disorder was predicted using DISOPRED. The region between SR9 and DH1 has a high probability of being disordered (cutoff >0.5). (D) Limited proteolysis of SR6-GEF1. His-SR6-GEF1 was incubated with increasing

concentrations of trypsin and select bands were identified using mass spectrometry. Relative abundance of identified peptides was plotted to determine composition of each band. The y-axis displays relative abundance of peptides and x-axis is 'amino acid position', which refers to the location in SR6-GEF1 that the peptide covers (with SR6-GEF1 diagram below). Band 1 (pink box around gel band at ~60kDa) comprises SR6-9 and Band 2 (blue box around band at ~40kDa) comprises GEF1. Therefore, SR6-9 and GEF1 form distinct stable domains.

To test directly for possible interactions between the SRs and GEF1 domain, we incubated SR6-GEF1 with an 11.4 Å spacer lysine crosslinker, BS3 (bis(sulfosuccinimidyl)suberate), and analyzed crosslinked peptides via mass spectrometry to identify sites in close enough proximity to crosslink. Several long-distance crosslinks were observed between the SRs and the GEF1 domain (Fig. 5A). Specifically, the SR:GEF1 interface includes a peptide in DH domain which is directly at the Rac1 binding interface (1429-1438, green in Fig. 2.5A) and a peptide in the PH domain important for stabilizing the Rac1 interaction (1529-1537, orange in Fig. 2.5A) (Fig. 2.5A)⁹⁰. Multiple regions originating in SR6-9 contact these peptides in the GEF domain. This suggests that SR6-GEF1 may be dynamic, with multiple conformational states captured by crosslinking. We hypothesize that these SR:GEF1 contacts likely disrupt Rac1 binding to GEF1.

We also performed chemical crosslinking on three variants in SR6-GEF1 to understand how intramolecular contacts may change in the variants. The SR6-GEF1 variants that display activated GEF activity, R1078Q and D1368V, both exhibited a loss of contact between SR6, 7, 9, and the GEF1 domain (Fig. 2.5B). In addition, R1078Q, but not D1368V, also reduced SR8:GEF1 contacts (Supplementary Table 2). In contrast, the SR6 variant, E883D, which reduced GEF activity, did not reduce intramolecular contacts with GEF1; in fact, new contacts appeared (SR7 and SR9 contacts, blue and purple arrowheads, Fig. 2.5B), suggesting this variant may reinforce intramolecular SR:GEF contacts (Fig. 2.5B).

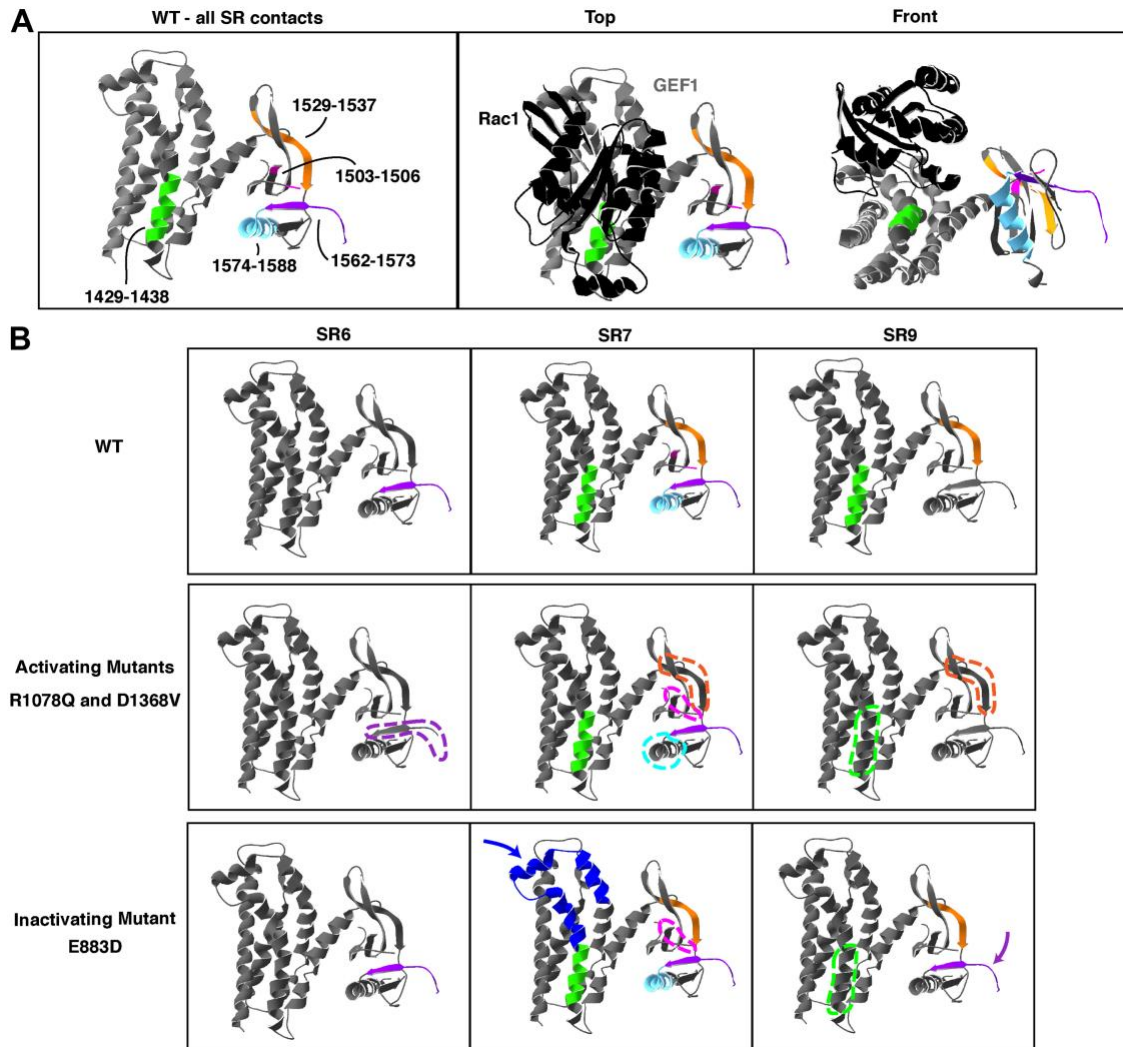


Fig. 2.5 The SRs interact with GEF1. Figure adapted from Bircher, Corcoran et al., 2022

(A) SR6-GEF1 was incubated with lysine crosslinker BS3 and crosslinked peptides were identified using mass spectrometry. Crystal structure of GEF1 alone (gray, left panel) and with Rac1 (black, right panel) (from PDB, ID = 2NZ8⁹⁰) with crosslinked peptides between SR6-9 and GEF1 (in WT case) shown in green (1429-1438), pink (1503-1506), orange (1529-1537), purple (1562-1588), and light blue (1574-1588). SR6-9 contacts the DH domain at a peptide that

likely interferes with Rac1 binding (1429-1438) and a region in the PH domain critical for stabilizing the Rac1 interaction (1529-1537)⁹⁰. (B) Representative activating mutants (R1078Q and D1368V) display fewer contacts between SR6-9 and GEF1 (lost contacts shown with dotted lines). Representative inactivating mutant (E883D) displays increased contacts between SR6-9 and GEF1 (New contacts shown with blue or purple arrows). Crosslinks were categorized based on their N-terminal crosslink site (in SR6, 7, or 9) and their C-terminal GEF1 contacts were visualized. For the activating mutants, the peptides that were *mutually* lost for both activating mutants were visualized here. For table of all mutant crosslinks between SR6-9 and GEF1, see Supplementary Table 2.

These data are consistent with a model in which specific intramolecular contacts between the SRs and GEF1 are altered in genetic variants with increased GEF1 activity.

2.3.6 The SRs reduce GEF1 binding to Rac1

Based on our crosslinking data, we hypothesized that an interaction between SRs 6-9 and PH1 may impair the ability of GEF1 to bind Rac1. We used BioLayer Interferometry to measure the association of nucleotide-free Rac1 with His-GEF1 or His-SR6-GEF1 immobilized on a Ni-NTA affinity chip. GEF1 bound to Rac1 with a $K_d = 151 \pm 49$ nM in nucleotide-free conditions (Fig. 2.6, A-C). SR6-GEF1 had a reduced affinity for Rac1, with a $K_d = 316 \pm 87$ nM (Fig. 2.6, A-C).

Taken together with the crosslinking data, this supports a model where the SRs contact the PH domain to impair GEF1 binding to Rac1, which likely contributes to the reduction in observed GEF1 activity.

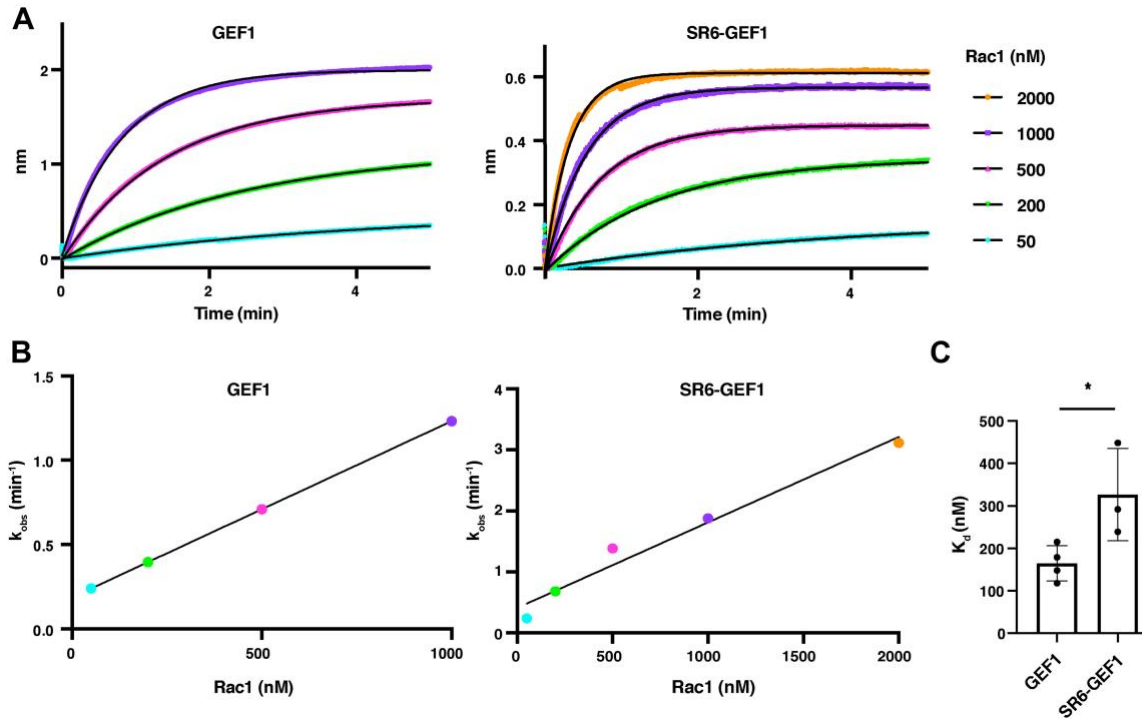


Fig. 2.6 Inclusion of SRs 6-9 reduce binding to Rac1. Figure adapted from Bircher, Corcoran et al., 2022

(A) His-GEF1 or His-SR6-GEF1 were immobilized on an Ni-NTA biosensor and the association of different concentrations of Rac1 was measured. Representative traces shown, with data in color and one phase exponential fits in black. Full concentration gradients (4-5 Rac1 concentrations) were performed at least three independent times. (B) k_{obs} values were extracted from each association curve and plotted against Rac1 concentration to calculate a K_d of GEF1 or SR6-GEF1 binding to Rac1. (C) SR6-GEF1 has a 2-fold weaker affinity for Rac1 than GEF1 (* = $p \leq 0.05$, unpaired t-test).

2.3.7 SRs 6-9 inhibit GEF1-induced cell spreading

Trio GEF1 activates Rac1 and RhoG to coordinate downstream cytoskeletal changes and mediate changes in cell morphology^{35, 39, 41, 54}. We first expressed Trio GEF1-GFP in HEK293 cells and quantified its impact on cell morphology (Fig. 2.7, A-C). When matched for GFP expression levels, GEF1 expressing cells had significantly increased cell area compared to GFP controls (Fig. 2.7 A-C). Cells expressing GEF1 appeared to be more spread with round lamellipodia encompassing the cell edge, a common result of Rac1 activation⁹⁴ (Fig. 2.7B). The area of cells expressing a catalytic-dead mutant of GEF1, GEF1 ND/AA (N1465A/D1466A), were similar to GFP controls, indicating a key role for GEF1 catalytic activity in this morphological change⁹⁵. In contrast to GEF1, SR6-GEF1 expressing cells had no measurable effect on cell area, but the SR8 mutant, SR6-GEF1_{R1078Q}, increased cell area over that of GFP and SR6-GEF1 WT (Fig. 2.7, B and C). Cells expressing SR6-GEF1_{R1078Q} also appeared qualitatively similar in morphology to those cells expressing GEF1 alone, with more full, rounded edges (Fig. 2.7B). Therefore, inclusion of SRs 6-9 inhibits Trio GEF1-dependent changes in cell morphology, and disease-associated variants can disrupt this inhibitory regulation.

We then expressed GFP-Trio9s, a predominant neuronal isoform throughout neurodevelopment, in HEK293 cells and quantified its impact on cell morphology⁹⁶ (Fig. 2.7, A and D-E). Interestingly, when matched for GFP expression levels, GFP-Trio9s expressing cells had significantly decreased cell area compared to GFP controls. Expressing two variants of Trio9s, the most

activated SR8 mutant, GFP-Trio9_{SR1078Q}, and a catalytic-dead mutant of GEF1, GFP-Trio9s ND/AA (N1465A/D1466A), decreased cell area compared to GFP alone (Fig. 2.7, *D* and *E*). Cells expressing any variant of GFP-Trio9s appeared very round, completely lacking lamellipodia or cell edge protrusions (Fig. 2.7, *D* and *E*). We speculate that activity of the Trio GEF2 domain, which targets RhoA to promote cytoskeleton contractility ⁹⁷, may dominate in this context, making it difficult to discern specific effects on GEF1 activity.

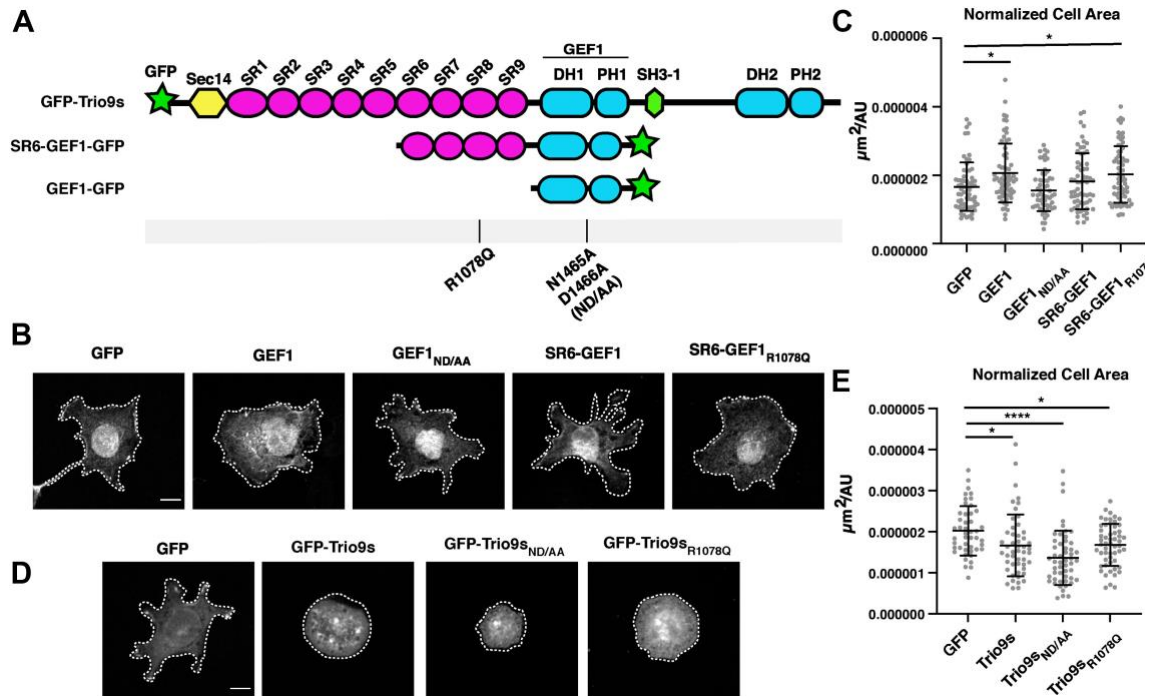


Fig. 2.7 SRs 6-9 reduce the impact of GEF1 on cell spreading. Figure adapted from Bircher, Corcoran et al., 2022

(A) Schematic of constructs used, with mutants shown below. (B) Constructs in A were transfected into HEK293 cells and plated on fibronectin. Cells were fixed and stained using anti-GFP to visualize GFP expression and cell morphology. Cells expressing GEF1 and SR6-GEF1_{R1078Q} appeared to have more rounded edges and circular shapes. Scale bar = 10 μm . Contrast was adjusted between images shown to best visualize cell edge; cell edge is outlined with a white dashed line. (C) Cell area, normalized to protein expression on a cell-by-cell basis, was quantified. Cell area increased upon expression of GEF1 and SR6-GEF1_{R1078Q}, while expression of a catalytic-dead GEF1 mutant (ND/AA) or SR6-GEF1 had no effect compared to GFP alone. (D) Cells visualized and analyzed

as in (B). Cells expressing Trio9s constructs all appeared rounder and lacked cell edge protrusions. (E) Cell area quantified as in (C). Cell area was decreased upon expression of all GFP-Trio9s constructs compared to GFP alone. Trio9^{SR1078Q} did not increase cell area to levels seen with GFP alone. Two biological replicates were performed for each set of constructs, with 25-40 cells analyzed per group per replicate (*= $p \leq 0.05$, ** = $p \leq 0.01$, *** = $p \leq 0.001$, one-way ANOVA between GFP control and each group and adjusted for multiple comparisons).

2.4 Discussion

We provide evidence here that the Trio SRs 6-9 directly inhibit GEF1 activity via intramolecular interactions *in vitro* and in cells. We demonstrate that NDD-associated variants in the SR8 and GEF1 domains release this autoinhibitory constraint, strongly suggesting that disruption of this GEF1 regulatory mechanism contributes to the pathophysiology of these disorders. Using chemical cross-linking and BioLayer Interferometry, we show that the SRs contact regions of GEF1 important for Rac1 binding, and that inclusion of the SRs is associated with reduced binding affinity for Rac1 *in vitro*. We present a model for how Trio GEF1 activity is regulated, and how this regulation is disrupted by disorder-associated variants.

2.4.1 Inclusion of Trio SRs autoinhibits GEF1 activity *in vitro*

Previous cell-based studies have shown that removing the SRs is associated with increased downstream Rac1 activity and Trio gain-of-function phenotypes *in vivo*, suggesting that the Trio SRs function to inhibit GEF1 activity^{56, 66, 98}. This hypothesis is supported by evidence that other RhoGEFs, like Tiam1, contain autoinhibitory N-terminally adjacent accessory domains^{46, 65, 99}. In most cases, how inhibition occurs and how it is released to activate GEF activity is unknown. Our results show that SR6-GEF1 is monomeric in solution and that inclusion of SRs significantly decreases GEF1 catalytic activity *in vitro*. Collectively, these observations suggest that the SRs are sufficient to inhibit GEF1 activity via intramolecular interactions *in cis*.

2.4.2 SRs make direct contact with GEF1 and impair interactions with Rac1

Within GEF1, the DH1 domain catalyzes GTP exchange onto Rac1 and serves as the main Rac1 binding interface. The PH domain plays a regulatory role in catalysis, but also serves to stabilize the Rac1:DH1 interaction^{36, 100}. Using chemical crosslinking, we demonstrate that SRs 6-9 make extensive contacts with the GEF1 domain, including at sites critical for Rac1 binding, suggesting that SR6-9 *sterically* blocks contact with Rac1. In addition, NDD-associated variants that activate GEF1 exhibit reduced contacts between the SRs and GEF1 and those that impair GEF1 activity exhibit increased contacts. Hence, altering the interaction between the SRs and GEF1 impacts catalytic activity⁹⁰.

We found that inclusion of SRs 6-9 reduces the affinity of GEF1 for Rac1 by 2-fold, compared to GEF1 alone. Whereas our catalytic rate measurements suggest the presence of SRs 6-9 results in a 6-fold decrease in activity, the reduction in affinity that we observed was smaller in magnitude. It is likely that engagement of the SRs with GEF1 impairs other steps in the catalytic cycle, as demonstrated by our catalytic efficiency data, in addition to impacting Rac1 binding affinity. Future studies will elucidate whether other components of the nucleotide exchange process are impacted by the SRs.

2.4.3 NDD associated mutations in SR8 and GEF1 disrupt SR-mediated GEF1 inhibition

Two rare variant clusters in *TRIO*, one in SR8 (Fig. 2A) and one in GEF1, have been linked to distinct endophenotypes in individuals with NDDs³². For example, *TRIO* SR8 variants are linked to developmental delay and macrocephaly in humans and cause increased Rac1 (GEF1) activity in cells, whereas most mutations in the GEF1 domain are linked to mild intellectual disability, microcephaly, and reduced Rac1 activity in cells. However, how SR8 variants increased Rac1 activity was completely unknown. We hypothesized that the increased Rac1 activity associated with SR8 domain variants resulted from disruption of SR-mediated GEF1 inhibition. We generated mutant SR6-GEF1 constructs harboring distinct disorder-associated variants and found that nearly all SR8 mutants increased SR6-GEF1 catalytic activity 4-8 fold. Interestingly, the one exception, N1080I, disrupts binding to neuroligin-1 and blocks neuroligin-1-mediated synaptogenesis¹⁰¹. We hypothesize that other sites, including N1080I, in the SRs serve as convergence points for upstream activators to regulate GEF1 activity, and discuss this in a following section. Together, these data demonstrate that many NDD variants in SR8 are sufficient to relieve SR-mediated GEF1 inhibition.

We also found that a GEF1 domain variant associated with Rac1 activation in cells likely impacts SR-mediated GEF1 inhibition. Unlike GEF1 disease variants that lie at the Rac1 binding interface and *decrease* GEF1 activity, this variant, D1368V, is distal to the Rac1 interface and *hyperactivates* Rac1 activity in cells

when introduced in the Trio9 splice isoform^{101 7, 24, 25}. Our results indicate that D1368V significantly increases GEF1 activity in the context of SR6-GEF1 but has no effect on GEF1 alone. We propose that D1368V enhances SR6-GEF1 activity by disrupting SR autoinhibition. Indeed, our crosslinking data suggests that contacts between the SRs and GEF1 are reduced for the D1368V variant.

2.4.4 NDD-associated variants in SR6 may reinforce SR-mediated GEF1 inhibition

We also generated two SR6-GEF1 constructs harboring individual disease variants in the SR6 domain, whose impact on Trio function remains completely unknown. The catalytic efficiency (k_{cat}/K_M) of SR6-GEF1_{E883D} was significantly slower than SR6-GEF1, suggesting that SR6 mutants decrease SR6-GEF1 catalytic activity. While the mechanism for this is unclear, one possibility is that SR6 acts as a hinge region allosterically governing the flexibility of the helices surrounding SR8, and that SR6 variants may decrease the ability for the SRs to release their inhibitory lock on the GEF1 domain. Indeed, we observed more contacts between SR7 and SR9 and the GEF1 domain in SR6-GEF1_{E883D}, suggesting that the intramolecular contacts are more stable or extensive in the variant case. This observation underscores the importance of understanding how dysregulation of Trio GEF1 activity contributes to NDDs.

2.4.5 The SRs may serve as a target for activators of Trio GEF1 activity

We demonstrated that the SRs inhibit Trio GEF1 activity, but it is unclear how inhibition may be released in a cellular context. SR domains are widely accepted as scaffolding proteins that coordinate cytoskeletal interactions with high spatial precision. Considering that Trio is known to act downstream of cell surface receptors to coordinate cytoskeletal rearrangements, we anticipate that the Trio SRs serve as a target of interaction partners to engage and activate Trio GEF1 activity in cells. Trio SRs interact with diverse cellular partners, including synaptic scaffolding proteins (Piccolo and Bassoon)⁸⁰, cell-adhesion molecules (VE-cadherin and Intercellular Adhesion Molecule 1 (ICAM1))^{102, 103}, and membrane trafficking proteins (RABIN8)⁸³. These SR binding partners may engage Trio to coordinate GEF1 activation and/or deactivation in a spatiotemporal manner. Indeed, several studies have shown that Trio interactions with binding partners impacts Rac1 activity in cells^{81, 101-104}. For example, VE-cadherin binds Trio SR5 and SR6, and this interaction locally increases Rac1 activity in cells¹⁰². Similarly, the ICAM1 intracellular tail binds Trio GEF1, and the Trio/ICAM1 interaction potentiates ICAM1 clustering at adhesion sites, promoting Rac1 activation in cells¹⁰³. Finally, the integral membrane protein Kidins220 regulates Rac1-dependent neurite outgrowth via interactions with the Trio SRs⁸¹. While these studies suggest that the Trio signaling partners may engage and activate Trio GEF1 activity, the specific interaction interfaces and binding stoichiometry that mediates GEF1 activation and how they are impacted by disorder-associated variants is presently unknown. Based on our evidence that SR8 variants relieve autoinhibitory

constraint, we anticipate that SR8 may be a convergence point for upstream activators and coordinated regulation of GEF1 activity.

2.5 Conclusions

TRIO has emerged as a significant risk gene for NDDs. Using biochemical and genetic tools, we identified a novel regulatory mechanism by which Trio SRs inhibit GEF1 activity and showed that disorder-associated variants are sufficient to relieve this autoinhibitory constraint. This discovery will serve as a model to understand how Trio GEF1 is regulated by physiological signals and how its disruption leads to NDDs. This mechanism may also offer a new target for therapeutic interventions for *TRIO*-associated NDDs.

2.6 Methods

2.6.1 Expression Cloning and Protein Purification

Human Trio SR6-GEF1 was PCR amplified and inserted into the pFastBac1 HTa vector (Invitrogen). Site-directed mutagenesis was used to insert point mutations into pFastBac1-Hta-SR6-GEF1 construct and confirmed by DNA sequencing. Primers used for cloning are included in Supplementary Table 1.

Recombinant baculoviruses were generated using Sf9 cells (Bac-to-Bac expression system, Thermo Fisher Scientific). Baculoviruses were used to infect Hi5 cells at an estimated multiplicity of infection = 1 for 48 hours before lysis in lysis buffer (20 mM HEPES pH 7.25, 500 mM KCl, 5 mM β -mercaptoethanol (BME), 5% glycerol, 1% Triton X-100, 20 mM imidazole, 1 mM DTT, 1 mM

phenylmethylsulfonyl fluoride (PMSF), 1x Roche cOmplete protease inhibitors (EDTA free) for 20 min at 4°C. Lysates were affinity purified using nitrilotriacetic acid (Ni-NTA) resin (Qiagen) and eluted with 250 mM imidazole. Elution fractions were further purified over an Sephadex 200 (S200) Increase 10/300 GL column into assay buffer (20 mM HEPES pH 7.25, 150 mM KCl, 5% glycerol, 0.01% Triton X-100, 1 mM DTT), aliquoted, and flash frozen for long-term storage.

Human Trio GEF1 and Rac1 were generated and affinity purified from bacterial cells as described in Blaise et al.⁸⁹. Point mutants were generated using site-directed mutagenesis. Following affinity purification, eluted protein was further purified over an S200 Increase column into assay buffer, aliquoted, and flash frozen for long-term storage.

Stokes radii of proteins were estimated based on the elution volume from the S200 Increase column, calculated based on a standard curve generated by running protein standards (Protein Standard Mix 15-600kDa, Supelco).

2.6.2 BODIPY-FL-GDP nucleotide exchange assays

12.8 μ M Rac1 was loaded with 3.2 μ M BODIPY-fluorescein (FL)-GDP (Invitrogen) in 1X assay buffer (20 mM HEPES pH 7.25, 150 mM KCl, 5% glycerol, 1 mM DTT, 0.01% Triton X-100) plus 2 mM EDTA to a total volume of 25 μ L per reaction, then incubated for 1 hour at room temperature. BODIPY-FL-GDP loading onto Rac1 was halted by the addition of 5 μ L of MgCl₂, for a total reaction volume of 30 μ L with a final MgCl₂ concentration of 5 mM. Prior to initiating the reaction with 100 nM Trio GEF, 30 μ L of GTPase (12.8 μ M) plus MgCl₂ (5 mM) mix or blank

(3.2 μ M BODIPY-FL-GDP, 2 mM EDTA, and 1X assay buffer) was added to appropriate wells. During the BODIPY-FL-GDP loading incubation period, GEF1-containing proteins were prepared in 1X assay buffer, 4 mM GTP, and 2 mM $MgCl_2$. Exchange reactions were initiated by adding 10 μ L of 100 nM Trio GEF mixture (as stated above) to each well, for a total reaction volume of 40 μ L. Real-time fluorescence data was measured every 10 seconds for 30 min monitoring BODIPY-FL fluorescence by excitation at 488 nm and emission at 535 nm, as per Blaise et al. ⁸⁹.

All k_{obs} measurements of GEF1 activity represent at least three experimental replicates with three technical replicates per experiment. Results are shown as the mean \pm standard deviation (SD) from multiple experiments. A one-way ANOVA was used to determine statistical significance between SR6-GEF1 and all other variants (two-tailed p-value <0.05) and adjusted using Dunnett's multiple comparisons test. Catalytic efficiencies (k_{cat}/K_M) of select SR6-GEF1 constructs were extracted from a linear fit of catalytic rate (k_{obs} , sec^{-1}) vs. GEF1 concentration (nM). Three experimental replicates were performed for each SR6-GEF1 construct, and the catalytic efficiency values were averaged. Results are shown as the mean \pm standard deviation (SD). A one-way ANOVA was used to determine statistical significance between SR6-GEF1 and all other variants (two-tailed p-value <0.05) and adjusted using Dunnett's multiple comparisons test.

2.6.3 Protein Structure Predictions

AlphaFold was used to access the predicted structure of human Trio spectrin repeats 1-GEF1 (amino acids 201-1600), entry number AF-O75962-F2⁹¹.⁹² Swiss pdb Viewer was used to model SR6-GEF1, amino acids 788-1599¹⁰⁵. DISOPRED was used to predict the probability of disorder of Trio SR6-GEF1, amino acids 788-1599⁹³.

2.6.4 Limited proteolysis

SR6-GEF1 in assay buffer plus 10 mM CaCl₂ was diluted to 0.4 mg/mL and incubated with increasing concentrations of trypsin (0.001 mg/mL to 0.11 mg/mL) for 1 hour at room temperature in a 25 µL total reaction volume. Reactions were quenched with 8 µL quench buffer (50 mM Tris-HCl pH 6.8, 4% SDS, 10% glycerol, 0.1% bromophenol blue, 5% BME, 1 mM PMSF, 4 mM EGTA, 4 mM EDTA) and immediately boiled for 10 min. Samples were immediately run on a 12% SDS-PAGE gel, and proteins were visualized by Coomassie R250 staining.

Major gel bands were excised and washed with 50:50 acetonitrile:water buffer containing 100 mM ammonium bicarbonate. Proteins in the gel were reduced with 4.5 mM DTT at 37°C for 20 min and alkylated with 10 mM iodoacetamide at room temperature for 20 min in the dark. Gel bands were washed twice with 50:50 acetonitrile:water containing 100 mM bicarbonate and dried for 10 min in a SpeedVac. Trypsin digestion was carried out (1:100 molar ratio of trypsin to protein) by incubation with the gel piece at 37°C overnight. The

digest samples were analyzed by LC–MS/MS using a Q-Exactive Plus mass spectrometer equipped with a Waters nanoACQUITY ultra-performance liquid chromatography (UPLC) system using a Waters Symmetry C18 180 μm by 20 mm trap column and a 1.7 μm (75 μm inner diameter by 250 mm) nanoACQUITY UPLC column (35°C) for peptide separation. Trapping was done at 15 $\mu\text{L}/\text{min}$ with 99% buffer A (100% water, 0.1% formic acid) for 1 min. Peptide separation was performed at 300 nL/min with buffer A and buffer B (100% acetonitrile, 0.1% formic acid) over a linear gradient. High-Energy collisional dissociation was utilized to fragment peptide ions via data-dependent acquisition. Mass spectral data were processed with Proteome Discoverer (v. 2.3) and protein database search was carried out in Mascot search engine (Matrix Science, LLC, Boston, MA; v. 2.6.0). Protein searches were conducted against the *Trichoplusia ni* protein database and the human Trio SR6-GEF1 sequence. Mascot search parameters included: parent peptide ion tolerance of 10.0 ppm; peptide fragment ion mass tolerance of 0.020 Da; strict trypsin fragments (enzyme cleavage after the C terminus of K or R, but not if it is followed by P); fixed modification of carbamidomethyl (C); and variable modification of phospho (S, T, Y), oxidation (M), and Propioamidation (C), and Deamidation (NQ). Peptide identification confidence was set at 95% confidence probability based on Mascot MOWSE score. Results were transferred to Scaffold software (Proteome Software, Portland, OR; v. 4) for further data analysis to look at peptide abundances in reference to their start position. These were utilized to plot in a frequency distribution to determine band identity.

2.6.5 Crosslinking mass spectrometry

Crosslinking experiments were performed as in Sanchez et al. ¹⁰⁶ with deviations noted below. 25 µg of protein was incubated in assay buffer with 100 µM BS3 (bis(sulfosuccinimidyl)suberate) (Thermo Fisher) for 30 min on ice. The reaction was quenched by adding Tris pH 7.25 to 10 mM final concentration. Protein was then acetone precipitated and the pellet was alkylated with iodoacetamide and digested with trypsin. Peptides were desalted on a 100 µL Omix C₁₈ tip (Agilent), dried, and reconstituted in 100 µL of 0.1% formic acid. Mass spectrometry was performed on an Orbitrap Exploris 480 equipped with an EasySpray nanoESI source, an EasySpray 75 µm x 15 cm C₁₈ column, and a FAIMS Pro ion mobility interface coupled with an UltiMate 3000 RSLCnano system (Thermo Scientific). Each sample was analyzed at four different FAIMS compensation voltages (CV= -40V, -50V, -60V, -70V) to provide gas-phase enrichment/fractionation of crosslinked peptide ions ¹⁰⁷. Each analysis was a separate injection (2.5 µL sample). The sample was loaded at 2% B at 600 nL/min for 35 min followed by a multi-segment elution gradient to 35% B at 200 nL/min over 70 min with the remaining time used for column washing and re-equilibration (buffer A: 0.1% formic acid (aq); buffer B: 0.1% formic acid in acetonitrile). Precursor ions were acquired at 120,000 resolving power and ions with charges 3-8+ were isolated in the quadrupole using a 1.6 m/z unit window and dissociated by HCD at 30% NCE. Product ions were measured at 30,000 resolving power. Peak lists were generated using PAVA (in house Python app), searched with Protein Prospector v6.3.23 ¹⁰⁸, and classified as unique residue pairs using Touchstone

(an in-house R library) at SVM.score ≥ 1.5 corresponding to a residue pair level FDR $< 0.1\%$ and then further summarized and presented as domain-domain pairs using Touchstone. A custom database consisting of the human Trio construct and a 10x longer decoy database (11 sequences total) was used in the Prospector search, using tryptic specificity with 2-missed cleavages and tolerance of 10/25 ppm (precursor/product). DSS/BS3 crosslinking was specified.

2.6.6 BioLayer interferometry

Kinetic binding assays were performed using a ForteBio BLItz instrument. Ni-NTA biosensors were pre-hydrated in assay buffer for 10 min prior to the experiment. Biosensors were first measured for a baseline signal for 30 seconds before loading His-GEF1 (0.5 μM) or SR6-GEF1 (2 μM) in assay buffer for 5 min (concentrations were optimized for reproducible biosensor loading and signal change). Biosensors were then re-equilibrated in assay buffer for 30 seconds before introducing varying concentrations of Rac1 (at least 4 concentrations per experiment) in assay buffer for 5 min to measure association. Association curves were fit to a one phase exponential curve to obtain a k_{obs} value and these values were plotted against Rac1 concentration to calculate a K_d from the linear fit of this line, where the y-intercept = k_{off} and slope = k_{on} ($K_d = k_{\text{off}}/k_{\text{on}}$). Concentration gradients were replicated at least three times independently, and the K_d measurements of each interaction were compared using an unpaired t-test. Reported values are mean \pm SD.

2.6.7 Measurement of GEF and SR6-GEF1 impact on cell morphology

Polyethylenimine was used to transfect HEK293 cells with 0.5-4 µg of DNA in 6-well dishes at a density of 3×10^5 cells per well. 24 hours after transfection, cells were trypsinized and replated at a density of 2.5×10^4 cells per coverslip on fibronectin-coated coverslips (10 µg/mL fibronectin). 24 hours post plating, cells were fixed and stained as in Lim et al. ¹⁰⁹. Cells were fixed for 5 min in 2% paraformaldehyde in cytoskeleton buffer (10 mM MES pH 6.8, 138 mM KCl, 3 mM MgCl₂, 2 mM EGTA, 320 mM sucrose). Cells were rinsed 3 times in Tris Buffered Saline (TBS) (20 mM Tris pH 7.4, 150 mM NaCl) and incubated with 5 µg/mL Alexa Fluor Wheat Germ Agglutinin 555 in TBS (Thermo Fisher) for 10 min to visualize the cell membrane when imaging. Cells were washed another three times in TBS, then permeabilized for 10 min in 0.3% TritonX-100/TBS and washed another 3 times in 0.1% TritonX-100/TBS. Cells were blocked for 30 min in antibody dilution buffer (ADB) (0.1% TritonX-100, 2% BSA, 0.1% NaN₃, 10% FBS, TBS) and incubated with primary antibody (ADB containing a 1:2000 dilution of Goat Anti-GFP, Rockland) at 4°C overnight. The next morning, cells were washed in 0.1% TritonX-100/TBS 3 times and incubated in secondary antibody for 1 hour at room temperature (in ADB, 1:2000 Alexa Fluor 488 Donkey Anti-Goat, Abcam). Cells were washed once in 0.1% TritonX-100/TBS, once in TBS, and then mounted onto glass slides using AquaMount (Lerner Laboratories). After drying, coverslips were sealed using clear nail polish and imaged using a 40x objective on a spinning disk confocal microscope (UltraVIEW VoX spinning disk confocal (Perkin Elmer) Nikon

Ti-E-Eclipse), collecting a full z-stack of images for each cell. Identical microscope settings were used between imaging samples.

After imaging cells, images were processed using Fiji/ImageJ ¹¹⁰ to generate a sum projection of the GFP channel for quantifying fluorescence as a proxy for total protein expression. Images were then analyzed using CellProfiler to semi-automatically detect cell edges and compute cell area ¹¹¹. Cell area was normalized for protein expression on a single cell basis by dividing the total area of the cell by the total GFP fluorescence of the cell (a proxy for total protein expression). Two biological replicates were performed, with 25-40 cells quantified per group per replicate. Statistical significance of differences in the normalized cell area was determined using a one-way ANOVA between the GFP control and all other groups (two-tailed p-value <0.05) and adjusted using Dunnett's multiple comparisons test.

Chapter 3

Studies Toward the Elucidation of Mechanisms of Trio GEF Activation and Regulation

3.1 Summary

My work presented in this chapter is currently unpublished and provides a foundation for future studies on elucidating mechanisms of Trio GEF activation and regulation in a cellular context and understanding how disruption of these processes contributes to disease pathology. The cellular perspective of how Trio GEF activity is regulated in cells builds on the novel mechanism of GEF1 autoinhibition I showed in Chapter 2. Here, I sought to identify the key mechanisms by which Trio GEF1 autoinhibitory constraint is relieved in a cellular context via (1) protein-protein interactions and/or (2) post-translational modifications. I generated and purified all constructs except for ADAM22, ADAM23, and L1CAM, which was done by Alyssa Blaise, Amanda Jeng, and Tony Koleske.

3.2 Determining whether and how receptors engage and activate Trio GEF1

3.2.1 Overview

As detailed extensively in Chapters 1 and 2, Trio acts downstream of cell surface receptors to coordinate cytoskeletal rearrangements. Work from our lab and others identified a list of cell surface receptors and kinases that have been shown to interact with Trio biochemically or genetically and are likely regulators of Trio GEF activity. However, the mechanisms by which these proteins engage Trio to active GEF activity are unclear.

Several receptors are known to signal through or interact functionally with Trio to regulate neuronal development and function and have downstream effects on Rac1 or RhoA activity (Table 4). We hypothesize that one or more of these receptors utilize their cytoplasmic domains to engage the SRs or Trio GEF1 to relieve autoinhibition.

In a neuronal context, we hypothesize that Trio engages DCC, ADAM22/ADAM23, Kidins220, L1CAM, and/or NLGN1 to regulate Rac1 and RhoA activity (Fig 3.1). DCC (Deleted in Colorectal Cancer) is a receptor for the Netrin-1 guidance factor. While it has been demonstrated that Trio is required for Netrin-1 mediated stimulation of Rac1 and neurite and axon outgrowth¹¹², the molecular mechanisms by which this occurs remains completely unknown.

Kidins220 (Kinase D interacting substrate of 220 kDa) is a transmembrane protein that integrates signals from Trk neurotrophin receptors. It has been demonstrated that Trio directly interacts with the N-terminal ankyrin repeats (aa 1-402) of Kidins220¹¹³, and overexpression of Kidins220-1-402 activates Rac1 activity in HEK293 cells¹¹³. While it has been demonstrated that the ankyrin repeats bind directly to both the N- and C-terminal regions of the spectrin repeats, it remains unclear whether this interaction directly activates Rac1 activity in cells.

Another class of candidate interactors to test as regulators of Trio GEF1 activity are proteins whose expression levels change upon loss of Trio, suggesting they may function in the same biochemical pathway as Trio. Our lab used mass spectrometry to analyze proteins whose expression levels changed in NEX-TRIO+/- cortex, and Amanda Jeng later identified L1CAM and ADAM23 as

significant hits. L1CAM is an Ig superfamily adhesion receptor that regulates cell:cell adhesion and neurite outgrowth and is decreased 45% in NEX TRIO +/- cortex. Others have shown that mutations in L1CAM are associated with CRASH syndrome, associated with defects in the corpus callosum and intellectual disability¹¹⁴. The *Drosophila* L1CAM ortholog interacts genetically with *TRIO* in mushroom body axonogenesis¹¹⁵.

The LGI1/ADAM22/ADAM23 complex promotes neurite outgrowth and anchors synaptic ion channels¹¹⁶⁻¹¹⁹. ADAM22 and ADAM23 are reduced 35-50% in *NEX-TRIO*^{-/-} cortex. Genetic variants in *ADAM23* are associated with increased epilepsy risk^{118, 120-123}. While our lab has demonstrated that Trio9s interacts with ADAM23 via pulldown assays with cell lysates overexpressing Trio9s, it remains to be tested whether this interaction is direct and whether this interaction is linked to Rac1 or RhoA activity.

Recent work by Tian et al. 2021 has implicated Neuroligin1 (NLGN1) as another candidate activator.¹⁰¹ Neuroligins are synaptic cell adhesion molecules that interact with neurexins to confer synapse formation. Neuroligin1 co-immunoprecipitated with Trio in rat brain homogenate and Hek293 lysate. Trio9 N1090I in HEK cells reduced the amount of Neuroligin immunoprecipitated by 50%. Intriguingly, Tian et al. demonstrated that replacing Trio and Kalirin with Trio9 N1080I in rat CA1 pyramidal neurons prevents neuroligin-induced increases in dendritic spine numbers in glutamatergic synapses. While this suggests Neuroligin1 interacts with Trio to regulate synaptogenesis, it is unknown whether this interaction is direct or whether Neuroligin1 directly activates Trio GEF1 activity.

It is interesting to note that the N1090I variant was the only SR8 variant that had no effect on SR6-GEF1 activity in Bircher and Corcoran et al. 2022.

In a non-neuronal context, other candidate activators that have been shown to function upstream of Trio and have downstream effects on Rac1 or RhoA activity include VE-Cadherin and ICAM. The cytosolic tails of both VE-Cadherin and ICAM1 have been shown to directly interact with Trio spectrin repeats and Trio GEF1, respectively, and both interactions are correlated with increased Rac1 activation in cells. However, the biochemical mechanisms underlying how these interactions directly activate Trio GEF1 activity have yet to be determined^{102, 103}.

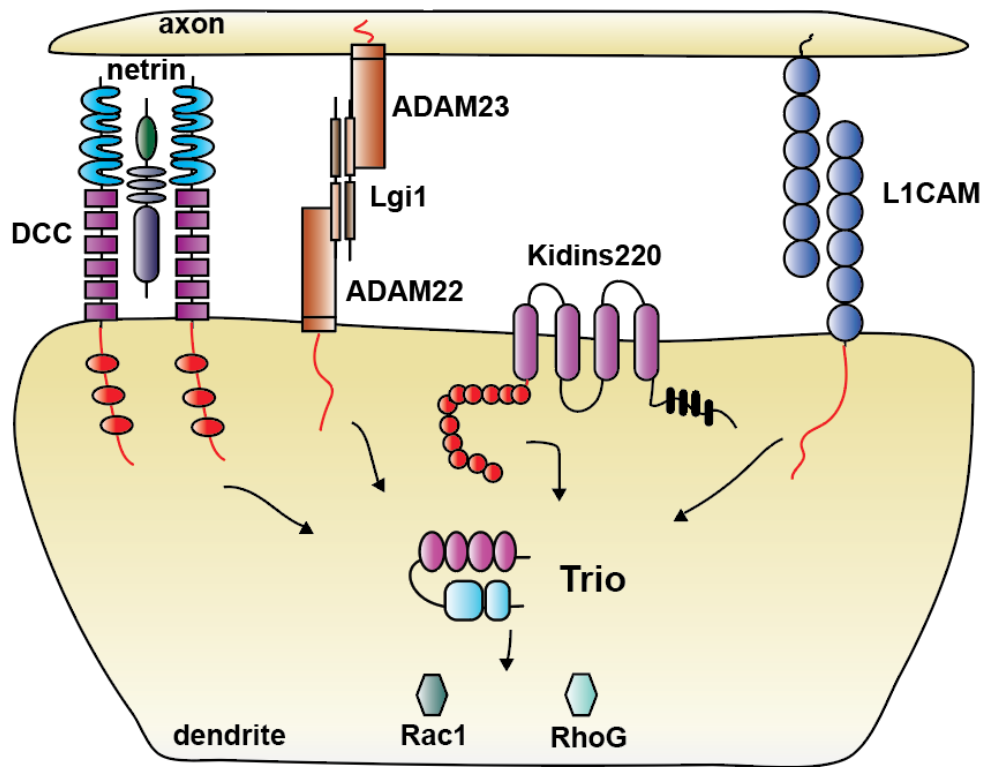


Fig 3.1 Candidate Trio GEF1 Activating Receptors.

Diagram of select candidate receptors (DCC, ADAM22/ADAM23, Kidins220, L1CAM) with cytosolic domains highlighted in red.

3.2.2 Generating Cytoplasmic Tails of Receptors that Functionally interact with Trio

Because these receptors all require their cytoplasmic domains to engage and activate intracellular binding events, I generated purified recombinant glutathione s-transferase (GST) fusions of the intracellular tails of each of these receptor tails (Fig 3.2). Given that each of these receptors dimerize or multimerize in cells upon activation, I chose GST to force the attach intracellular domains to dimerize. I purified each intracellular tail following the GST purification protocol detailed in Chapter one (Blaise et al. 2022) but did not cleave the GST tag after purification (Fig 3.3). After purification, each construct was run over the S200 Increase column or G25 Sephadex buffer exchange column into standard assay buffer (20 mM Hepes pH 7.25, 150 mM KCl, 5% glycerol, 0.01% Triton X-100, 1 mM DTT), aliquoted, and flash frozen for long-term storage. Each construct was confirmed to be soluble and behaving as a monodisperse population prior to assay use. A detailed table including pertinent information for each construct is in the Appendix section of this thesis (Table 5).

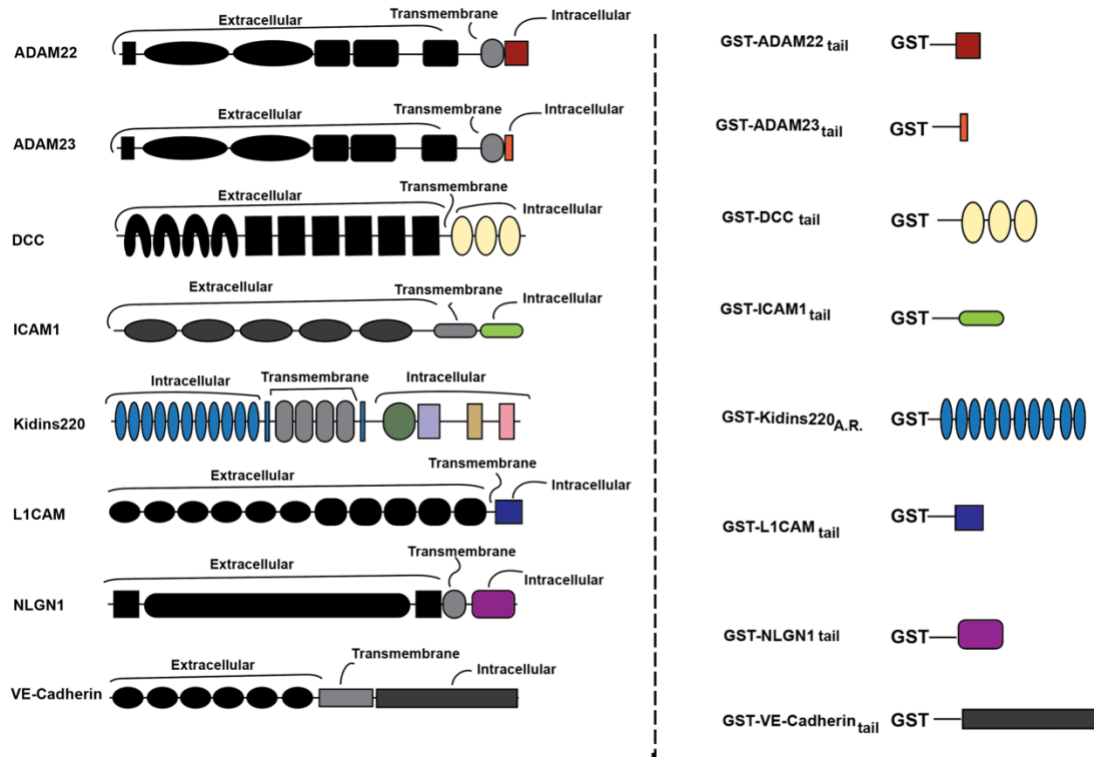


Fig 3.2 Schematic of Purifying Intracellular Tails of Candidate Trio Activators.

Left: Schematic of full-length candidate Trio activators with extracellular regions indicated in black, transmembrane regions indicated in gray and intracellular regions colored. The ADAM22 intracellular tail (red), ADAM23 intracellular tail (orange), DCC intracellular P1-P3 domains (yellow), ICAM1 intracellular tail (green), Kidins220 ankyrin repeats (blue), L1CAM intracellular tail (indigo), NLGN1 intracellular tail (violet), and VE-Cadherin intracellular tails (black) were isolated and purified as recombinant proteins. Right: Schematic of recombinant fragments generated and purified. Each intracellular tail was generated as a GST fusion.

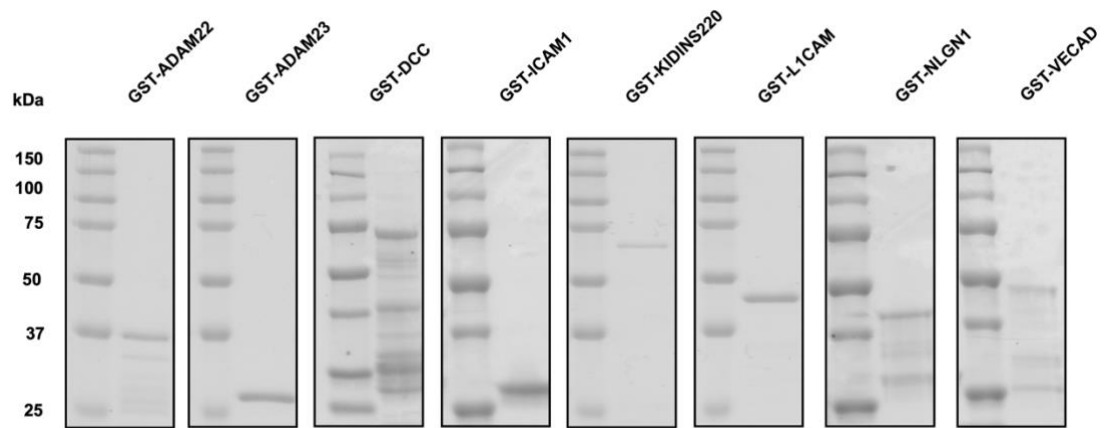


Fig 3.3 Purified Candidate Trio Activator Tail Constructs.

Samples (approximately 5 μ g) of purified cytosolic tails of candidate Trio activators were analyzed by SDS-PAGE and stained with Coomassie Blue R250 to assess purity.

3.2.3 Measuring receptor binding and activation of Trio SR6-GEF1

3.2.3.1 Methods

To first determine whether Trio directly interacts with any of these intracellular tails of candidate activators, I set up an in vitro binding matrix to determine whether each intracellular tail was sufficient to pull down Trio His GEF1, Trio His-SR6-GEF1, or Trio His-SR6-SH3-1 out of solution.¹²⁴

To prepare the bait beads, I purified each intracellular tail and buffer exchanged each into standard assay buffer (20 mM Hepes pH 7.25, 150 mM KCl, 5% glycerol, 0.01% TritonX100, 1 mM DTT), detailed in Section 3.2.2 of this thesis, for each intracellular tail to serve as the bait for each binding reaction. I linked an equimolar amount of each GST-tagged intracellular tail to amino link beads (5 μ M) with NaCNBH₃ (20 μ L/mL) overnight at 4 °C, and the following day blocked unoccupied binding sites with ethanolamine (50 mM), also rotating overnight at 4 °C.

Prior to assay use, the beads were washed 5 times with NaCl (1 M) and resuspended in standard assay buffer/binding buffer. Binding buffer was added to make a 50%-50% ratio of bead to buffer slurry.

Three different Trio constructs served as the “prey” proteins, Trio His-GEF1, Trio His-SR6-GEF1, and Trio His-SR6-SH3-1 (Fig 1.10). Trio His-GEF1 was purified from bacterial cells as described in Section 1.4.3 of this thesis, and Trio His-SR6-GEF1 and Trio SR6-SH3-1 were purified from insect cells as described in Section 2.6.1 of this thesis. Prior to incubation with each intracellular tail, Trio

constructs were diluted to 5 - 10 μ M in binding buffer and pre-cleared with GST-bound aminolink beads (5 μ M) for 1 hr at 4 $^{\circ}$ C (7.5 μ L beads per 500 μ L reaction) to minimize non-specific interactions. Pre-cleared Trio constructs (500 μ L) were incubated with 7.5 μ L beads of each intracellular tail (15 μ L slurry) for 1 hr at $^{\circ}$ C. Beads were washed quickly 5 times with RIPA buffer (10 mM Tris-HCl pH 8.0, 1 mM EDTA, 0.5 mM EGTA, 1 % Triton X-100, 0.1% Sodium Deoxycholate, 0.1% SDS, 140 mM NaCl), resuspended in 25 μ L 1x LSB, and analyzed by SDS-PAGE and stained with Coomassie Blue.

3.2.3.2 Trio directly interacts with each candidate activator intracellular region

Preliminary results from the in vitro binding matrix suggest that the Trio SR6-GEF1 and SR6-SH3(1) regions are sufficient to interact with the cytosolic regions of ADAM22, ADAM23, DCC, ICAM1, Kidins220, L1CAM, NLGN1, and VE-Cadherin. These results are consistent with data from other labs that indicate that Trio GEF1 directly interacts with ICAM1, Trio SR 5-6 directly interacts with VE-Cadherin, and Kidins220 interacts with Trio SRs 1-4 and SRs 5-9^{81, 102, 103}.

During the initial trials for this binding matrix, the initial limitation was that the GST beads alone, meant to serve as a negative control, were pulling down all Trio constructs, suggesting non-specific binding was occurring despite pre-clearing with control aminolink beads blocked with ethanolamine. Therefore, while the preliminary results indicate that DCC, Kidins220, NLGN1, and ICAM all directly bind to Trio (Fig 3.4). Further validation with these constructs with more stringent pre-clearing and washing conditions will be needed to verify these results.

In subsequent binding assays, to minimize non-specific interactions, pre-clearing was performed with GST beads instead of control aminolink beads, and instead of washing the beads quickly two times with binding buffer, washing stringency was increased to five times with RIPA buffer. While Trio GEF1 appeared to have enhanced binding to each of the intracellular tails compared to GST alone as a negative control, non-specific binding with GST continued to be a limitation with the Trio GEF1 construct. However, pulldowns with GST as a negative control was minimized for both the Trio SR6-GEF1 and Trio SR6-SH3-1 constructs. GST-ADAM22, ADAM23, L1CAM, and VE-Cadherin pulled Trio SR6-GEF1 and Trio SR6-SH3-1 (Fig 3.5- Fig 3.6) out of solution, suggesting that Trio directly interacts with the cytosolic regions of each of these cell surface receptors. While promising preliminary results, more rigorous biochemical assays are required to determine whether interaction can reach saturable levels, and quantitative binding assays such as supernatant depletion assays or BioLayer Interferometry should be utilized to determine the binding affinity for each direct interaction.

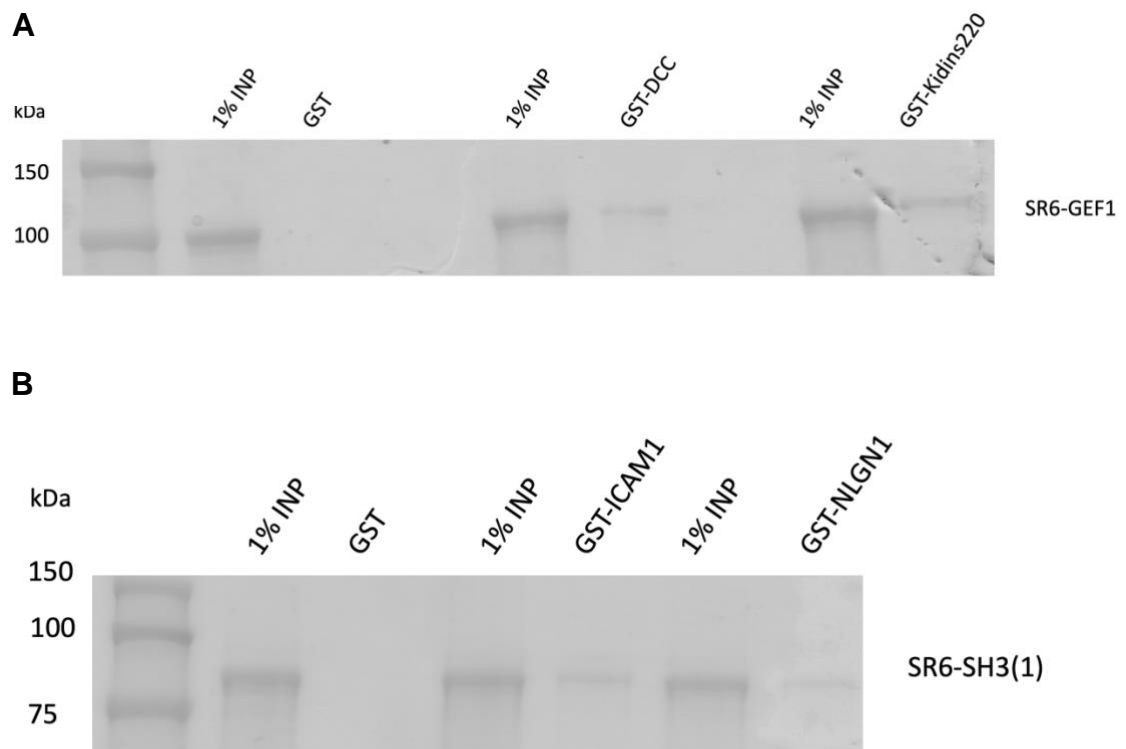


Fig 3.4 DCC, Kidins220, ICAM1 and NLGN1 interact with Trio.

(A) Trio SR6-GEF1 (10 μ M) was incubated with GST-DCC and GST-Kidins220 linked to aminolink beads (5 μ M). Bound Trio SR6-GEF1 was analyzed by SDS-PAGE and stained with Coomassie Blue. (B) Trio SR6-SH3-1 (5 μ M) was incubated with GST-ICAM1 and GST-NLGN1 linked to aminolink beads (5 μ M). Bound Trio SR6-GEF1 was analyzed by SDS-Page and Stained with Coomassie Blue.

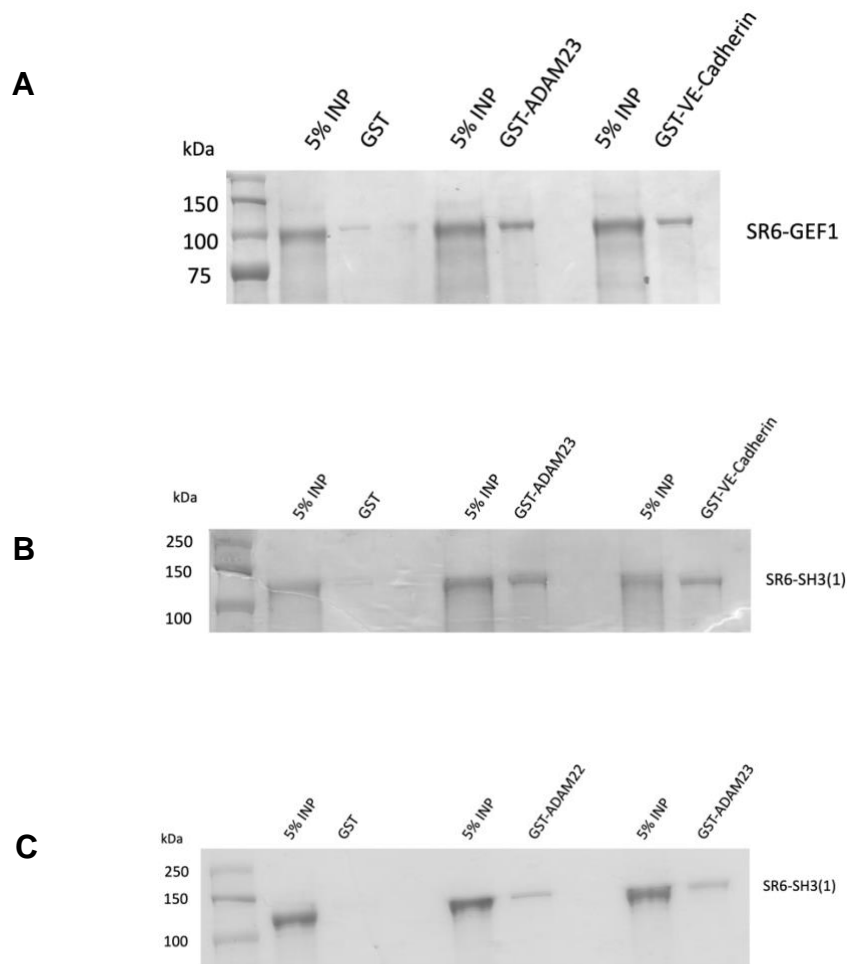


Fig 3.5 ADAM22, ADAM23, and VE-Cadherin directly interact with Trio.

(A) Trio SR6-GEF1 (10 μ M) was incubated with GST-ADAM23 and GST-VE-Cadherin linked to aminolink beads (5 μ M). Bound Trio SR6-GEF1 was analyzed by SDS-PAGE and stained with Coomassie Blue. (B) Trio SR6-SH3-1 (5 μ M) was incubated with GST-ADAM23 and GST-VE-Cadherin linked to aminolink beads (5 μ M). Bound Trio SR6-GEF1 was analyzed by SDS-PAGE and stained with Coomassie Blue. (B) Trio SR6-SH3-1 (5 μ M) was incubated with GST-

ADAM22 and GST-ADAM23 linked to aminolink beads (5 μ M). Bound Trio SR6-SH3-1 was analyzed by SDS-Page and Stained with Coomassie Blue.

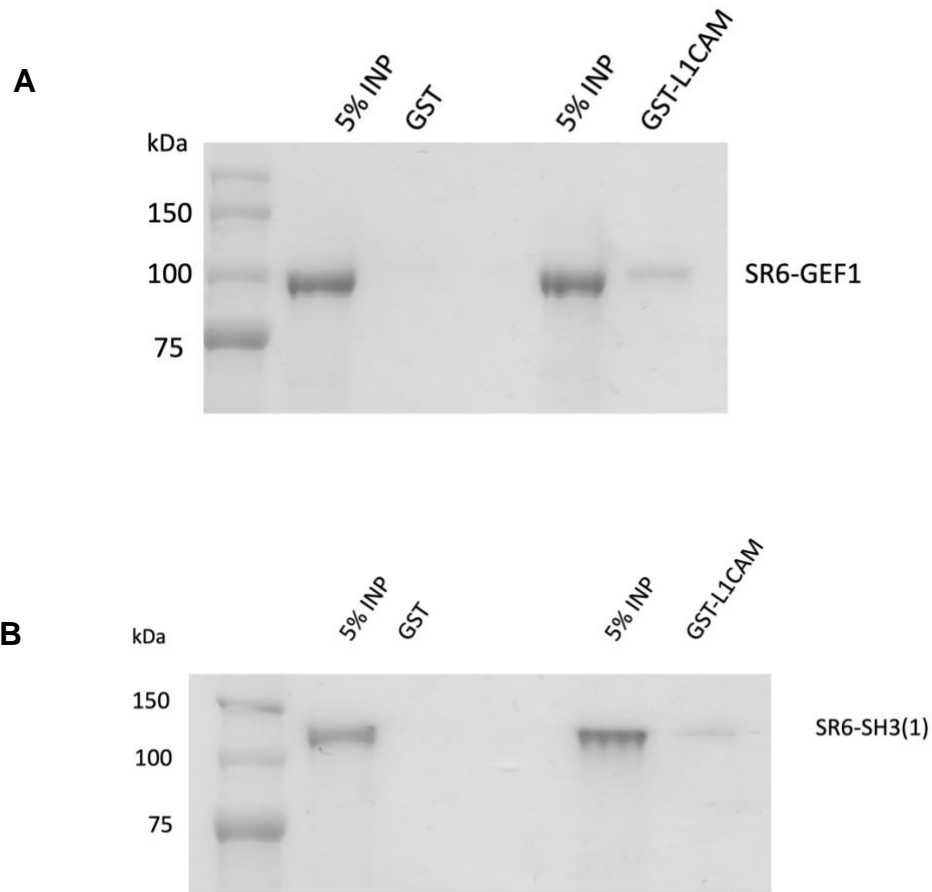


Fig 3.6 L1CAM directly interacts with Trio.

Trio SR6-GEF1 (10 μ M) was incubated with GST-L1CAM linked to aminolink beads (5 μ M). Bound Trio SR6-GEF1 was analyzed by SDS-Page and Stained with Coomassie Blue. (B) Trio SR6-SH3-1 (5 μ M) was incubated with GST-L1CAM linked to aminolink beads (5 μ M). Bound Trio SR6-SH3-1 was analyzed by SDS-PAGE and stained with Coomassie Blue.

3.2.3.3 No receptor tail candidate activates Trio SR6-GEF1 in vitro

To determine whether any of these candidate activator receptor tails are sufficient to impact SR6-GEF1 activity in a concentration dependent manner, I titrated in increasing amounts (0 – 2 μ M) of each GST-receptor cytoplasmic domain with a fixed amount of SR6-GEF1 (100 nM) and compared to changes in SR6-GEF1 activity relative to GST alone.

These preliminary tests suggested that titrating in each activator into solution is not sufficient to impact SR6-GEF1 activity in a concentration dependent manner (Fig 3.7), suggesting that other factors are needed to engage and activate SR6-GEF2 in vitro.

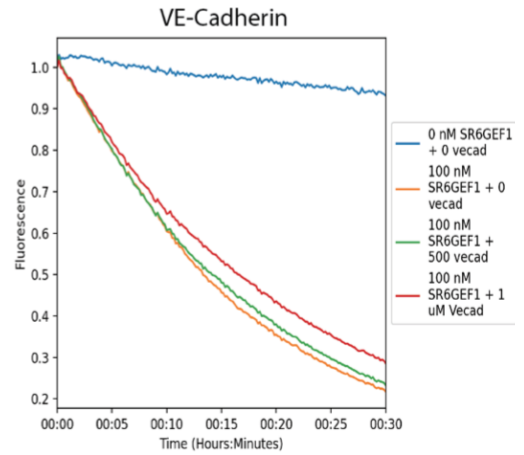
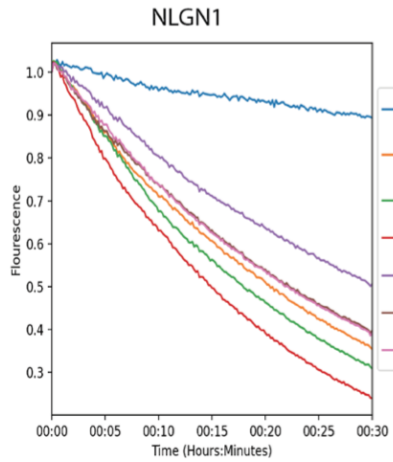
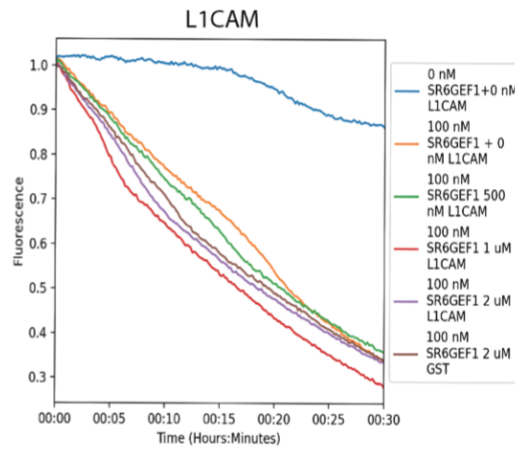
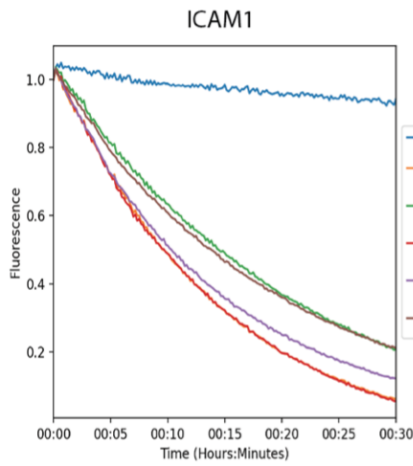
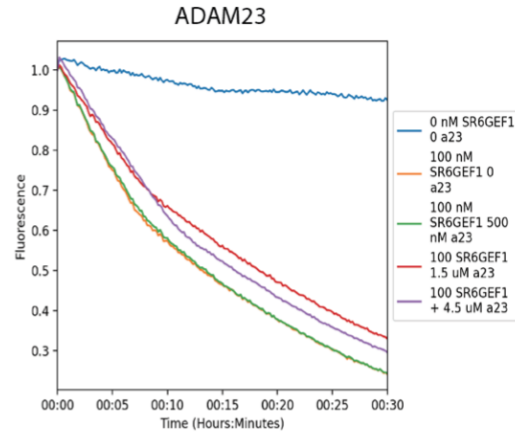
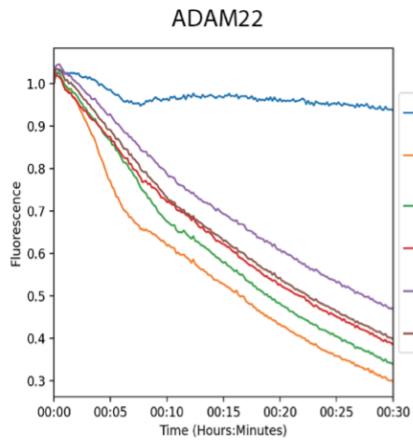


Fig 3.7 Candidate activator tails do not activate Trio SR6-GEF1 in vitro.

Sample GEF assay traces of SR6-GEF1 with titrating increasing amounts of ADAM22, ADAM23, ICAM1, L1CAM, NLGN1, VE-Cadherin. No intracellular tail had a significant impact on Trio SR6-GEF1 activity.

3.3 Determining whether and how phosphorylation impacts Trio GEF activity

3.3.1 Overview

Many RhoGEFs contain accessory domains that block GEF activity via intramolecular inhibition, and in all cases, it is hypothesized that activation of GEF activity occurs through the relief of autoinhibitory constraint interaction with other cellular binding partners or post-translational modifications ⁶⁵.

For example Vav, a RhoGEF that functions downstream of cell surface receptors such as EGFR and PDGFR, is activated by transient phosphorylation by members of the Src and Syk tyrosine kinase families, resulting in the activation of its catalytic activity ^{65, 125-129}

Therefore, in addition to testing the hypothesis that Trio GEF1 is activated via interactions with upstream cell surface receptors, I also sought to assess whether and how phosphorylation impacts Trio GEF activity. Limited mapping of Trio phosphorylation has been performed, and one of the few early Trio publications including a map of Trio tyrosine phosphorylation showed that only the Ig and kinase domains of FL-Trio are tyrosine phosphorylated, and that Trio spectrin repeats appear only to be phosphorylated on serine residues ^{35, 130}.

While phosphorylation mapping on the Trio SR6-GEF1 region is limited, the Eipper/Mains group has done extensive work to investigate phosphorylation on the Trio paralog Kalirin and identified several residues phosphorylated using Kalirin immunopurified from murine brain ^{131, 132}. In addition, Herring et al. 2016

demonstrated that CAMKII phosphorylation of Kalirin is sufficient to enhance AMPAR synaptic transmission, supporting the hypothesis that Kalirin and Trio activity may be tightly coordinated via phosphorylation ¹³³.

I performed sequence alignment between Trio and Kalirin and found that the majority of the Kalirin phosphorylation sites are conserved in Trio and positioned at the SR:GEF1 interface of our model (Fig 3.8, Table 6, Table 7). Therefore, I hypothesized that phosphorylation may impact autoregulation of GEF1 activity by the SRs.

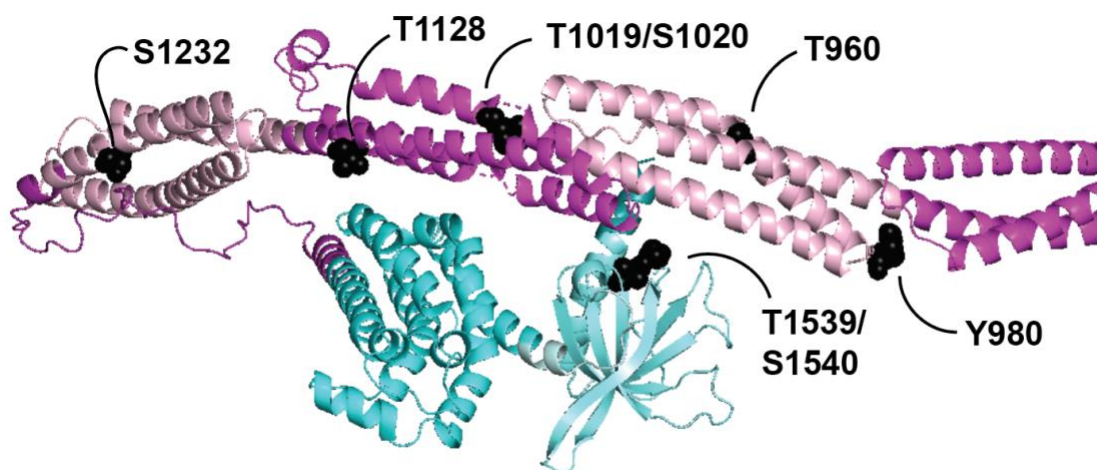


Fig 3.8 Conserved phosphorylation sites mapped on Trio SR6-GEF1.

Several residues are phosphorylated on the Trio paralog Kalirin immunopurified from brain. These sites are conserved in Trio and positioned at the SR6:GEF1 interface in our model.

3.3.2 Generating and testing Trio Sr6-GEF1 isosteric phosphomimic constructs

To test whether phosphorylation impacts our model of SR6-GEF1 autoinhibition in vitro, I generated and purified eight isosteric phosphomimic residues (S to D, T to E) within SR6-GEF1 (Fig 3.9), following the same protocol outlined in Chapter 2 for generating the SR6-GEF1 disease mutant constructs (Table 8). Similar to the workflow of measuring changes in catalytic activity of the SR8 disease mutant constructs in Chapter 2, I tested whether these phosphomimic constructs had any changes in catalytic rate (k_{obs}) when measured at equimolar amounts.

Surprisingly, my preliminary results indicated that none of the isosteric mutants had any change in catalytic activity compared to SR6-GEF1 (Fig 3.10). While this data suggests that phosphorylation of these sites alone is not sufficient to relieve autoinhibition, phosphorylation of these sites may still be critical to other modes of regulation, such as impacting binding with other regulatory proteins or impacting subcellular localization.

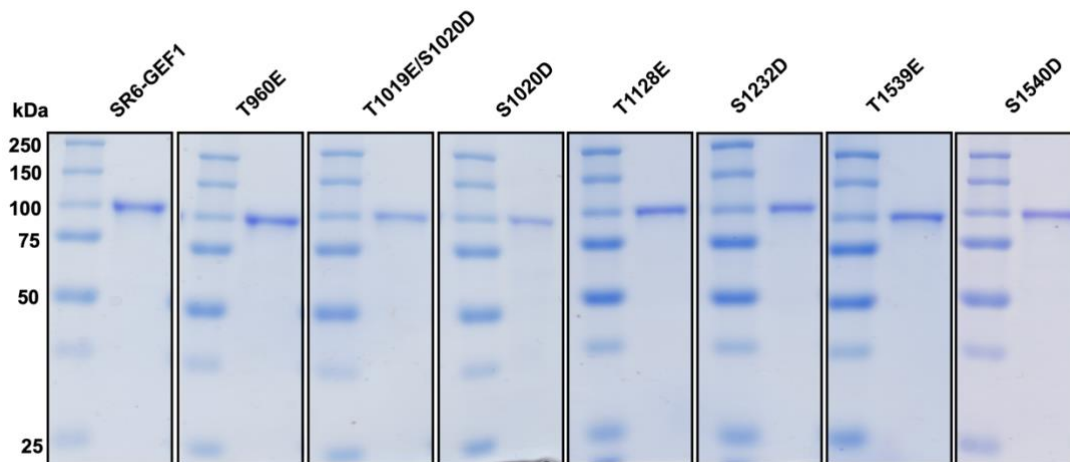


Fig 3.9 Isosteric Phosphomimic Trio SR6-GEF1 constructs.

Samples (approximately 5 μ g) of purified SR6-GEF1 isosteric phosphomimic mutants were analyzed by SDS-PAGE and stained with Coomassie Blue R250 to assess purity.

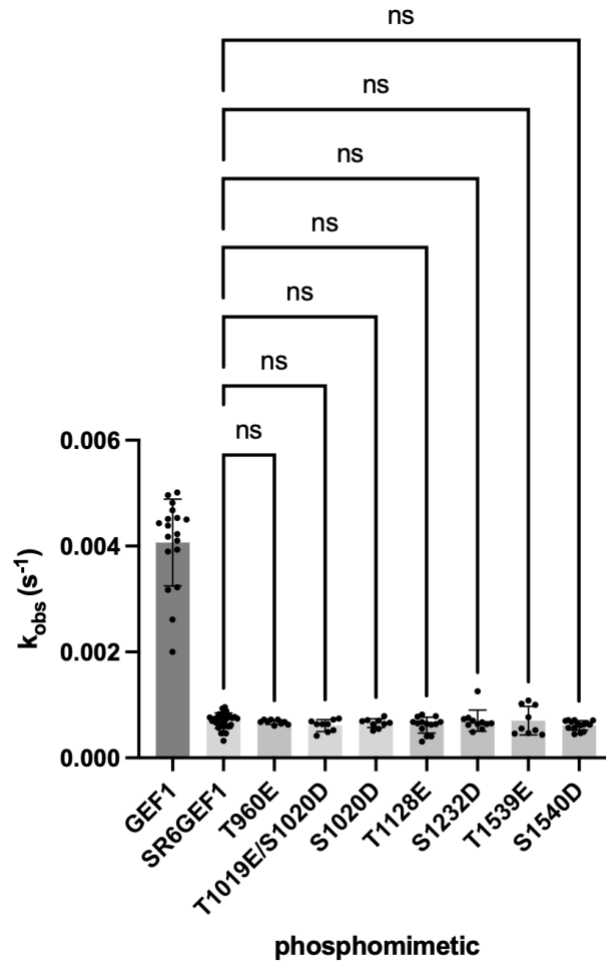


Fig 3.10 Phosphomimetic Trio SR6-GEF1 constructs do not have altered catalytic activity.

Isosteric phosphomimetic SR6-GEF1 constructs do not have significantly enhanced catalytic rates, k_{obs} , at equal molar amounts (100 nM). Significant difference was compared to SR6-GEF1 in a one-way ANOVA adjusted for multiple comparisons ($n \geq 9$).

3.4 Discussion

Chapter Three details my unpublished work to uncover how Trio GEF1 is regulated in a cellular context. My results suggest that ADAM22, ADAM23, DCC, ICAM1, Kidins220, L1CAM, NLGN1, and VE-Cadherin directly interact with Trio SR6-GEF1. However, none of the intracellular tails were able to activate Trio SR6-GEF1 in vitro.

There are several explanations as to why this may be; from a technical standpoint, it could be a limitation of the fluorescence-based assay; a more sensitive assay might be needed to detect changes in GEF activity, a different buffer may be needed to facilitate binding and subsequent activation in vitro, or a different Trio construct could be tested to see if any different changes in activity are observed (ex. GEF1 or SR6-SH6-SH3(1)).

Another possibility as to why no changes in SR6-GEF1 activity were observed is that other cellular factors may be needed to engage and activate SR6-GEF1 in vitro. In Chapter 4, I discuss the future directions of this project and possible avenues to determine how Trio SR6-GEF1 is regulated in a cellular context.

I also tested the hypothesis that phosphorylation relieves autoinhibition by generating isosteric phosphomimic constructs of conserved phosphorylation sites and measuring catalytic activity in vitro. My results indicated that phosphorylation alone does not impact Trio SR6-GEF1 activity in vitro, suggesting that either phosphorylation does not impact Trio GEF1 regulation, or other cellular factors are required.

While phosphorylation and direct competition are two likely modes for relief of autoinhibition of Trio SR6-GEF1 given its known interactions with upstream cell surface receptors, there are several ways that autoinhibition can be regulated in cells, such as other post-translational modifications (acetylation, methylation, sumoylation, etc.) or mechanical relief. In Chapter Four, I discuss future directions to probe Trio GEF1 regulation in cells.

Chapter 4

Ongoing Work and Future Directions

4.1 Summary

Chapter Four serves as both a brief overview of ongoing work to elucidate how Trio GEF1 is regulated in a cellular context and a discussion of future directions of this project. The experiments proposed are a cumulative result of fruitful discussions with Tony Koleske, Josie Bircher, Amanda Jeng, Pauline Pan, and me.

4.2 Do candidate activators increase Trio SR6-GEF1 activity in cells?

Because titrating in increasing amounts of intracellular tails did not impact Trio SR6-GEF1 *in vitro*, it is likely that other cellular factors are needed to engage and activate SR6-GEF1. Therefore, a cell-based assay is the first possible approach to understand whether and how any of the candidate Trio activators engage and activate Trio SR6-GEF1 in cells. For example, the cell-based FRET Rac1 biosensor assay previously used by our lab may be used in the future to determine whether co-expression of each FL candidate receptor and Trio SR6-GEF1 impacts Rac1 activation compared to SR6-GEF1 alone (Fig 4.1) ⁷.

In addition to binding partner interactions and phosphorylation, other modes of autoinhibitory regulation must be considered.

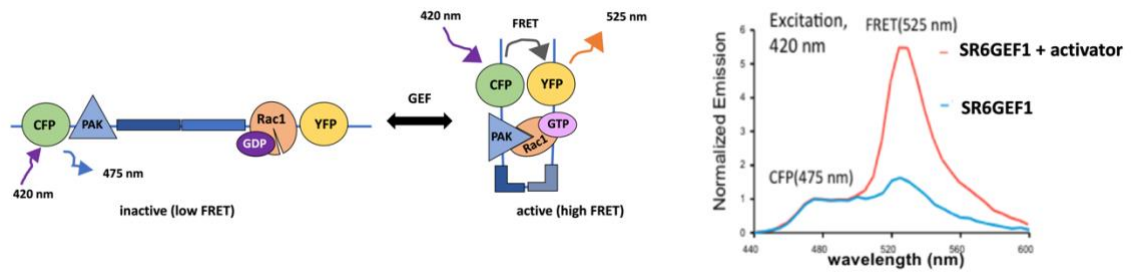


Fig 4.1 Cell-based assay for Trio SR6-GEF1 activity. Figure adapted from *Katrancha et al. 2017*.

(A) The Rac1 biosensor has high FRET activity when GTP is bound to Rac1. (B) Expression of activated Trio GEF1 would yield a significant change in FRET at 525 nm (red traces) in the Rac1 biosensor (blue traces).

4.3 What are other Trio signaling pathways?

While our list of candidate Trio activators is a solid foundation for investigating Trio signaling pathways that regulate GEF1 activity, the list of candidate Trio interactors continues to emerge with growing proteomic and phosphoproteomic data.

To determine whether I could identify any novel interactors that interact with the Trio SR6-SH3-1 interface specifically, and therefore may be more likely to engage Trio SR6-GEF1 and activate GEF1 via relief of autoinhibition, I conducted preliminary pulldown assays to determine whether Trio SR6-SH3-1 pulled any proteins out of mouse whole brain lysate by incubating 8 μL Trio SR6-SH3-1 aminolink beads (1 μM) in 500 μL brain lysate, following the protocol outlined in Miller et al. 2010¹³⁴. Faint bands were visualized via Coomassie Blue Silver Stain, yet the amount of protein bound was too low to send out for mass spectrometry sequencing to identify the interactors. While one possibility is that the concentration of mouse brain lysate or Trio SR6-SH3-1 linked to beads was too low to get a detectable signal, another possibility to consider is that because Trio has been shown to interact with cell surface receptors, most Trio interactors may be present in the insoluble fraction of the cell lysate, and therefore would not be detectable by this method.

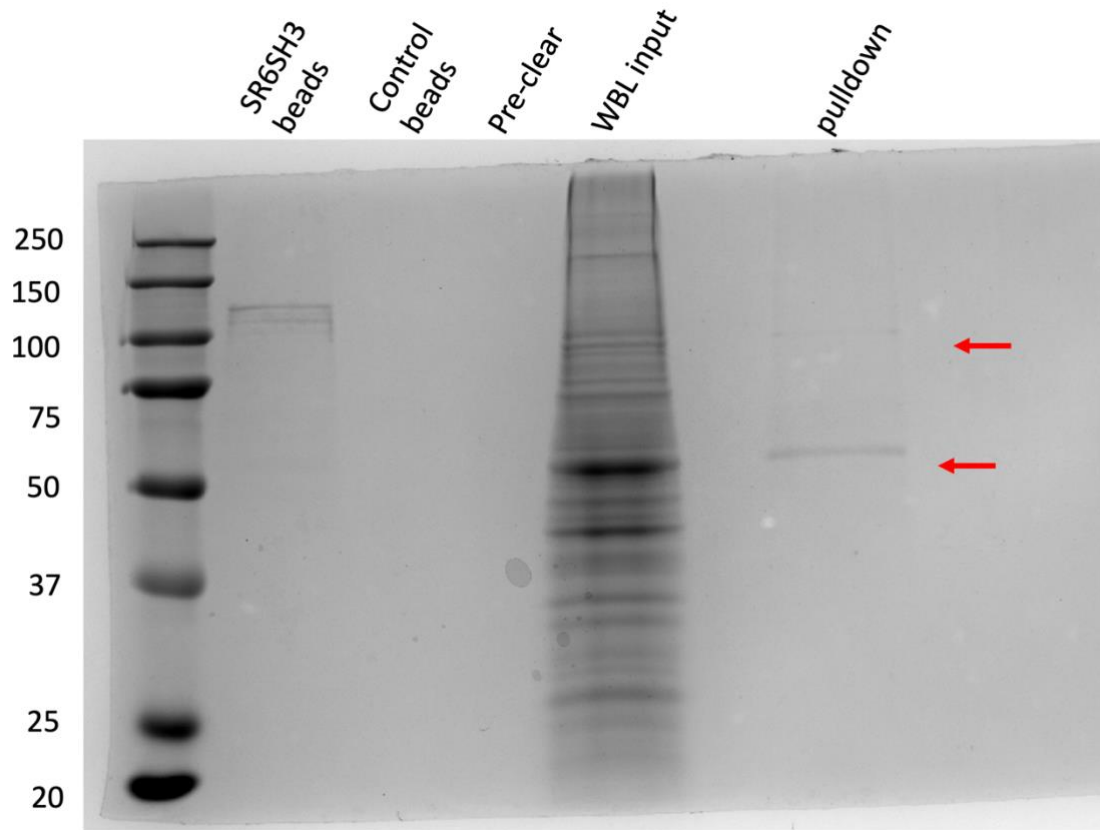


Fig 4.2 Preliminary identification of Trio interactors from mouse brain extract.

Trio SR6-SH3-1 (1 μ M) was incubated with 500 μ L mouse brain abstract (1 mg/mL). Bound proteins were analyzed by SDS-PAGE and stained with Coomassie Blue Silver.

4.4 Is there crosstalk between Trio GEF1 and GEF2?

When using AlphaFold to make structural predictions about Trio SR6-GEF1, we also generated a model of SR6-GEF2⁹¹. Intriguingly, the model predicts GEF2 docking close to GEF1, and both being nested within the spectrin repeats. This led us to hypothesize that one potential mode of Trio GEF1 regulation is by the GEF2 domain. This hypothesis is corroborated by our results shown in Fig 2.7, where cells expressing any variant of GFP-Trio9s lacked lamellipodia or cell edge protrusions, suggesting that the activity of GEF2 dominates over GEF1 in cells.

To better understand the biochemical mechanisms of cross-talk between GEF1 and GEF2, I generated a construct that extended from Trio SR6-GEF2 and purified from insect cells like Trio SR6-GEF1, detailed in Chapter 2. However, unlike Trio SR6-GEF1, SR6-GEF2 was significantly degraded even despite testing several standard different infection conditions. Therefore, we predict different purification methods will need to be tested to obtain SR6-GEF2 pure enough to test in biochemical assays, such as using dual tag affinity chromatography or ion exchange chromatography.

Once pure SR6-GEF2 is obtained, *in vitro* GEF assays can be used as the first step to understanding whether GEF2 activity impacts GEF1 activity. To do this, the catalytic rate of SR6-GEF2 could be measured with Rac1 bound to GDP-FL-BODIPY alone, or with both Rac1:GDP-FL-BODIPY and RhoA bound to non-fluorescent GDP added to the reaction mix. This experiment set-up could then be switched, with RhoA being bound to GDP-FL-BODIPY, to determine whether GEF2 activity is impacted by GEF1.

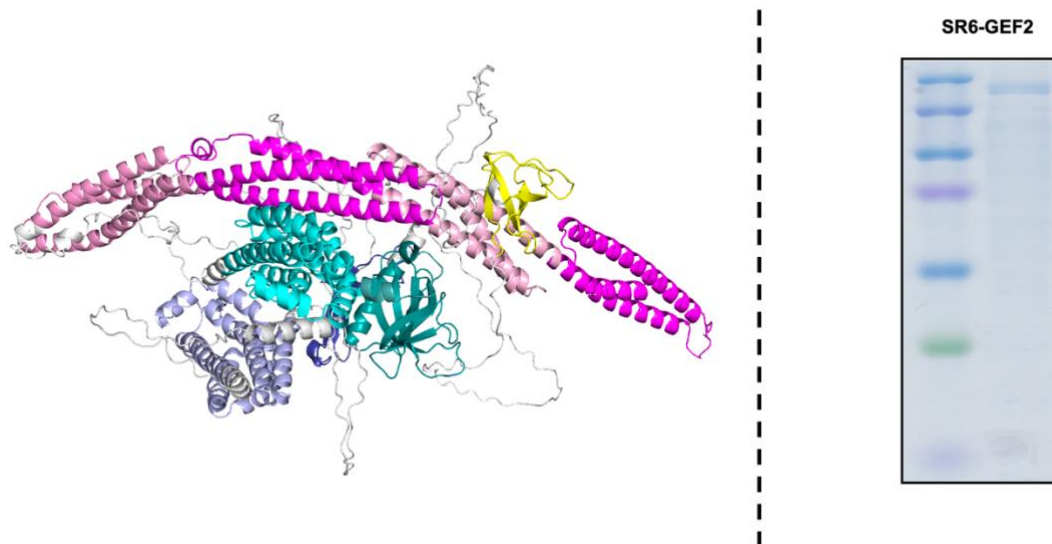


Fig 4.3 Structural Prediction and Purification of Trio SR6-GEF2.

Left: AlphaFold model of human Trio SR6-GEF1. SR6, 8 in dark pink, SR 7,9 in light pink, linker region in gray, GEF1 in blue, SH3-1 in yellow, GEF2 in purple.

Right: Purified Trio SR6-GEF2 (5 μg) was analyzed by SDS-PAGE and stained with Coomassie Blue R250 to assess purity.

4.5 Concluding Remarks

In this thesis, I sought to answer one fundamental Trio signaling question, which is how Trio GEF1 is regulated in cells. In Chapter One, I detail the set of biochemical tools I generated to probe Trio GEF1 signaling. Chapter Two includes my co-first author paper with former graduate student Josie Bircher, where we discovered a novel mechanism of autoinhibition of Trio GEF1 activity by the adjacent spectrin repeats. In Chapter Three, I describe my unpublished work to understand how Trio GEF1 is engaged and activated in a cellular context and discuss avenues for future directions of this work in Chapter Four. By understanding the mechanism of Trio GEF1 regulation in cells, understanding how disease variants disrupts these processes will be critical to guide the development of targeted therapeutic intervention.

Appendix

Table 1: Recombinant Trio Fragments

Construct	Strain Database code	Sequencing	Expression	Solubility	Affinity tag	MW (tag included)	Collaborator
pfB SR1 – GEF1	AJK2149 AJK2150	Sequenced approved; but only contains His Tag; MBP tag out of frame***	Expresses	Not Soluble	His ₆ (MBP out of frame)	162 kDa	Tony Koleske
PMAL SR1-GEF1	AJK2157 AJK2158	Sequence approved	Not Tested	Not Tested	MBP tag	204 kDa	Tony Koleske
pfB SR4-GEF1	AJK2151 AJK2152	Sequenced approved; only contains His tag; MBP tag out of frame	Expresses	Not Soluble	His (MBP out of frame)	120 kDa	Tony Koleske
pMAL SR4-GEF1	AJK2161 AJK2162	Sequence approved	Not Tested	Not Tested	MBP	120 kDa	Tony Koleske
pfB SR6-GEF1	AJK2153 AJK2154	Sequence approved	Expresses	Soluble	His ₆ ,	94 kDa	Tony Koleske
pfB SR6-GEF1 (WTS)	AJK2447	Sequence approved; stop codon inserted before out of frame MBP	Expresses	Soluble	His ₆	94 kDa	Made by Tony Koleske and Josie Bircher
pfB GEF1	AJK2147 AJK2148	Sequenced approved; only contains His tag	Not Tested	Not Tested	His ₆	42 kDa	Tony Koleske
pMAL GEF1	AJK2155 AJK2156	Sequence Approved	Not Tested	Not Tested	MBP	84 kDa	Tony Koleske
pET GEF1	AJK2080	Sequence Approved	Expresses	Soluble	His ₆	42 kDa	Made by Amanda Jeng and Tony Koleske
pGEX SR1-3	AJK2626	Sequence Approved	Expresses	Soluble	GST	69 kDa	Tony Koleske
pGEX SR4-6	AJK2627	Sequence Approved	Expresses	Soluble	GST	66 kDa	Tony Koleske
pGEX SR7-9	AJK2628	Sequence Approved	Expresses	Not Soluble	GST	66 kDa	Tony Koleske
pGEX SR6	AJK2577	Sequence Approved	Expresses	Soluble	GST	41 kDa	N.A.

pGEX SR8	AJK2578	Sequence Approved	Expresses	Soluble	GST	42 kDa	N.A.
pFB SR 1-9	AJK2317	Sequence approved	Expresses	Not Soluble	His ₆ , MBP	165 kDa	N.A.
pMAL SR1-9	AJK2220 AJK2221	Sequence Approved	Expresses	Not Soluble	MBP	165 kDa	N.A.
pGEX SR1-9	AJK2321	Sequence Approved	Expresses	Not Soluble	GST	150 kDa	Tony Koleske
pFB SR4-9	AJK2318	Sequence Approved	Expresses	Soluble	His	123 kDa	Tony Koleske
pMAL SR4-9	AJK2320	Sequence Approved	Expresses	Not soluble	MBP	123 kDa	N.A.
pGEX SR4-9	AJK2322	Sequence Approved	Expresses	Not soluble	GST	107 kDa	Tony Koleske
pFB SR6-9	AJK2319	Sequence Approved	Expresses	Soluble	His ₆ , MBP	97 kDa	Tony Koleske
pGEX SR6-9	AJK2323	Sequence Approved	Expresses	Soluble, difficult to get pure	GST	77 kDa	Tony Koleske
pGEX SR6-9	AJK2454	Sequence Approved	Expresses	Soluble	GST, His ₆	77 kDa	Josie Bircher, Tony Koleske
pFB SR1-SH3 (1)	AJK2690	Sequence Approved	Expresses	Not Soluble	His ₆	175 kDa	Josie Bircher, Tony Koleske
pFB SR4-SH3(1)	AJK2691	Sequence Approved	Expresses	Not Soluble	His ₆	133 kDa	Josie Bircher, Tony Koleske
pFB SR6 – SH31	AJK2692	Sequence Approved	Expresses	Soluble	His ₆	107 kDa	Josie Bircher, Tony Koleske
pGEX SH3 (1)	AJK2695	Sequence Approved	Expresses	Soluble	GST	33 kDa	N.A.
pET GEF2	AJK2080	Sequence Approved	Expresses	Soluble	His ₆	42 kDa	Made by Amanda Jeng and Tony Koleske
pGEX SH3 (2)	AJK2696	Sequence approved	Expresses	Soluble	GST	33 kDa	N.A.
pMAL Ig Kinase	AJK2222 AJK2223	Sequence approved	Expresses	Soluble	MBP	87 kDa	N.A.
pMAL Ig Kinase	AJK2434	Sequence approved	Expresses	Soluble	MBP, His ₆	87 kDa	Tony Koleske, Amand Jeng
Pfb SR1-GEF2	AJ2579	Not Sequence approved;	Not Tested	Not tested	His ₆	238 kDa	Tony Koleske

pFB SR6-GEF2	AJK2580	Sequence approved	Low Expression	Soluble, significant degradation	His ₆	169 kDa	Tony Koleske
Trio Duet (GEF2 – Kinase)	Not added; construct did not express	Sequence Approved, but doesn't express;	Does not express; something wrong	Not Tested	His ₆ , MBP	145 kDa	Tony Koleske

Table 2: Recombinant Trio Primer sequences

Construct	Strain Database code	Forward Primer	Reverse Primer	cDNA region amplified (FL Trio)	Notes
pfB SR1 – GEF1 (HTA-MCS-Precision-MBP)	AJK2149 AJK2150	GATCGAATTC CAGCTAACTC CTGAGTTTGAT	GATCCTCTA GATTTCCCT TCAGGTGG ATCGT	nt 589 - 4797	Trouble with solubility, crashes out running over S200
PMAL SR1-GEF1 (pMAL-TEV)	AJK2157 AJk2158	GATCGAATTC CAGCTAACTC CTGAGTTTGAT	GATCTCTA GATTATCCC TTCAGGTG GATCGT	nt 589 - 4797	Not tested, likely too big to purify from bacteria
pFB SR4-GEF1 (HTA-MCS-Precision-MBP)	AJK2151 AJK2152	GATCGAATTC AGGCTGCAGC TGTGTGTTTTTC	GATCCTCTA GATTTCCCT TCAGGTGG ATCGT	nt 1693 - 4797	Purifies but does not make over S200 in standard buffer
pMAL SR4-GEF1 (pMAL-TEV)	AJK2161 AJk2162	GATCGAATTC AGGCTGCAGC TGTGTGTTTTTC	GATCTCTA GATTATCCC TTCAGGTG GATCGT	nt 1693 - 4797	Not tested, likely too big to purify from bacteria
pfB SR6-GEF1 (HTA-MCS-Precision-MBP)	AJK2153 AJK2154	GATCGAATTC CTGCGCATCT TCGAGAGGGA C	GATCCTCTA GATTTCCCT TCAGGTGG ATCGT	nt 2362 - 4797	No stop codon, 12 extra aa at c-term
pfB SR6-GEF1 (WTS) (HTA-MCS-Precision-MBP)	AJK2447	GATCGAATTC CTGCGCATCT TCGAGAGGGA C	GATCCTCTA GACTATTTTC CCTTCAGG TGGATCGT	nt 2362 - 4797	Construct used in Bircher Corcoran 2022
pFB GEF1 (HTA-MCS-Precision-MBP)	AJK2147 AJK2148	GATCGAATTCT TGGAAAAAGC CCTGGGGATT	GATCCTCTA GATTTCCCT TCAGGTGG ATCGT	nt 3724 - 4797	No stop codon, 12 extra aa at c-term
pMAL GEF1 (pMAL-TEV)	AJK2155 AJK2156	GATCGAATTCT TGGAAAAAGC CCTGGGGATT	GATCTCTA GATTATCCC TTCAGGTG GATCGT	nt 3724 - 4797	Includes linker between SR9 and GEF1
petHIS GEF1	AJK2080	See Blaise et al., 2022	See Blaise et al., 2022	See Blaise et al., 2022	Made by Amanda Jeng and Tony Koleske

pGEX SR1-3 (pGEX-6p1)	AJK2626	GATCCGGAAT TCCCAGCTAA CTCCTGAGTTT GAT	GATCCTCG AGTTACTGA TGCAGCCG GACCTT	nt 589 - 1692	Sequenced and stop codon present!
pGEX SR4-6 (pGEX-6p1)	AJK2627	GATCGAATTC AGGCTGCAGC TGTGTGTTTTTC	GATCGCGG CCGCTTAC TGCTCCAG GTGTTTCC G	nt 1693 - 2715	Sequenced and stop codon present!
pGEX SR7-9 (pGEX-6p1)	AJK2628	GATCGAATTCT GCGTGCAGCT GCGCCACCTG	GATCGCGG CCGCTTAA GAGTCCCT GTAATTCTC	nt 2716 - 3723	Sequenced and stop codon present!
pGEX SR6 (pGEX-6p1)	AJK2577	GATC GAATTC CTGCGCATCT TCGAGAGGGA CGCCATCGAC ATT	GATCGCGG CCGCCTAC TGCTCCAG GTGTTTCC GATGCTGC TCTGC	nt 2362 - 2715	Never purified, only performed solubility test; primers made by Josie Bircher
pGEX SR8 (pGEX-6p1)	AJK2578	GATC GAATTC TCTGTGCTTTT CTACAAAACCT CAGAGCAGGT CTGCA	GATC GCGGCCGC CTACTG GTCCAG CCGTCT CTTCC	nt 3037 – 3408	Soluble, purifies; Primers made by Josie Bircher
pFB SR 1-9 (HTA-MCS- Precision- MBP)	AJK2317	GATCGAATTC CAGCTAACTC CTGAGTTTGAT	GATCTCTA GATTAAGA GGTCCTGT ACTTCTC	nt 589 - 3723	Trouble with solubility, crashes out running over S200
pMAL SR1-9 (pMAL-TEV)	AJK2220 AJK2221	GATCGAATTC CAGCTAACTC CTGAGTTTGAT	GATCTCTA GATTAAGA GGTCCTGT ACTTCTC	nt 589 - 3723	Trouble with solubility- try different buffer conditions
pGEX SR1-9 (pGEX-6p1)	AJK2321	GATCCGGAAT TCCCAGCTAA CTCCTGAGTTT GAT	GATCGCGG CCGCTTTAA GAGTCCCT GTAATTCT	nt 589 - 3723	Trouble with solubility- try different buffer conditions
pFB SR4-9 (HTA-MCS- Precision- MBP)	AJK2318	GATCGAATTC AGGCTGCAGC TGTGTGTTTTTC	GATCTCTA GATTAAGA GGTCCTGT ACTTCTC	nt 1693 - 3723	Trouble with solubility- try different buffer conditions
pMAL SR4-9 (pMAL-TEV)	AJK2320	GATCGAATTC AGGCTGCAGC TGTGTGTTTTTC	GATCTCTA GATTAAGA GGTCCTGT ACTTCTC	nt 1693 - 3723	Trouble with solubility- try different buffer conditions
pGEX SR4-9 (pGEX-6p1)	AJK2322	GATCCGGAAT TCCAGGCTGC AGCTGTGTGT TTT	GATCGCGG CCGCTTTAA GAGTCCCT GTAATTCT	nt 1693 - 3723	Trouble with solubility- try different buffer conditions
pFB SR6-9	AJK2319	GATCGAATTC CTGCGCATCT	GATCTCTA GATTAAGA	nt 2362 - 3723	Hard to get pure

(HTA-MCS-Precision-MBP)		TCGAGAGGGG C	GGTCCTGT ACTTCTC		
pMAL SR6-9 (pMAL-TEV)	AJK2323	GATCGAATTC CTGCGCATCT TCGAGAGGGG C	GATCTCTA GATTAAGA GGTCCTGT ACTTCTC	nt 2362 - 3723	Soluble in Tris 8
pFB SR1-SH3 (1) (HTA-MCS-Precision-MBP)	AJK2690	Made by JEB	Made by JEB	nt 589 - 5136	Primers made by Josie Bircher and Tony Koleske
pFB SR4-SH3(1) (HTA-MCS-Precision-MBP)	AJK2691	Made by JEB	Made by JEB	nt 1693 - 5136	Primers made by Josie Bircher and Tony Koleske
pFB SR6 – SH3(1) (HTA-MCS-Precision-MBP)	AJK2692	Made by JEB	Made by JEB	nt 2362 - 5136	Primers made by Josie Bircher and Tony Koleske
pGEX SH3 (1) (pGEX-6p1)	AJK2695	GATCGGATCC GGTGGCTGTG AGCTGACAGT G	GATCGAATT CTTAGGGG ACCAGGCC TTCTGCCG C	nt 4966 – 5136	Purifies well
Pet His GEF2	AJK2080	See Blaise et al., 2022	See Blaise et al., 2022	See Blaise et al., 2022	Made by Amanda Jeng and Tony Koleske
pGEX SH3 (2) (pGEX-6p1)	AJK2696	GATCGGATCC AGCAACATCT CCACCATGTT G	GATCGAATT CTTATGCAC TGGTGTGG CCCAGGAC	nt 7651 - 7848	Initial construct did not contain stop codon; had to remake
pMAL Ig Kinase (pMAL-TEV)	AJK2222 AJK2223	GATCGGATCC CCAGAATTCG TCATTCCATTG	GATCAAGC TTTTAGGCC TGCAGCCA CTGCTC	nt 8053 - 9294	Soluble, tag able to be cleaved and separated
pMAL Ig Kinase, His ₆ tag (pMAL TEV)	AJK2434	Made by ATJ	Made by ATJ	nt 8053 - 9294	Purifies well; primers made by Amanda Jeng

Pfb SR1- GEF2 (HTA-MCS- Precision- MBP)	AJ2579	GATCGAATTC CAGCTAACTC CTGAGTTTGAT	GATCTCTA GATTACCCT TCTAAAATT TGGTTGAT	nt 589 - 6813	Tried to express and does not work; do not use
pFB SR6- GEF2 (HTA-MCS- Precision- MBP)	AJ2580	GATCGAATTC CTGCGCATCT TCGAGAGGGA C	GATCTCTA GATTACCCT TCTAAAATT TGGTTGAT	nt 2362 - 6813	Significant degradation
Trio Duet (GEF2 – Kinase) (HTA-MCS- Precision- MBP)	Not added	GATC CGT CGA CGA AACACCCTGC GCAAGTGG	GATCTCTA GAAACTCTA GGCAGAAG CCTGCT	nt 5311 – 9291	Does not express but sequencing looks good; would still remake

Table 3: Primer sequences and vectors used for Trio constructs. Table adapted from Bircher, Corcoran et al., 2022

construct	nt change	primer seq fwd (5'-3')	primer seq rev (5'-3')	vector
R877W	c2629t	AGAGATGTAGACATGGCAACTGGGTCCAGGAC	GTCTGGACCCAAGTTGCCATGTCTACATCTCT	pFb-HTA
T1075I	c3224t	TTCTGAAGGCTTGATCCTTGCTCGGAGG	CCTCCGAGCAAGGATGCAAGCCTTCAGGAA	pFb-HTA
T1075P	a3223c	CCTGAAGGCTTGCCCCCTTGCTCGGAG	CTCCGAGCAAGGGGCAAGCCTTCAGG	pFb-HTA
R1078W	c3232t	GGCTTGACCCCTTGCTGGAGGAATGCAG	CTGCATTCTCCAAGCAAGGGTGCAAGCC	pFb-HTA
R1078G	c3232g	GGCTTGACCCCTTGCTGGAGGAATGCAG	CTGCATTCTCCAAGCAAGGGTGCAAGCC	pFb-HTA
R1078Q	g3233a	CTTGACCCCTTGCTCAGAGGAATGCAGACGT	ACGTCTGCATTCTCTGAGCAAGGGTGCAAG	pFb-HTA
R1145G	a3433g	TACGTGGTCTTTGAGGGGAGTCCAAGCAGG	CCTGCTGGCACTCCCCTCAAAGACCAAGTA	pFb-HTA
E883D	g2649t	GTCCAGGACCTGCTGGATTTCTCATGAAAACAG	CTGTTTTTCATGAAGAAAATCCAGCAGGTCCTGGAC	pFb-HTA
D1368V	a4103t	gtaacaaacaatgtccaacaacctctggcaactgttcatt	aatatgaacagttgccagaggttgggacattgtttgttac	pFb-HTA
SR6-GEF1	WT	GATCGAATTCCTGCGCATCTTCGAGAGGGAC	GATCCTTAGActaTTCCCTTCAGGTGGATCGT	pFb-HTA
N1080I	a3239t	gaagacgtctgcaatcctccgagcaagggt	acccttctggaggattgcagacgtcttc	pFb-HTA
L1124S	t3371c	tggtccaagtaatgcgataacctgttctccggtg	caacgggagaacagggtatgcattactggacca	pFb-HTA
GEF1	see Blaise et al, 2021			pET-His-TT
Rac1	see Blaise et al, 2021			pGEX-6P1
px1-GEF1-GFP	WT	GATCGTTAACGGCTCAGAGGTGAAACTTCGAGATGCTGCTC	GATCGCGCCGCTCCCTTCAGGTGGATCGTCCGCTCCTGGATGA	px1-HA-GFP
px1-SR6-GEF1-GFP	WT	GATCGTTAACCTGCGCATCTTCGAGAGGGACGCCATCGACA	GATCGCGCCGCTCCCTTCAGGTGGATCGTCCGCTCCTGGATGA	px1-HA-GFP
px1-GEF1-GFP ND/AA	a4393g/a4394c/a439t	GTC CCG AAG CGA GCC GCT GCC GCC ATG CAC CTC AG	CTG AGG TGC ATG GCG GCA GCG GCT CGC TTC GGC AC	px1-HA-GFP

Table 4: Candidate Protein Activators of Trio

Activator	Protein Class	Known impact on Trio Signaling	Known Interaction	Reference
ADAM22	Adhesion	Lower ADAM22 expression levels are correlated with loss of Trio	Unknown	Katrancha et al, 2019
ADAM23	Adhesion	Lower ADAM23 expression levels are correlated with loss of Trio	GST-ADAM23 pulls down Trio9s from cell lysate (preliminary data from Josie Bircher)	Katrancha et al., 2019
DCC	Netrin receptor	Trio is required for Netrin-1 mediated stimulation of Rac1 and neurite and axon outgrowth	Unknown	Briancon-Marjollet et al., 2008
ICAM1	Adhesion	Trio directly interacts with ICAM1 intracellular tail; ICAM1 clustering promotes Rac1 activation in cells	Pulling down Myc-Trio FL or Myc-Trio GEF1 pulls down ICAM1 when both overexpressed in cells	Van rijssel et al., 2012
Kidins220	Adaptor	Trio SRs directly interact with Kidins220; interaction correlates with increased Rac1 levels in cells	Trio Sec14, SR 1-4, SR5-9 directly interact with Kidins220 ankryin repeats	Neubrand et al., 2010
L1CAM	Adhesion	Lower expression levels of L1	Unknown	Katrancha et al., 2019

NLGN1	Adhesion	ASD mutation N1080I (SR8) inhibits interaction with NLGN1, blocks NLGN-1 mediated synaptogenesis in cells	Coimmunoprecipitates with Trio9; CO-IP reduced with N1080I mutation	Tian et al., 2021
VE-Cadherin	Adhesion	Trio SRs directly interact with VE-Cadherin intracellular tail; interaction correlates with increased Rac1 levels in cells	Trio SRs 5-6 interact with VE-Cadherin tail	Timmerman et al, 2015

Table 5: Primer sequences used for candidate activators of Trio

Construct	Strain Database Code	Forward Primer	Reverse Primer	Region of protein amplified	Notes
ADAM22 _{tail}	AJK2411	Made by ATJ	Made by ATJ	aa 804-859	Generated by Amanda Jeng and Tony Koleske
ADAM23 _{tail}	AJK2328	Made by ATJ	Made by ATJ	aa 814-832	Generated by Amanda Jeng and Tony Koleske
DCC _{tail}	AJK2693	GATC GAATTC atttgaccgacgct ctca	GATCCTCGA Gttaaaggct gagcctgtgaT	aa 1120-1445	Trouble with solubility
ICAM1 _{tail}	AJK2581	GAT CGA ATT CAA CCG CCA GCG GAA GAT CAAGAAATA CAG AC	GATCGCG GCCGCTC AGGGAG GCGTGCC TTGT	aa 504-532	Purifies well; primers made by Josie Bircher
Kidins220 ankyrin repeats	AJK2629	GATC GAATTC GGGATGTCA GTTCTTATAT CACAG	GATCGC GGCCGC TTATTTG TTGGGTC TG TAGAG	aa 1-402	Trouble with Solubility
L1CAM _{tail}	AJK2325	Made by ATJ	Made by ATJ	aa 1144-1257	Generated by Amanda Jeng and Tony Koleske
NLGN1 _{tail}	AJK2631	GATC GAATTC AGACATGATGTC CACCGGAGG	GATCGCGG CCGCCTATA CCCTGGTTG TTGAATG	aa 714-843	Some degradation
VE-Cadherin _{tail}	AJK2630	GATC GAATTC CGGCGGCGGCT CCGGAAGCAGG CCCGCGCG	GATCGC GGCCGC CTAATAC AGCAGCT CCTCCCG GGGGTC CGAGCC GT	aa 621-784	Relatively low expression ; primers made by Josie Bircher

Table 6: Trio and Kalirin phosphorylation peptide sequences

residue hTrio	domain hTrio	peptide sequence hTrio	Peptide sequence kalirin
S109	SR3	RRLIpSYLACIPSEEVCKRG	K.LVpTYLASVPSEDEVCKR.G
T517	SR3	KSLLDKLRPLpTPGSSDSL TASA NYSKA	K.AL LDVLRPLpSPGNSESLTATAN YSK.A
T622	SR4	KRHEDFEEVAQNTYpTNAKI	K.RHDDFEEVAQNTYpTNADK.I
T637	SR4	KLLEAAEQLAQpTGECDP EEIYQA	K.LLEAAEQLAQpTGECDP EEIYK.A
S702	SR5	KELLDDVYAEpSVEAVQDLIKR	K.EVLEDVCADpSVD AVQELIK.Q
T960	SR7	KpTHQSALQVQQKA	K.pTHQSALQVQQK.A
Y980	SR7	KAEAMLQANH pYDMDMIRDCAEK V	K.AEALLQAGH pYDADAIRECAEK.V
T1019	SR8	KpTSEQVCSVLESLEQEYRR	K.pTSEQVCSVLESLEQEYR.R
S1020	SR8	KTpSEQVCSVLESLEQEYRR	K.TpSEQVCSVLESLEQEYR.R
T1128	SR8	VLHYWpTMRK	R.VLHFWpTLK.K
S1232	SR9	RDFpSLRM	R.DFpSLR.M
T1539	PH1	KLFpTSELGVTEGHVEDPCKF	K.LLpTSELGVTEHVEGD PCK.F
S1540	PH1	KLFTpSELGVTEHGVEDPCKF	K.LLTpSELGVTEHVEGD PCK.F
S1627	linker	RRDG- EDLDpSQGDGSSQPDTISIASRT	K.RDGVEDGDpSQGDGSSQPDTISIA SR.T
S1632	linker	RDG- EDLDSQGDGpSSQPDTISIASRT	R.DGVEDGDSQGDGpSSQPDTISIAS R.T

Table 7: Evolutionarily conserved Trio and Kalirin phosphorylation residues

residue hTrio	domain hTrio	kinase	evolution conservation
S109	SR3	CAMKII, PKA, PKC	yes
T517	SR3	n.a	yes
T622	SR4	Fyn - 591	no
T637	SR4	n.a	yes - kalrn trio same gene
S702	SR5	n.a	yes
T960	SR7	n.a	yes
Y980	SR7	n.a	yes
T1019	SR8	CKII, CAMKII	yes
S1020	SR8	CKII, CAMKII	yes
T1128	SR8	n.a	yes
S1232	SR9	n.a	yes - kalrn trio same gene
T1539	PH1	n.a	yes
S1540	PH1	CKII, CAMKII, PKC	yes - kalrn trio same gene
S1627	linker	CKII	yes
S1632	linker	n.a	yes

Table 8: Primer sequences and vectors used for isosteric phosphomimic Trio SR6-GEF1 constructs

Construct	Strain Database Code	Forward Primer	Reverse Primer	Vector
T960E	AJK2682	agcgcgctctgatgctctttctc aatggcatgctggaactgc	gcagttccagcatgccattgaga aagagcatcagagcgcgct	pFB-HTA
T1019E, S1020D	AJK2683	cgctgcagacctgctcatcctc ttgtagaaagcgacagaggc gttgacgag	ctcgtcaacgcctctgctgctttct acaaagaggatgagcaggctc gcagcg	pFB-HTA
T1019E	AJK2684	gcagacctgctctgactctttgt agaaagcgacagaggcgttg	caacgcctctgctgctttctacaa agagtcaagcagcaggctctgc	pFB-HTA
S1020D	AJK2685	ggacgctgcagacctgctcat cggttttgtagaaagcgaca	tgtcgtttctacaaaaccgatga gcaggctgcagcgtcc	pFB-HTA
T1128E	AJK2686	ccagccgtctcttctcatctcc cagtaatgaataacctg	cagggattgcattactgggaga tgaggaagagacggctgg	pFB-HTA
S1232D	AJK2687	gtacttctccatccgcagatcg aaatctctgtacctcttatcc	ggataagaggtacagagattc gatctgcggatggagaagtac	pFB-HTA
T1539E	AJK2688	tgtgacaccaactctgactca aacaattgctttataaaggta ctgcttctcc	ggagaagcaagtacctttataa aagcaaattggttgagtcagagtt gggtgtcaca	pFB-HTA
S1540D	AJK2689	ttaacatgttctgtgacacca actcatcggtaaacaattgctt tataaaggta	taccttataaaaagcaaattgtta ccgatgagttgggtgtcacagaa catgtgaa	pFB-HTA

References

1. Murray CJ, Collaborators USBoD. The state of US health, 1990-2010: burden of diseases, injuries, and risk factors. *JAMA*. 2013;310(6):591-608. Epub 2013/07/12. doi: 10.1001/jama.2013.13805. PubMed PMID: 23842577; PMCID: PMC5436627.
2. Knapp M, Mangalore R, Simon J. The global costs of schizophrenia. *Schizophr Bull*. 2004;30(2):279-93. Epub 2004/07/29. doi: 10.1093/oxfordjournals.schbul.a007078. PubMed PMID: 15279046.
3. Cloutier M, Greene M, Guerin A, Touya M, Wu E. The economic burden of bipolar I disorder in the United States in 2015. *Journal of Affective Disorders*. 2018;226:45-51. doi: <https://doi.org/10.1016/j.jad.2017.09.011>.
4. Keshavan MS, Lawler AN, Nasrallah HA, Tandon R. New drug developments in psychosis: Challenges, opportunities and strategies. *Prog Neurobiol*. 2017;152:3-20. Epub 2016/08/16. doi: 10.1016/j.pneurobio.2016.07.004. PubMed PMID: 27519538; PMCID: PMC5362348.
5. Remington G, Foussias G, Fervaha G, Agid O, Takeuchi H, Lee J, Hahn M. Treating Negative Symptoms in Schizophrenia: an Update. *Curr Treat Options Psychiatry*. 2016;3:133-50. Epub 2016/07/05. doi: 10.1007/s40501-016-0075-8. PubMed PMID: 27376016; PMCID: PMC4908169.
6. Owen MJ, Sawa A, Mortensen PB. Schizophrenia. *Lancet*. 2016;388(10039):86-97. Epub 2016/01/19. doi: 10.1016/s0140-6736(15)01121-6. PubMed PMID: 26777917; PMCID: PMC4940219.
7. Katrancha SM, Wu Y, Zhu M, Eipper BA, Koleske AJ, Mains RE. Neurodevelopmental disease-associated de novo mutations and rare sequence variants affect TRIO GDP/GTP exchange factor activity. *Hum Mol Genet*. 2017;26(23):4728-40. Epub 2017/10/04. doi: 10.1093/hmg/ddx355. PubMed PMID: 28973398; PMCID: PMC5886096.
8. Smrt RD, Zhao X. Epigenetic regulation of neuronal dendrite and dendritic spine development. *Front Biol (Beijing)*. 2010;5(4):304-23. doi: 10.1007/s11515-010-0650-0. PubMed PMID: 25635180.
9. Kulkarni VA, Firestein BL. The dendritic tree and brain disorders. *Mol Cell Neurosci*. 2012;50(1):10-20. Epub 2012/04/03. doi: 10.1016/j.mcn.2012.03.005. PubMed PMID: 22465229.
10. van Spronsen M, Hoogenraad CC. Synapse pathology in psychiatric and neurologic disease. *Curr Neurol Neurosci Rep*. 2010;10(3):207-14. Epub 2010/04/29. doi: 10.1007/s11910-010-0104-8. PubMed PMID: 20425036; PMCID: PMC2857788.
11. Blanpied TA, Ehlers MD. Microanatomy of dendritic spines: emerging principles of synaptic pathology in psychiatric and neurological disease. *Biol Psychiatry*. 2004;55(12):1121-7. Epub 2004/06/09. doi: 10.1016/j.biopsych.2003.10.006. PubMed PMID: 15184030.
12. Glantz LA, Lewis DA. Decreased dendritic spine density on prefrontal cortical pyramidal neurons in schizophrenia. *Arch Gen Psychiatry*. 2000;57(1):65-73. Epub 2000/01/13. doi: 10.1001/archpsyc.57.1.65. PubMed PMID: 10632234.

13. Konopaske GT, Lange N, Coyle JT, Benes FM. Prefrontal cortical dendritic spine pathology in schizophrenia and bipolar disorder. *JAMA Psychiatry*. 2014;71(12):1323-31. Epub 2014/10/02. doi: 10.1001/jamapsychiatry.2014.1582. PubMed PMID: 25271938; PMCID: PMC5510541.
14. Hutsler JJ, Zhang H. Increased dendritic spine densities on cortical projection neurons in autism spectrum disorders. *Brain Res*. 2010;1309:83-94. Epub 2009/11/10. doi: 10.1016/j.brainres.2009.09.120. PubMed PMID: 19896929.
15. Fromer M, Pocklington AJ, Kavanagh DH, Williams HJ, Dwyer S, Gormley P, Georgieva L, Rees E, Palta P, Ruderfer DM, Carrera N, Humphreys I, Johnson JS, Roussos P, Barker DD, Banks E, Milanova V, Grant SG, Hannon E, Rose SA, Chambert K, Mahajan M, Scolnick EM, Moran JL, Kirov G, Palotie A, McCarroll SA, Holmans P, Sklar P, Owen MJ, Purcell SM, O'Donovan MC. De novo mutations in schizophrenia implicate synaptic networks. *Nature*. 2014;506(7487):179-84. Epub 2014/01/22. doi: 10.1038/nature12929. PubMed PMID: 24463507.
16. Jiang Y, Han Y, Petrovski S, Owzar K, Goldstein DB, Allen AS. Incorporating Functional Information in Tests of Excess De Novo Mutational Load. *American journal of human genetics*. 2015;97(2):272-83. Epub 2015/07/30. doi: 10.1016/j.ajhg.2015.06.013. PubMed PMID: 26235986.
17. Penzes P, Cahill ME, Jones KA, VanLeeuwen J-E, Woolfrey KM. Dendritic spine pathology in neuropsychiatric disorders. *Nat Neurosci*. 2011;14(3):285-93. doi: 10.1038/nn.2741. PubMed PMID: 21346746.
18. Lee SH, Wray NR. Genetic relationship between five psychiatric disorders estimated from genome-wide SNPs. *Nat Genet*. 2013;45(9):984-94. Epub 2013/08/13. doi: 10.1038/ng.2711. PubMed PMID: 23933821; PMCID: PMC3800159.
19. McCarthy SE, Gillis J, Kramer M, Lihm J, Yoon S, Berstein Y, Mistry M, Pavlidis P, Solomon R, Ghiban E, Antoniou E, Kelleher E, O'Brien C, Donohoe G, Gill M, Morris DW, McCombie WR, Corvin A. De novo mutations in schizophrenia implicate chromatin remodeling and support a genetic overlap with autism and intellectual disability. *Mol Psychiatry*. 2014;19(6):652-8. Epub 2014/04/29. doi: 10.1038/mp.2014.29. PubMed PMID: 24776741.
20. Zhou Y, Kaiser T, Monteiro P, Zhang X, Van der Goes MS, Wang D, Barak B, Zeng M, Li C, Lu C, Wells M, Amaya A, Nguyen S, Lewis M, Sanjana N, Zhou Y, Zhang M, Zhang F, Fu Z, Feng G. Mice with Shank3 Mutations Associated with ASD and Schizophrenia Display Both Shared and Distinct Defects. *Neuron*. 2016;89(1):147-62. Epub 2015/12/10. doi: 10.1016/j.neuron.2015.11.023. PubMed PMID: 26687841.
21. Anttila V, Murray R. Analysis of shared heritability in common disorders of the brain. *Science*. 2018;360(6395). Epub 2018/06/23. doi: 10.1126/science.aap8757. PubMed PMID: 29930110; PMCID: PMC6097237.
22. Sanders SJ, Murtha MT, Gupta AR, Murdoch JD, Raubeson MJ, Willsey AJ, Ercan-Sencicek AG, DiLullo NM, Parikshak NN, Stein JL, Walker MF, Ober GT, Teran NA, Song Y, El-Fishawy P, Murtha RC, Choi M, Overton JD, Bjornson RD, Carriero NJ, Meyer KA, Bilguvar K, Mane SM, Sestan N, Lifton RP, Gunel M, Roeder K, Geschwind DH, Devlin B, State MW. De novo mutations revealed by

- whole-exome sequencing are strongly associated with autism. *Nature*. 2012;485(7397):237-41. Epub 2012/04/13. doi: 10.1038/nature10945. PubMed PMID: 22495306; PMCID: PMC3667984.
23. De Rubeis S, Buxbaum JD. Synaptic, transcriptional and chromatin genes disrupted in autism. *Nature*. 2014;515(7526):209-15. Epub 2014/11/05. doi: 10.1038/nature13772. PubMed PMID: 25363760; PMCID: PMC4402723.
24. Pengelly RJ, Greville-Heygate S, Schmidt S, Seaby EG, Jabalameli MR, Mehta SG, Parker MJ, Goudie D, Fagotto-Kaufmann C, Mercer C, Study DDD, Debant A, Ennis S, Baralle D. Mutations specific to the Rac-GEF domain of TRIO cause intellectual disability and microcephaly. *J Med Genet*. 2016;53(11):735-42. Epub 2016/07/16. doi: 10.1136/jmedgenet-2016-103942. PubMed PMID: 27418539; PMCID: PMC5264232.
25. Sadybekov A, Tian C, Arnesano C, Katritch V, Herring BE. An autism spectrum disorder-related de novo mutation hotspot discovered in the GEF1 domain of Trio. *Nat Commun*. 2017;8(1):601. Epub 2017/09/21. doi: 10.1038/s41467-017-00472-0. PubMed PMID: 28928363; PMCID: PMC5605661.
26. Iossifov I, O'Roak BJ, Sanders SJ, Ronemus M, Krumm N, Levy D, Stessman HA, Witherspoon KT, Vives L, Patterson KE, Smith JD, Paepers B, Nickerson DA, Dea J, Dong S, Gonzalez LE, Mandell JD, Mane SM, Murtha MT, Sullivan CA, Walker MF, Waqar Z, Wei L, Willsey AJ, Yamrom B, Lee YH, Grabowska E, Dalkic E, Wang Z, Marks S, Andrews P, Leotta A, Kendall J, Hakker I, Rosenbaum J, Ma B, Rodgers L, Troge J, Narzisi G, Yoon S, Schatz MC, Ye K, McCombie WR, Shendure J, Eichler EE, State MW, Wigler M. The contribution of de novo coding mutations to autism spectrum disorder. *Nature*. 2014;515(7526):216-21. Epub 2014/11/05. doi: 10.1038/nature13908. PubMed PMID: 25363768; PMCID: PMC4313871.
27. de Ligt J, Willemsen MH, van Bon BW, Kleefstra T, Yntema HG, Kroes T, Vulto-van Silfhout AT, Koolen DA, de Vries P, Gilissen C, del Rosario M, Hoischen A, Scheffer H, de Vries BB, Brunner HG, Veltman JA, Vissers LE. Diagnostic exome sequencing in persons with severe intellectual disability. *N Engl J Med*. 2012;367(20):1921-9. Epub 2012/10/05. doi: 10.1056/NEJMoa1206524. PubMed PMID: 23033978.
28. Rauch A, Wieczorek D, Graf E, Wieland T, Ende S, Schwarzmayr T, Albrecht B, Bartholdi D, Beygo J, Di Donato N, Dufke A, Cremer K, Hempel M, Horn D, Hoyer J, Joset P, Ropke A, Moog U, Riess A, Thiel CT, Tzschach A, Wiesener A, Wohlleber E, Zweier C, Ekici AB, Zink AM, Rump A, Meisinger C, Grallert H, Sticht H, Schenck A, Engels H, Rappold G, Schrock E, Wieacker P, Riess O, Meitinger T, Reis A, Strom TM. Range of genetic mutations associated with severe non-syndromic sporadic intellectual disability: an exome sequencing study. *Lancet*. 2012;380(9854):1674-82. Epub 2012/10/02. doi: 10.1016/s0140-6736(12)61480-9. PubMed PMID: 23020937.
29. Ba W, Yan Y, Reijnders MR, Schuurs-Hoeijmakers JH, Feenstra I, Bongers EM, Bosch DG, De Leeuw N, Pfundt R, Gilissen C, De Vries PF, Veltman JA, Hoischen A, Mefford HC, Eichler EE, Vissers LE, Nadif Kasri N, De Vries BB. TRIO loss of function is associated with mild intellectual disability and affects dendritic branching and synapse function. *Hum Mol Genet*. 2016;25(5):892-902. Epub

- 2016/01/02. doi: 10.1093/hmg/ddv618. PubMed PMID: 26721934; PMCID: PMC4754042.
30. Large-scale discovery of novel genetic causes of developmental disorders. *Nature*. 2015;519(7542):223-8. Epub 2014/12/24. doi: 10.1038/nature14135. PubMed PMID: 25533962; PMCID: PMC5955210.
31. Singh T, Daly MJ. Exome sequencing identifies rare coding variants in 10 genes which confer substantial risk for schizophrenia. medRxiv. 2020:2020.09.18.20192815. doi: 10.1101/2020.09.18.20192815.
32. Barbosa S, Debant A, Schmidt S, Baralle D. Opposite Modulation of RAC1 by Mutations in TRIO Is Associated with Distinct, Domain-Specific Neurodevelopmental Disorders. *Am J Hum Genet*. 2020;106(3):338-55. Epub 2020/02/29. doi: 10.1016/j.ajhg.2020.01.018. PubMed PMID: 32109419; PMCID: PMC7058823.
33. Lek M, MacArthur DG. Analysis of protein-coding genetic variation in 60,706 humans. *Nature*. 2016;536(7616):285-91. Epub 2016/08/19. doi: 10.1038/nature19057. PubMed PMID: 27535533; PMCID: PMC5018207.
34. Samocha KE, Robinson EB, Sanders SJ, Stevens C, Sabo A, McGrath LM, Kosmicki JA, Rehnstrom K, Mallick S, Kirby A, Wall DP, MacArthur DG, Gabriel SB, DePristo M, Purcell SM, Palotie A, Boerwinkle E, Buxbaum JD, Cook EH, Jr., Gibbs RA, Schellenberg GD, Sutcliffe JS, Devlin B, Roeder K, Neale BM, Daly MJ. A framework for the interpretation of de novo mutation in human disease. *Nat Genet*. 2014;46(9):944-50. Epub 2014/08/05. doi: 10.1038/ng.3050. PubMed PMID: 25086666; PMCID: PMC4222185.
35. Debant A, Serra-Pages C, Seipel K, O'Brien S, Tang M, Park SH, Streuli M. The multidomain protein Trio binds the LAR transmembrane tyrosine phosphatase, contains a protein kinase domain, and has separate rac-specific and rho-specific guanine nucleotide exchange factor domains. *Proc Natl Acad Sci U S A*. 1996;93(11):5466-71. Epub 1996/05/28. doi: 10.1073/pnas.93.11.5466. PubMed PMID: 8643598; PMCID: PMC39269.
36. Bellanger JM, Estrach S, Schmidt S, Briancon-Marjollet A, Zugasti O, Fromont S, Debant A. Different regulation of the Trio Dbl-Homology domains by their associated PH domains. *Biol Cell*. 2003;95(9):625-34. Epub 2004/01/15. PubMed PMID: 14720465.
37. Bateman J, Van Vactor D. The Trio family of guanine-nucleotide-exchange factors: regulators of axon guidance. *J Cell Sci*. 2001;114(Pt 11):1973-80. Epub 2001/08/09. PubMed PMID: 11493634.
38. Miller MB, Yan Y, Eipper BA, Mains RE. Neuronal Rho GEFs in synaptic physiology and behavior. *Neuroscientist*. 2013;19(3):255-73. Epub 2013/02/13. doi: 10.1177/1073858413475486. PubMed PMID: 23401188; PMCID: PMC3927235.
39. Hall A. Rho GTPases and the actin cytoskeleton. *Science*. 1998;279(5350):509-14. Epub 1998/02/07. doi: 10.1126/science.279.5350.509. PubMed PMID: 9438836.
40. Hall A, Lalli G. Rho and Ras GTPases in axon growth, guidance, and branching. *Cold Spring Harb Perspect Biol*. 2010;2(2):a001818. Epub 2010/02/26.

- doi: 10.1101/cshperspect.a001818. PubMed PMID: 20182621; PMCID: PMC2828272.
41. Penzes P, Johnson RC, Kambampati V, Mains RE, Eipper BA. Distinct roles for the two Rho GDP/GTP exchange factor domains of kalirin in regulation of neurite growth and neuronal morphology. *J Neurosci*. 2001;21(21):8426-34. Epub 2001/10/19. PubMed PMID: 11606631.
 42. Bellanger JM, Lazaro JB, Diriong S, Fernandez A, Lamb N, Debant A. The two guanine nucleotide exchange factor domains of Trio link the Rac1 and the RhoA pathways in vivo. *Oncogene*. 1998;16(2):147-52. Epub 1998/02/17. doi: 10.1038/sj.onc.1201532. PubMed PMID: 9464532.
 43. Blangy A, Vignal E, Schmidt S, Debant A, Gauthier-Rouviere C, Fort P. TrioGEF1 controls Rac- and Cdc42-dependent cell structures through the direct activation of rhoG. *J Cell Sci*. 2000;113 (Pt 4):729-39. Epub 2000/02/01. PubMed PMID: 10652265.
 44. Vishwanatha KS, Wang YP, Keutmann HT, Mains RE, Eipper BA. Structural organization of the nine spectrin repeats of Kalirin. *Biochemistry*. 2012;51(28):5663-73. Epub 2012/06/29. doi: 10.1021/bi300583s. PubMed PMID: 22738176; PMCID: PMC3447990.
 45. Saito K, Tautz L, Mustelin T. The lipid-binding SEC14 domain. *Biochim Biophys Acta*. 2007;1771(6):719-26. Epub 2007/04/13. doi: 10.1016/j.bbali.2007.02.010. PubMed PMID: 17428729.
 46. Schiller MR, Ferraro F, Wang Y, Ma XM, McPherson CE, Sobota JA, Schiller NI, Mains RE, Eipper BA. Autonomous functions for the Sec14p/spectrin-repeat region of Kalirin. *Experimental cell research*. 2008;314(14):2674-91. doi: 10.1016/j.yexcr.2008.05.011. PubMed PMID: 18585704; PMCID: 2613971.
 47. McPherson CE, Eipper BA, Mains RE. Multiple novel isoforms of Trio are expressed in the developing rat brain. *Gene*. 2005;347(1):125-35. doi: <https://doi.org/10.1016/j.gene.2004.12.028>.
 48. Portales-Casamar E, Briançon-Marjollet A, Fromont S, Triboulet R, Debant A. Identification of novel neuronal isoforms of the Rho-GEF Trio. *Biology of the Cell*. 2006;98(3):183-93. doi: 10.1042/bc20050009.
 49. Awasaki T, Saito M, Sone M, Suzuki E, Sakai R, Ito K, Hama C. The Drosophila trio plays an essential role in patterning of axons by regulating their directional extension. *Neuron*. 2000;26(1):119-31. Epub 2000/05/08. doi: 10.1016/s0896-6273(00)81143-5. PubMed PMID: 10798397.
 50. Bateman J, Shu H, Van Vactor D. The guanine nucleotide exchange factor trio mediates axonal development in the Drosophila embryo. *Neuron*. 2000;26(1):93-106. Epub 2000/05/08. doi: 10.1016/s0896-6273(00)81141-1. PubMed PMID: 10798395.
 51. Bellanger JM, Astier C, Sardet C, Ohta Y, Stossel TP, Debant A. The Rac1- and RhoG-specific GEF domain of Trio targets filamin to remodel cytoskeletal actin. *Nat Cell Biol*. 2000;2(12):888-92. Epub 2001/01/09. doi: 10.1038/35046533. PubMed PMID: 11146652.
 52. O'Brien SP, Seipel K, Medley QG, Bronson R, Segal R, Streuli M. Skeletal muscle deformity and neuronal disorder in Trio exchange factor-deficient mouse

- embryos. *Proceedings of the National Academy of Sciences*. 2000;97(22):12074-8. doi: 10.1073/pnas.97.22.12074.
53. Katrancha SM, Shaw JE, Zhao AY, Myers SA, Cocco AR, Jeng AT, Zhu M, Pittenger C, Greer CA, Carr SA, Xiao X, Koleske AJ. Trio Haploinsufficiency Causes Neurodevelopmental Disease-Associated Deficits. *Cell Rep*. 2019;26(10):2805-17 e9. Epub 2019/03/07. doi: 10.1016/j.celrep.2019.02.022. PubMed PMID: 30840899; PMCID: PMC6436967.
54. Steven R, Kubiseski TJ, Zheng H, Kulkarni S, Mancillas J, Ruiz Morales A, Hogue CW, Pawson T, Culotti J. UNC-73 activates the Rac GTPase and is required for cell and growth cone migrations in *C. elegans*. *Cell*. 1998;92(6):785-95. Epub 1998/04/07. doi: 10.1016/s0092-8674(00)81406-3. PubMed PMID: 9529254.
55. Liebl EC, Forsthoefel DJ, Franco LS, Sample SH, Hess JE, Cowger JA, Chandler MP, Shupert AM, Seeger MA. Dosage-sensitive, reciprocal genetic interactions between the Abl tyrosine kinase and the putative GEF trio reveal trio's role in axon pathfinding. *Neuron*. 2000;26(1):107-18. Epub 2000/05/08. doi: 10.1016/s0896-6273(00)81142-3. PubMed PMID: 10798396.
56. Newsome TP, Schmidt S, Dietzl G, Keleman K, Asling B, Debant A, Dickson BJ. Trio combines with dock to regulate Pak activity during photoreceptor axon pathfinding in *Drosophila*. *Cell*. 2000;101(3):283-94. Epub 2000/06/10. doi: 10.1016/s0092-8674(00)80838-7. PubMed PMID: 10847683.
57. Iyer SC, Wang D, Iyer EP, Trunnell SA, Meduri R, Shinwari R, Sulkowski MJ, Cox DN. The RhoGEF trio functions in sculpting class specific dendrite morphogenesis in *Drosophila* sensory neurons. *PLoS One*. 2012;7(3):e33634. Epub 2012/03/24. doi: 10.1371/journal.pone.0033634. PubMed PMID: 22442703; PMCID: PMC3307743.
58. Govek EE, Newey SE, Van Aelst L. The role of the Rho GTPases in neuronal development. *Genes Dev*. 2005;19(1):1-49. Epub 2005/01/05. doi: 10.1101/gad.1256405. PubMed PMID: 15630019.
59. Ron D, Zannini M, Lewis M, Wickner RB, Hunt LT, Graziani G, Tronick SR, Aaronson SA, Eva A. A REGION OF PROTO-DBL ESSENTIAL FOR ITS TRANSFORMING ACTIVITY SHOWS SEQUENCE SIMILARITY TO A YEAST-CELL CYCLE GENE, CDC24, AND THE HUMAN BREAKPOINT CLUSTER GENE, BCR. *New Biologist*. 1991;3(4):372-9. PubMed PMID: WOS:A1991GK71900010.
60. Katzav S, Cleveland JL, Heslop HE, Pulido D. Loss of the amino-terminal helix-loop-helix domain of the vav proto-oncogene activates its transforming potential. *Molecular and cellular biology*. 1991;11(4):1912-20. doi: 10.1128/mcb.11.4.1912. PubMed PMID: 2005887.
61. Miki T, Smith CL, Long JE, Eva A, Fleming TP. Oncogene *ect2* is related to regulators of small GTP-binding proteins. *Nature*. 1993;362(6419):462-5. doi: 10.1038/362462a0.
62. van Leeuwen FN, van der Kammen RA, Habets GG, Collard JG. Oncogenic activity of *Tiam1* and *Rac1* in NIH3T3 cells. *Oncogene*. 1995;11(11):2215-21. Epub 1995/12/07. PubMed PMID: 8570171.

63. Kawasaki Y, Senda T, Ishidate T, Koyama R, Morishita T, Iwayama Y, Higuchi O, Akiyama T. Asef, a link between the tumor suppressor APC and G-protein signaling. *Science*. 2000;289(5482):1194-7. Epub 2000/08/19. doi: 10.1126/science.289.5482.1194. PubMed PMID: 10947987.
64. Bos JL, Rehmann H, Wittinghofer A. GEFs and GAPs: critical elements in the control of small G proteins. *Cell*. 2007;129(5):865-77. Epub 2007/06/02. doi: 10.1016/j.cell.2007.05.018. PubMed PMID: 17540168.
65. Schmidt A, Hall A. Guanine nucleotide exchange factors for Rho GTPases: turning on the switch. *Genes Dev*. 2002;16(13):1587-609. Epub 2002/07/09. doi: 10.1101/gad.1003302. PubMed PMID: 12101119.
66. Estrach S, Schmidt S, Diriong S, Penna A, Blangy A, Fort P, Debant A. The Human Rho-GEF trio and its target GTPase RhoG are involved in the NGF pathway, leading to neurite outgrowth. *Curr Biol*. 2002;12(4):307-12. Epub 2002/02/28. doi: 10.1016/s0960-9822(02)00658-9. PubMed PMID: 11864571.
67. Speicher DW, Marchesi VT. Erythrocyte spectrin is comprised of many homologous triple helical segments. *Nature*. 1984;311(5982):177-80. Epub 1984/09/13. doi: 10.1038/311177a0. PubMed PMID: 6472478.
68. Stabach PR, Simonovic I, Ranieri MA, Aboodi MS, Steitz TA, Simonovic M, Morrow JS. The structure of the ankyrin-binding site of beta-spectrin reveals how tandem spectrin-repeats generate unique ligand-binding properties. *Blood*. 2009;113(22):5377-84. Epub 2009/01/27. doi: 10.1182/blood-2008-10-184291. PubMed PMID: 19168783; PMCID: PMC2689040.
69. Djinovic-Carugo K, Gautel M, Ylanne J, Young P. The spectrin repeat: a structural platform for cytoskeletal protein assemblies. *FEBS Lett*. 2002;513(1):119-23. Epub 2002/03/26. doi: 10.1016/s0014-5793(01)03304-x. PubMed PMID: 11911890.
70. Liem RK. Cytoskeletal Integrators: The Spectrin Superfamily. *Cold Spring Harb Perspect Biol*. 2016;8(10). Epub 2016/10/05. doi: 10.1101/cshperspect.a018259. PubMed PMID: 27698030; PMCID: PMC5046693.
71. Lenne PF, Raae AJ, Altmann SM, Saraste M, Hörber JKH. States and transitions during forced unfolding of a single spectrin repeat. *FEBS Letters*. 2000;476(3):124-8. doi: 10.1016/S0014-5793(00)01704-X.
72. Amann KJ, Renley BA, Ervasti JM. A cluster of basic repeats in the dystrophin rod domain binds F-actin through an electrostatic interaction. *The Journal of biological chemistry*. 1998;273(43):28419-23. Epub 1998/10/17. doi: 10.1074/jbc.273.43.28419. PubMed PMID: 9774469.
73. Li X, Bennett V. Identification of the spectrin subunit and domains required for formation of spectrin/adducin/actin complexes. *The Journal of biological chemistry*. 1996;271(26):15695-702. Epub 1996/06/28. doi: 10.1074/jbc.271.26.15695. PubMed PMID: 8663089.
74. Otey CA, Pavalko FM, BurrIDGE K. An interaction between alpha-actinin and the beta 1 integrin subunit in vitro. *The Journal of Cell Biology*. 1990;111(2):721. doi: 10.1083/jcb.111.2.721.
75. Sampath R, Gallagher PJ, Pavalko FM. Cytoskeletal interactions with the leukocyte integrin beta2 cytoplasmic tail. Activation-dependent regulation of associations with talin and alpha-actinin. *The Journal of biological chemistry*.

- 1998;273(50):33588-94. Epub 1998/12/05. doi: 10.1074/jbc.273.50.33588. PubMed PMID: 9837942; PMCID: PMC2823626.
76. Carpen O, Pallai P, Staunton DE, Springer TA. Association of intercellular adhesion molecule-1 (ICAM-1) with actin-containing cytoskeleton and alpha-actinin. *The Journal of Cell Biology*. 1992;118(5):1223. doi: 10.1083/jcb.118.5.1223.
77. Heiska L, Kantor C, Parr T, Critchley DR, Vilja P, Gahmberg CG, Carpen O. Binding of the cytoplasmic domain of intercellular adhesion molecule-2 (ICAM-2) to alpha-actinin. *The Journal of biological chemistry*. 1996;271(42):26214-9. Epub 1996/10/18. doi: 10.1074/jbc.271.42.26214. PubMed PMID: 8824270.
78. Wechsler A, Teichberg VI. Brain spectrin binding to the NMDA receptor is regulated by phosphorylation, calcium and calmodulin. *Embo j*. 1998;17(14):3931-9. Epub 1998/07/22. doi: 10.1093/emboj/17.14.3931. PubMed PMID: 9670010; PMCID: PMC1170728.
79. Wyszynski M, Lin J, Rao A, Nigh E, Beggs AH, Craig AM, Sheng M. Competitive binding of alpha-actinin and calmodulin to the NMDA receptor. *Nature*. 1997;385(6615):439-42. Epub 1997/01/30. doi: 10.1038/385439a0. PubMed PMID: 9009191.
80. Terry-Lorenzo RT, Torres VI, Wagh D, Galaz J, Swanson SK, Florens L, Washburn MP, Waites CL, Gundelfinger ED, Reimer RJ, Garner CC. Trio, a Rho Family GEF, Interacts with the Presynaptic Active Zone Proteins Piccolo and Bassoon. *PLOS ONE*. 2016;11(12):e0167535. doi: 10.1371/journal.pone.0167535.
81. Neubrand VE, Thomas C, Schmidt S, Debant A, Schiavo G. Kidins220/ARMS regulates Rac1-dependent neurite outgrowth by direct interaction with the RhoGEF Trio. *Journal of Cell Science*. 2010;123(12):2111. doi: 10.1242/jcs.064055.
82. Beck KA. Spectrins and the Golgi. *Biochim Biophys Acta*. 2005;1744(3):374-82. Epub 2005/06/01. doi: 10.1016/j.bbamcr.2005.04.008. PubMed PMID: 15921768.
83. Tao T, Sun J, Peng Y, Li Y, Wang P, Chen X, Zhao W, Zheng YY, Wei L, Wang W, Zhou Y, Liu J, Shi YS, Zhu MS. Golgi-resident TRIO regulates membrane trafficking during neurite outgrowth. *The Journal of biological chemistry*. 2019;294(28):10954-68. Epub 2019/06/04. doi: 10.1074/jbc.RA118.007318. PubMed PMID: 31152060; PMCID: PMC6635450.
84. Yan Y, Eipper BA, Mains RE. Kalirin-9 and Kalirin-12 Play Essential Roles in Dendritic Outgrowth and Branching. *Cereb Cortex*. 2015;25(10):3487-501. Epub 2014/08/21. doi: 10.1093/cercor/bhu182. PubMed PMID: 25146373; PMCID: PMC4585498.
85. Yan Y, Eipper BA, Mains RE. Kalirin is required for BDNF-TrkB stimulated neurite outgrowth and branching. *Neuropharmacology*. 2016;107:227-38. Epub 2016/04/03. doi: 10.1016/j.neuropharm.2016.03.050. PubMed PMID: 27036892; PMCID: PMC4912856.
86. Katrancha SM, Shaw JE, Zhao AY, Myers SA, Cocco AR, Jeng AT, Zhu M, Pittenger C, Greer CA, Carr SA, Xiao X, Koleske AJ. Trio Haploinsufficiency Causes Neurodevelopmental Disease-Associated Deficits. *Cell reports*.

- 2019;26(10):2805-17.e9. Epub 2019/03/07. doi: 10.1016/j.celrep.2019.02.022. PubMed PMID: 30840899.
87. Bircher JE, Koleske AJ. Trio family proteins as regulators of cell migration and morphogenesis in development and disease - mechanisms and cellular contexts. *J Cell Sci.* 2021;134(3). Epub 2021/02/12. doi: 10.1242/jcs.248393. PubMed PMID: 33568469; PMCID: PMC7888718.
88. Paskus JD, Herring BE, Roche KW. Kalirin and Trio: RhoGEFs in Synaptic Transmission, Plasticity, and Complex Brain Disorders. *Trends Neurosci.* 2020;43(7):505-18. Epub 2020/06/10. doi: 10.1016/j.tins.2020.05.002. PubMed PMID: 32513570; PMCID: PMC7321888.
89. Blaise AM, Corcoran EE, Wattenberg ES, Zhang Y-L, Cottrell JR, Koleske AJ. In vitro fluorescence assay to measure GDP/GTP exchange of guanine nucleotide exchange factors of Rho family GTPases. *Biology Methods and Protocols.* 2021. doi: 10.1093/biomethods/bpab024.
90. Chhatriwala MK, Betts L, Worthylake DK, Sondek J. The DH and PH domains of Trio coordinately engage Rho GTPases for their efficient activation. *J Mol Biol.* 2007;368(5):1307-20. Epub 2007/03/30. doi: 10.1016/j.jmb.2007.02.060. PubMed PMID: 17391702; PMCID: PMC1890047.
91. Jumper J, Evans R, Pritzel A, Green T, Figurnov M, Ronneberger O, Tunyasuvunakool K, Bates R, Zidek A, Potapenko A, Bridgland A, Meyer C, Kohl SAA, Ballard AJ, Cowie A, Romera-Paredes B, Nikolov S, Jain R, Adler J, Back T, Petersen S, Reiman D, Clancy E, Zielinski M, Steinegger M, Pacholska M, Berghammer T, Bodenstein S, Silver D, Vinyals O, Senior AW, Kavukcuoglu K, Kohli P, Hassabis D. Highly accurate protein structure prediction with AlphaFold. *Nature.* 2021;596(7873):583-9. Epub 2021/07/16. doi: 10.1038/s41586-021-03819-2. PubMed PMID: 34265844; PMCID: PMC8371605.
92. Varadi M, Anyango S, Deshpande M, Nair S, Natassia C, Yordanova G, Yuan D, Stroe O, Wood G, Laydon A, Židek A, Green T, Tunyasuvunakool K, Petersen S, Jumper J, Clancy E, Green R, Vora A, Lutfi M, Figurnov M, Cowie A, Hobbs N, Kohli P, Kleywegt G, Birney E, Hassabis D, Velankar S. AlphaFold Protein Structure Database: massively expanding the structural coverage of protein-sequence space with high-accuracy models. *Nucleic Acids Research.* 2021;50(D1):D439-D44. doi: 10.1093/nar/gkab1061.
93. Ward JJ, McGuffin LJ, Bryson K, Buxton BF, Jones DT. The DISOPRED server for the prediction of protein disorder. *Bioinformatics.* 2004;20(13):2138-9. Epub 2004/03/27. doi: 10.1093/bioinformatics/bth195. PubMed PMID: 15044227.
94. Wells CM, Walmsley M, Ooi S, Tybulewicz V, Ridley AJ. Rac1-deficient macrophages exhibit defects in cell spreading and membrane ruffling but not migration. *J Cell Sci.* 2004;117:1259-68.
95. Debreceni B, Gao Y, Guo F, Zhu K, Jia B, Zheng Y. Mechanisms of guanine nucleotide exchange and Rac-mediated signaling revealed by a dominant negative trio mutant. *The Journal of biological chemistry.* 2004;279(5):3777-86. Epub 2003/11/03. doi: 10.1074/jbc.M308282200. PubMed PMID: 14597635.
96. McPherson CE, Eipper BA, Mains RE. Multiple novel isoforms of Trio are expressed in the developing rat brain. *Gene.* 2005;347(1):125-35. doi: 10.1016/j.gene.2004.12.028. PubMed PMID: 15715966.

97. van Rijssel J, Hoogenboezem M, Wester L, Hordijk PL, Van Buul JD. The N-terminal DH-PH domain of Trio induces cell spreading and migration by regulating lamellipodia dynamics in a Rac1-dependent fashion. *PloS one*. 2012;7(1):e29912. Epub 2012/01/13. doi: 10.1371/journal.pone.0029912. PubMed PMID: 22238672; PMCID: PMC3253119.
98. Schiller MR, Chakrabarti K, King GF, Schiller NI, Eipper BA, Maciejewski MW. Regulation of RhoGEF activity by intramolecular and intermolecular SH3 domain interactions. *The Journal of biological chemistry*. 2006;281(27):18774-86. Epub 2006/04/29. doi: 10.1074/jbc.M512482200. PubMed PMID: 16644733.
99. Xu Z, Gakhar L, Bain FE, Spies M, Fuentes EJ. The Tiam1 guanine nucleotide exchange factor is auto-inhibited by its pleckstrin homology coiled-coil extension domain. *The Journal of biological chemistry*. 2017;292(43):17777-93. Epub 2017/09/09. doi: 10.1074/jbc.M117.799114. PubMed PMID: 28882897; PMCID: PMC5663878.
100. Kubiseski TJ, Culotti J, Pawson T. Functional analysis of the *Caenorhabditis elegans* UNC-73B PH domain demonstrates a role in activation of the Rac GTPase in vitro and axon guidance in vivo. *Mol Cell Biol*. 2003;23(19):6823-35. Epub 2003/09/16. doi: 10.1128/MCB.23.19.6823-6835.2003. PubMed PMID: 12972602; PMCID: PMC193939.
101. Tian C, Paskus JD, Fingleton E, Roche KW, Herring BE. Autism Spectrum Disorder/Intellectual Disability-Associated Mutations in Trio Disrupt Neuroigin 1-Mediated Synaptogenesis. *J Neurosci*. 2021;41(37):7768-78. Epub 2021/08/07. doi: 10.1523/JNEUROSCI.3148-20.2021. PubMed PMID: 34353896; PMCID: PMC8445058.
102. Timmerman I, Heemskerk N, Kroon J, Schaefer A, van Rijssel J, Hoogenboezem M, van Unen J, Goedhart J, Gadella TW, Jr., Yin T, Wu Y, Huveneers S, van Buul JD. A local VE-cadherin and Trio-based signaling complex stabilizes endothelial junctions through Rac1. *J Cell Sci*. 2015;128(18):3514. Epub 2015/09/17. doi: 10.1242/jcs.179424. PubMed PMID: 26374854; PMCID: PMC6518322.
103. van Rijssel J, Kroon J, Hoogenboezem M, van Alphen FP, de Jong RJ, Kostadinova E, Geerts D, Hordijk PL, van Buul JD. The Rho-guanine nucleotide exchange factor Trio controls leukocyte transendothelial migration by promoting docking structure formation. *Mol Biol Cell*. 2012;23(15):2831-44. Epub 2012/06/15. doi: 10.1091/mbc.E11-11-0907. PubMed PMID: 22696684; PMCID: PMC3408411.
104. Son K, Smith TC, Luna EJ. Supervillin binds the Rac/Rho-GEF Trio and increases Trio-mediated Rac1 activation. *Cytoskeleton (Hoboken)*. 2015;72(1):47-64. Epub 2015/02/28. doi: 10.1002/cm.21210. PubMed PMID: 25655724.
105. Guex N, Peitsch MC. Swiss-Model and the Swiss-pdbViewer: An environment for comparative protein modeling. *Electrophoresis*. 1997;18:2714-23.
106. Sanchez NA, Kallweit LM, Trnka MJ, Clemmer CL, Al-Sady B. Heterodimerization of H3K9 histone methyltransferases G9a and GLP activates methyl reading and writing capabilities. *The Journal of biological chemistry*. 2021;297(5):101276. Epub 2021/10/08. doi: 10.1016/j.jbc.2021.101276. PubMed PMID: 34619147; PMCID: PMC8564726.

107. Schnirch L, Nadler-Holly M, Siao SW, Frese CK, Viner R, Liu F. Expanding the Depth and Sensitivity of Cross-Link Identification by Differential Ion Mobility Using High-Field Asymmetric Waveform Ion Mobility Spectrometry. *Anal Chem.* 2020;92(15):10495-503. Epub 2020/07/10. doi: 10.1021/acs.analchem.0c01273. PubMed PMID: 32643919.
108. Trnka MJ, Baker PR, Robinson PJ, Burlingame AL, Chalkley RJ. Matching cross-linked peptide spectra: only as good as the worse identification. *Mol Cell Proteomics.* 2014;13(2):420-34. Epub 2013/12/18. doi: 10.1074/mcp.M113.034009. PubMed PMID: 24335475; PMCID: PMC3916644.
109. Lim C, Berk JM, Blaise A, Bircher J, Koleske AJ, Hochstrasser M, Xiong Y. Crystal structure of a guanine nucleotide exchange factor encoded by the scrub typhus pathogen *Orientia tsutsugamushi*. *Proc Natl Acad Sci U S A.* 2020;117(48):30380-90. Epub 2020/11/14. doi: 10.1073/pnas.2018163117. PubMed PMID: 33184172; PMCID: PMC7720168.
110. Schindelin J, Arganda-Carreras I, Frise E, Kaynig V, Longair M, Pietzsch T, Preibisch S, Rueden C, Saalfeld S, Schmid B, Tinevez J-Y, White DJ, Hartenstein V, Eliceiri K, Tomancak P, Cardona A. Fiji: an open-source platform for biological-image analysis. *Nature Methods.* 2012;9(7):676-82. doi: 10.1038/nmeth.2019.
111. McQuin C, Goodman A, Chernyshev V, Kamensky L, Cimini BA, Karhohs KW, Doan M, Ding LY, Rafelski SM, Thirstrup D, Wiegand W, Singh S, Becker T, Caicedo JC, Carpenter AE. CellProfiler 3.0: Next-generation image processing for biology. *Plos Biol.* 2018;16(7). doi: ARTN e2005970 10.1371/journal.pbio.2005970. PubMed PMID: WOS:000440397800026.
112. Briancon-Marjollet A, Ghogha A, Nawabi H, Triki I, Auziol C, Fromont S, Piche C, Enslin H, Chebli K, Cloutier JF, Castellani V, Debant A, Lamarche-Vane N. Trio mediates netrin-1-induced Rac1 activation in axon outgrowth and guidance. *Mol Cell Biol.* 2008;28(7):2314-23. Epub 2008/01/24. doi: 10.1128/MCB.00998-07. PubMed PMID: 18212043; PMCID: PMC2268419.
113. Neubrand VE, Thomas C, Schmidt S, Debant A, Schiavo G. Kidins220/ARMS regulates Rac1-dependent neurite outgrowth by direct interaction with the RhoGEF Trio. *J Cell Sci.* 2010;123(Pt 12):2111-23. doi: 10.1242/jcs.064055. PubMed PMID: 20519585.
114. Yamasaki M, Thompson P, Lemmon V. CRASH syndrome: mutations in L1CAM correlate with severity of the disease. *Neuropediatrics.* 1997;28(3):175-8. Epub 1997/06/01. doi: 10.1055/s-2007-973696. PubMed PMID: 9266556; PMCID: PMC1563987.
115. Goossens T, Kang YY, Wuytens G, Zimmermann P, Callaerts-Végh Z, Pollarolo G, Islam R, Hortsch M, Callaerts P. The *Drosophila* L1CAM homolog Neuroglian signals through distinct pathways to control different aspects of mushroom body axon development. *Development.* 2011;138(8):1595-605. Epub 2011/03/11. doi: 10.1242/dev.052787. PubMed PMID: 21389050; PMCID: PMC3062427.
116. Fukata Y, Adesnik H, Iwanaga T, Bredt DS, Nicoll RA, Fukata M. Epilepsy-related ligand/receptor complex LGI1 and ADAM22 regulate synaptic transmission. *Science.* 2006;313(5794):1792-5. Epub 2006/09/23. doi: 10.1126/science.1129947. PubMed PMID: 16990550.

117. Fukata Y, Lovero KL, Iwanaga T, Watanabe A, Yokoi N, Tabuchi K, Shigemoto R, Nicoll RA, Fukata M. Disruption of LGI1-linked synaptic complex causes abnormal synaptic transmission and epilepsy. *Proc Natl Acad Sci U S A*. 2010;107(8):3799-804. Epub 2010/02/06. doi: 10.1073/pnas.0914537107. PubMed PMID: 20133599; PMCID: PMC2840530.
118. Owuor K, Harel NY, Englot DJ, Hisama F, Blumenfeld H, Strittmatter SM. LGI1-associated epilepsy through altered ADAM23-dependent neuronal morphology. *Mol Cell Neurosci*. 2009;42(4):448-57. Epub 2009/10/03. doi: 10.1016/j.mcn.2009.09.008. PubMed PMID: 19796686; PMCID: PMC2783222.
119. van Sonderen A, Petit-Pedrol M, Dalmau J, Titulaer MJ. The value of LGI1, Caspr2 and voltage-gated potassium channel antibodies in encephalitis. *Nat Rev Neurol*. 2017;13(5):290-301. Epub 2017/04/19. doi: 10.1038/nrneurol.2017.43. PubMed PMID: 28418022.
120. Gu W, Brodtkorb E, Steinlein OK. LGI1 is mutated in familial temporal lobe epilepsy characterized by aphasic seizures. *Annals of neurology*. 2002;52(3):364-7. Epub 2002/09/03. doi: 10.1002/ana.10280. PubMed PMID: 12205652.
121. Kalachikov S, Evgrafov O, Ross B, Winawer M, Barker-Cummings C, Martinelli Boneschi F, Choi C, Morozov P, Das K, Teplitskaya E, Yu A, Cayanis E, Penchaszadeh G, Kottmann AH, Pedley TA, Hauser WA, Ottman R, Gilliam TC. Mutations in LGI1 cause autosomal-dominant partial epilepsy with auditory features. *Nat Genet*. 2002;30(3):335-41. Epub 2002/01/26. doi: 10.1038/ng832. PubMed PMID: 11810107; PMCID: PMC2606053.
122. Morante-Redolat JM, Gorostidi-Pagola A, Piquer-Sirerol S, Sáenz A, Poza JJ, Galán J, Gesk S, Sarafidou T, Mautner VF, Binelli S, Staub E, Hinzmann B, French L, Prud'homme JF, Passarelli D, Scannapieco P, Tassinari CA, Avanzini G, Martí-Massó JF, Kluwe L, Deloukas P, Moschonas NK, Michelucci R, Siebert R, Nobile C, Pérez-Tur J, López de Munain A. Mutations in the LGI1/Epitempin gene on 10q24 cause autosomal dominant lateral temporal epilepsy. *Hum Mol Genet*. 2002;11(9):1119-28. Epub 2002/04/30. doi: 10.1093/hmg/11.9.1119. PubMed PMID: 11978770.
123. Koskinen LL, Seppälä EH, Belanger JM, Arumilli M, Hakosalo O, Jokinen P, Nevalainen EM, Viitmaa R, Jokinen TS, Oberbauer AM, Lohi H. Identification of a common risk haplotype for canine idiopathic epilepsy in the ADAM23 gene. *BMC Genomics*. 2015;16(1):465. Epub 2015/06/19. doi: 10.1186/s12864-015-1651-9. PubMed PMID: 26084559; PMCID: PMC4470040.
124. Lapetina S, Gil-Henn H. A guide to simple, direct, and quantitative in vitro binding assays. *J Biol Methods*. 2017;4(1):e62. Epub 20170120. doi: 10.14440/jbm.2017.161. PubMed PMID: 31453222; PMCID: PMC6708923.
125. Crespo P, Schuebel KE, Ostrom AA, Gutkind JS, Bustelo XR. Phosphotyrosine-dependent activation of Rac-1 GDP/GTP exchange by the vav proto-oncogene product. *Nature*. 1997;385(6612):169-72. doi: 10.1038/385169a0. PubMed PMID: 8990121.
126. Han J, Das B, Wei W, Van Aelst L, Mosteller RD, Khosravi-Far R, Westwick JK, Der CJ, Broek D. Lck regulates Vav activation of members of the Rho family of GTPases. *Mol Cell Biol*. 1997;17(3):1346-53. doi: 10.1128/MCB.17.3.1346. PubMed PMID: 9032261; PMCID: PMC231859.

127. Teramoto H, Salem P, Robbins KC, Bustelo XR, Gutkind JS. Tyrosine phosphorylation of the vav proto-oncogene product links FcepsilonRI to the Rac1-JNK pathway. *The Journal of biological chemistry*. 1997;272(16):10751-5. doi: 10.1074/jbc.272.16.10751. PubMed PMID: 9099726.
128. Miranti CK, Leng L, Maschberger P, Brugge JS, Shattil SJ. Identification of a novel integrin signaling pathway involving the kinase Syk and the guanine nucleotide exchange factor Vav1. *Curr Biol*. 1998;8(24):1289-99. doi: 10.1016/s0960-9822(07)00559-3. PubMed PMID: 9843681.
129. Salojin KV, Zhang J, Delovitch TL. TCR and CD28 are coupled via ZAP-70 to the activation of the Vav/Rac-1-/PAK-1/p38 MAPK signaling pathway. *J Immunol*. 1999;163(2):844-53. PubMed PMID: 10395678.
130. Medley QG, Buchbinder EG, Tachibana K, Ngo H, Serra-Pages C, Streuli M. Signaling between focal adhesion kinase and trio. *The Journal of biological chemistry*. 2003;278(15):13265-70. Epub 2003/01/29. doi: 10.1074/jbc.M300277200. PubMed PMID: 12551902.
131. Kiraly DD, Stone KL, Colangelo CM, Abbott T, Wang Y, Mains RE, Eipper BA. Identification of kalirin-7 as a potential post-synaptic density signaling hub. *J Proteome Res*. 2011;10(6):2828-41. Epub 20110425. doi: 10.1021/pr200088w. PubMed PMID: 21488700; PMCID: PMC3107868.
132. Miller MB, Yan Y, Machida K, Kiraly DD, Levy AD, Wu YI, Lam TT, Abbott T, Koleske AJ, Eipper BA, Mains RE. Brain Region and Isoform-Specific Phosphorylation Alters Kalirin SH2 Domain Interaction Sites and Calpain Sensitivity. *ACS Chem Neurosci*. 2017;8(7):1554-69. Epub 20170425. doi: 10.1021/acscchemneuro.7b00076. PubMed PMID: 28418645; PMCID: PMC5517348.
133. Herring BE, Nicoll RA. Kalirin and Trio proteins serve critical roles in excitatory synaptic transmission and LTP. *Proc Natl Acad Sci U S A*. 2016;113(8):2264-9. Epub 2016/02/10. doi: 10.1073/pnas.1600179113. PubMed PMID: 26858404; PMCID: PMC4776457.
134. Miller MM, Lapetina S, MacGrath SM, Sfakianos MK, Pollard TD, Koleske AJ. Regulation of actin polymerization and adhesion-dependent cell edge protrusion by the Abl-related gene (Arg) tyrosine kinase and N-WASp. *Biochemistry*. 2010;49(10):2227-34. Epub 2010/02/12. doi: 10.1021/bi901721u. PubMed PMID: 20146487; PMCID: PMC2836179.